

3D printing of Green Water Purification Filters

Design towards Sustainable and Scalable Biocomposite Materials

Natalia Fijot



3D printing of Green Water Purification Filters

Design towards Sustainable and Scalable Biocomposite Materials

Natalia Fijol

Academic dissertation for the Degree of Doctor of Philosophy in Materials Chemistry at Stockholm University to be publicly defended on Friday 22 September 2023 at 13.00 in Magnélisalen, Kemiska övningslaboratoriet, Svante Arrhenius väg 16 B.

Abstract

The globally escalating water pollution and water scarcity necessitates the development of efficient and sustainable water treatment technologies. This thesis investigates the feasibility of utilizing renewable and waste materials in the form of green composites for the fabrication of water purification filters via Fused Deposition Modelling (FDM).

The first system studied within this thesis is based on the biobased thermoplastic polymer - polylactic acid (PLA), which serves as a composite matrix that is reinforced and functionalized with an array of green materials including fish-scale extracted hydroxyapatite (HAp), 2,2,6,6 - tetramethylpiperidine-1-oxyl (TEMPO) - oxidized cellulose nanofibers (TCNF), chitin nanofibers (ChNF), and bioinspired metal-organic framework - SU-101. All the developed PLA-based biocomposites exhibited great design flexibility and excellent printability, leading to the development of high surface-finish quality water purification filters of various geometries and porosity architectures. The developed filters successfully removed various contaminants from water. High capability for removal of metal ions from both, model solutions (reaching removal capacity towards Cu^{2+} ions of 208 mg/g_{NF} and 234 mg/g_{NF} for ChNF/PLA and TCNF/PLA filters, respectively, compared to only 4 mg/g for PLA filters), as well as from an actual mine effluent, reaching removal efficiency towards i.a. Mn^{2+} ions of over 50 % was demonstrated. Moreover, the developed TCNF/PLA and ChNF/PLA filters successfully removed microplastics from laundry effluent with over 70 % separation efficiency. The PLA-based biocomposite filters surface-functionalized with SU-101 were also suitable for the removal of cationic dye, methylene blue (MB), from water with removal efficiencies of over 40 %.

The second composite system explored the possibility of using post-consumer polycotton textile waste as a functional entity for the polyethylene terephthalate glycol (PETG) matrix, for the fabrication of 3D printing filaments, which can be further processed into highly functional water purification filters by the FDM. The conducted TEMPO-mediated oxidation of the polycotton garments introduced negatively charged carboxylic groups onto the 3D printing filament's surface and consequently, onto the 3D printed structures, yielding filters suitable for removal of cationic dyes, such as MB, from water.

Apart from being evaluated for their ability to remove various contaminants from water, the filters have been subjected to a series of tests to assess the homogeneity of the filler dispersion in the polymer matrix as well as the filters' permeability and mechanical stability. The high throughput character of the filters was demonstrated, as e.g., for the HAp/PLA filters the calculated flux reached $2 \times 10^6 \text{ L m}^{-2} \text{ h}^{-1} \text{ bar}^{-1}$. The reinforcing impact of the nanospecies on the polymer matrix in the gradient porosity filters was investigated and so, it was shown that the addition of ChNF and TCNF fibers into PLA increases their Young's modulus value from $550.7 \pm 2.8 \text{ MPa}$, to $622.7 \pm 1.6 \text{ MPa}$ and $702.9 \pm 5.4 \text{ MPa}$, respectively. Moreover, the lifespan of the filters was assessed by subjecting them to an accelerated ageing procedure in water, which have shown that the TCNF/PLA and ChNF/PLA filters could serve up to eight and five months, respectively, while maintaining their functionality and good mechanical performance. Furthermore, the study revealed that the filters are indeed biodegradable, as after prolonged exposure to water at elevated temperatures, they have fully disintegrated.

Overall, the obtained results demonstrate the feasibility of combining renewable and recycled materials with 3D printing technology to create water purification filters suitable for the removal of a wide variety of contaminants from water.

Keywords: 3D printing, water treatment, polylactic acid, nanocellulose, nanochitin, hydroxyapatite, green metal-organic frameworks.

Stockholm 2023

<http://urn.kb.se/resolve?urn=urn:nbn:se:su:diva-219886>

ISBN 978-91-8014-416-2

ISBN 978-91-8014-417-9

Department of Materials and Environmental
Chemistry (MMK)

Stockholm University, 106 91 Stockholm



Stockholm
University

3D PRINTING OF GREEN WATER PURIFICATION FILTERS

Natalia Fijot

3D printing of Green Water Purification Filters

Design towards Sustainable and Scalable Biocomposite Materials

Natalia Fijoł

©Natalia Fijoł, Stockholm University 2023

ISBN print 978-91-8014-416-2

ISBN PDF 978-91-8014-417-9

Printed in Sweden by Universitetsservice US-AB, Stockholm 2023

To my loved ones

“Nothing in life is to be feared, it is only to be understood.
Now is the time to understand more, so that we may fear less.”

— Maria Skłodowska-Curie

“I knew exactly what to do. But in a much more real sense, I
had no idea what to do.”

— Michael Scott, *The Office*, Season 5: Stress Relief

Abstract

The globally escalating water pollution and water scarcity necessitates the development of efficient and sustainable water treatment technologies. This thesis investigates the feasibility of utilizing renewable and waste materials in the form of green composites for the fabrication of water purification filters via Fused Deposition Modelling (FDM).

The first system studied within this thesis is based on the biobased thermoplastic polymer - polylactic acid (PLA), which serves as a composite matrix that is reinforced and functionalized with an array of green materials including fish-scale extracted hydroxyapatite (HAp), 2,2,6,6 – tetramethylpiperdine-1-oxyl (TEMPO) - oxidized cellulose nanofibers (TCNF), chitin nanofibers (ChNF), and bioinspired metal-organic framework – SU-101. All the developed PLA-based biocomposites exhibited great design flexibility and excellent printability, leading to the development of high surface-finish quality water purification filters of various geometries and porosity architectures. The developed filters successfully removed various contaminants from water. High capability for removal of metal ions from both, model solutions (reaching removal capacity towards Cu^{2+} ions of 208 mg/g_{NF} and 234 mg/g_{NF} for ChNF/PLA and TCNF/PLA filters, respectively compared to only 4 mg/g for PLA filters), as well as from an actual mine effluent, reaching removal efficiency towards i.a. Mn^{2+} ions of over 50 % was demonstrated. Moreover, the developed TCNF/PLA and ChNF/PLA filters successfully removed microplastics from laundry effluent with over 70 % separation efficiency. The PLA-based biocomposite filters surface-functionalized with SU-101 were also suitable for the removal of cationic dye, methylene blue (MB), from water with removal efficiencies of over 40 %.

The second composite system explored the possibility of using post-consumer polycotton textile waste as a functional entity for the polyethylene terephthalate glycol (PETG) matrix, for the fabrication of 3D printing filaments, which were further processed into highly functional water purification filters by the FDM. The conducted TEMPO-mediated oxidation of the upcycled polycotton garments introduced negatively charged carboxylic groups onto the 3D printing filament's surface and consequently, onto the 3D printed structures, yielding filters suitable for removal of cationic dyes, such as MB, from water. Apart from being evaluated for their ability to remove various contaminants from water, the filters have been subjected to a series of tests to assess the homogeneity of the filler dispersion in the polymer matrix as well as the filters' permeability and mechanical stability. The high throughput character of the filters was demonstrated, as e.g. for the HAp/PLA filters the calculated flux reached $2 \times 10^6 \text{ L m}^{-2} \text{ h}^{-1} \text{ bar}^{-1}$. The reinforcing impact of the nanospecies on the polymer matrix in the gradient porosity filters was investigated and so, it was shown that the addition of ChNF and TCNF fibers into PLA increases their Young's modulus value from $550.7 \pm 2.8 \text{ MPa}$, to $622.7 \pm 1.6 \text{ MPa}$ and $702.9 \pm 5.4 \text{ MPa}$, respectively.

Moreover, the lifespan of the filters was assessed by subjecting them to an accelerated ageing procedure in water, which have shown that the TCNF/PLA and ChNF/PLA filters could serve up to eight and five months, respectively, while maintaining their functionality and good mechanical performance. Furthermore, the study revealed that the filters are indeed biodegradable, as after prolonged exposure to water at elevated temperatures, they have fully disintegrated.

Overall, the obtained results demonstrate the feasibility of combining renewable and recycled materials with 3D printing technology to create water purification filters suitable for the removal of a wide variety of contaminants from water.

Keywords: 3D printing, water treatment, polylactic acid, nanocellulose, nanochitin, hydroxyapatite, green metal-organic frameworks.

Sammanfattning

De globalt eskalerande vattenföroreningarna och vattenbristen kräver utveckling av effektiva och hållbara vattenreningsteknologier. Denna avhandling undersöker genomförbarheten att använda förnybara och/eller återvunna avfallsmaterial i form av kompositer för tillverkning av vattenreningsfilter via Fused Deposition Modelling (FDM).

Det första systemet bygger på den biobaserade termoplastiska polymeren – polylaktid (PLA), som fungerar som en kompositmatris vilken förstärkts och funktionaliserats med olika gröna material, inklusive fiskfjälls-extraherad hydroxyapatit (HAp), 2,2,6,6 - tetrametylipiperidin-1-oxyl (TEMPO)-oxiderade cellulosa-nanofibrer (TCNF), kitin-nanofibrer (ChNF) och det bioinspirerade metallbelagda organiska ramverket - SU-101. Samtliga framställda PLA-baserade biokompositer visade stor designflexibilitet och utmärkt utskriftsbarhet, vilket ledde till utvecklingen av vattenreningsfilter med hög yttjämnhet och olika geometrier och porositetsstrukturer. De utvecklade filtren avlägsnade framgångsrikt olika föroreningar från vatten. En hög förmåga att avlägsna metalljoner från modellösningar (uppnådde borttagningskapacitet av t.ex. Cu^{2+} joner på 208 mg/g_{NF} och 234 mg/g_{NF} för ChNF/PLA och TCNF/PLA-filter, jämfört med 4 mg/g för PLA-filter), samt från ett verkligt gruvavloppsflöde, där borttagningskapaciteten av t.ex. Mn^{2+} var över 50 %, demonstrerades. Dessutom avlägsnade TCNF/PLA- och ChNF/PLA-filtren framgångsrikt mikroplaster från tvättvatten med över 70 % separationskapacitet. De biokomposita filtren som ytfunktionaliserats med SU-101 var även lämpliga för att avlägsna ett katjoniskt färgämne, metylenblå (MB), från vatten med en borttagningskapacitet på över 40 %.

Det andra kompositsystemet undersökte möjligheten att använda återvunnet textilavfall från konsumenter som en funktionell enhet för polyetentereftalatglykol (PETG)-matrisen, för tillverkning av 3D-filament, som sedan kan användas för att producera högfungerande vattenreningsfilter genom FDM. Genomförd TEMPO-oxidation av återvunnet polycotton-klädesplagg ledde till introduktionen av negativt laddade kemiska grupper på 3D-filamentets yta och därigenom på de 3D-utskrivna strukturerna, vilket resulterar i filter som är lämpliga för avlägsnande av katjoniska färgämnen, som MB, från vatten.

Utöver att utvärderas för sin förmåga att avlägsna olika föroreningar från vatten, har filtren genomgått en serie tester för att bedöma bland annat homogeniteten i fyllmedlets dispersion i polymermatrisen samt filtrens permeabilitet och mekaniska stabilitet. Filtrens höga genomströmningsegenskaper demonstrerades, t.ex. för HAp/PLA-filtret nådde den beräknade flödes hastigheten $2 \times 10^6 \text{ L m}^{-2} \text{ h}^{-1} \text{ bar}^{-1}$. Förstärkande egenskaper hos nanospecier i gradientporositetsfilter på polymermatrisen undersöktes och

det visades att tillsats av ChNF- och TCNF-fibrer till PLA ökar dess Young's modul-värde från 550.7 ± 2.8 MPa till 622.7 ± 1.6 MPa respektive 702.9 ± 5.4 MPa. Dessutom utvärderades filtrens livslängd genom att utsättas för en accelererad åldrandeprocess i vatten, vilket ledde till slutsatsen att filtren kan fungera i upp till åtta månader och behålla sin funktionalitet och goda mekaniska prestanda. Vidare visade studien att filtren faktiskt är biologiskt nedbrytbara, eftersom de efter långvarig exponering i vatten vid förhöjd temperatur helt brutits ner.

Sammanfattningsvis visar de erhållna resultaten att det är genomförbart att kombinera förnybara och återvunna material med 3D-utskriftsteknik för att skapa vattenreningsfilter lämpliga för att avlägsna olika föroreningar från vatten. Ytterligare forskning krävs för att optimera kompositsystemets design, så att det inkorporerar ett större antal funktionskomponenter och därmed förbättrar dess totala prestanda och effektivitet.

Streszczenie

Eskalujący problem globalnego zanieczyszczenia wód wymaga opracowania nowoczesnych i skutecznych technologii oczyszczania wody działających w ramach zrównoważonego rozwoju. W kontekście niniejszej rozprawy doktorskiej przeprowadzono badania mające na celu wykorzystanie odnawialnych biomateriałów, a także poddanych recyklingowi materiałów odpadowych, do produkcji filtrów do oczyszczania wody za pomocą technologii druku trójwymiarowego (3D), konkretnie metody Osadzania Topionego Materiału (*ang.* Fused Deposition Modelling (FDM)).

W badaniach skoncentrowano się na dwóch różnych systemach kompozytowych. Pierwszy system opierał się na biodegradowalnym polimerze termoplastycznym - kwasie polilaktydowym (PLA), który pełnił rolę lepiszcza kompozytu. Lepiszcz było następnie wzmacniane i funkcjonalizowane przy użyciu materiałów pochodzenia naturalnego tj. hydroksyapatytem (HAp) ekstraktowanym z rybich łusek, nanowłóknami celulozy (CNF) utlenionej 2,2,6,6-tetrametylo-1-oksopiperydyną (TEMPO) - TCNF, nanowłóknami chitynowymi (ChNF) oraz zielonym szkieletem metalo-organicznym bazującym na kwasie elagowym (SU-101). Wszystkie otrzymane biokompozyty oparte na PLA charakteryzowały się dużą elastycznością w zakresie projektowania i doskonałą zdolnością do przetwarzania przy użyciu komercyjnych drukarek 3D, co pozwoliło na stworzenie filtrów o wysokiej jakości wykonania, a także o różnych geometriach i architekturach porowatości. Opracowane materiały skutecznie usuwały różne substancje zanieczyszczające z wody. Filtry wykazały wysoką zdolność do usuwania jonów metali zarówno z roztworów modelowych (uzyskując m.in. zdolność usuwania jonów Cu^{2+} na poziomie 208 $\text{mg/g}_{\text{nanowłókna(NW)}}$ i 234 mg/g_{NW} dla filtrów ChNF/PLA i TCNF/PLA, w porównaniu do 4 mg/g dla filtrów wykonanych z czystego PLA), jak i z rzeczywistych zrzutów kopalnianych, osiągając skuteczność usuwania jonów Mn^{2+} powyżej 50 %. Ponadto, opracowane filtry TCNF/PLA i ChNF/PLA wykazywały potencjał do separacji mikroplastików z odpływu z prania z efektywnością separacji powyżej 70 %. Natomiast zrecyklingowane filtry biokompozytowe powierzchniowo funkcjonalizowane SU-101 wykazały się również zdolnością do usuwania barwnika kationowego, błękitu metylenowego (MB), z wody z wydajnością usuwania powyżej 40 %.

Drugi badany system kompozytowy koncentrował się na wykorzystaniu zużytych tekstyliów bawełniano-poliestrowych jako komponentu konstrukcyjnego dla lepiszcza glikolu polietylenotereftalanowego (PETG) do produkcji termoplastycznych filamentów do druku 3D. Otrzymane filamenty zostały przetworzone w wysoko funkcjonalne filtry do oczyszczania wody przy użyciu technologii FDM. Oksydacja tekstyliów katalizowana TEMPO przeprowadzona przed przetwarzaniem materiału, zarówno w wylączarce jednoślakowej, jak i drukarce 3D, umożliwiła wprowadzenie na powierzchnię filamentu, a ostatecznie także filtrów, grup chemicznych o ładunku

ujemnym. Otrzymane filtry były więc odpowiednio zaprojektowane do usuwania jonowych substancji z ładunkiem dodatnim, takich jak np. MB, z wody.

Oprócz oceny zdolności filtrów do usuwania różnych substancji zanieczyszczających z wody, przeprowadzono również szereg testów mających na celu ocenę m.in. jednorodności rozproszenia nanokomponentów w lepiszczu polimerowym, przepuszczalności, a także stabilności termomechanicznej filtrów. Wykazano na przykład, że przepływ wody dla filtrów wykonanych z kompozytu HAp/PLA wynosił $2 \times 10^6 \text{ L m}^{-2} \text{ h}^{-1} \text{ bar}^{-1}$. Badano również wpływ nanocząstek wzmacniających na lepiszcze polimerowe i wykazano, że dodatek włókien chityny i celulozy do PLA zwiększał odpowiednio moduł Younga wydrukowanych porowatych filtrów z $550.7 \pm 2.8 \text{ MPa}$ do $622.7 \pm 1.6 \text{ MPa}$ i $702.9 \pm 5.4 \text{ MPa}$. Ponadto, oceniono okres użytkowania filtrów poprzez przyspieszone procesy starzenia w wodzie, które potwierdziły, że filtry TCNF/PLA mogą służyć przez okres do ośmiu miesięcy, zachowując swoją funkcjonalność i właściwości mechaniczne.

Podsumowując, prezentowany zbiór publikacji stanowiący rozprawę doktorską dowodzi możliwości wykorzystania odnawialnych i zrecyklingowanych materiałów i technologii druku 3D w celu stworzenia filtrów do oczyszczania wody, zdolnych do usuwania szerokiej gamy substancji zanieczyszczających. Dalsze badania, służące optymalizacji składu chemicznego badanych kompozytów, są wskazane. Ponadto, należy przeprowadzić środowiskową ocenę cyklu życia wykonanych filtrów, tak aby kontynuować postęp w dziedzinie oczyszczania wody w ramach idei zrównoważonego rozwoju.

Słowa kluczowe: Druk 3D, oczyszczenie wody, kwas polilaktydowy, nanowłókna celulozowe i chitynowe, hydroksyapatyt, zielony szkielec metalo-organiczny.

List of publications

This thesis is based on the following publications:

- i. **3D-printed monolithic biofilters based on a polylactic acid (PLA) – hydroxyapatite (HAp) composite for heavy metal removal from an aqueous medium**

Natalia Fijol, Hani Nasser Abdelhamid, Binsi Pillai, Stephen A. Hall, Nebu Thomas and Aji P. Mathew. *RSC Advances* (2021), 11, 32408.

Scientific contribution: conceptualization, methodology, validation, investigation, data curation, writing – original draft, visualization.

- ii. **3D printed polylactic acid (PLA) filters reinforced with polysaccharide nanofibers for metal ions capture and microplastics separation from water**

Natalia Fijol, Andrea Aguilar-Sanchez, Maria-Ximena Ruiz-Caldas, Jakob Redlinger-Pohn, Andreas Mautner and Aji P. Mathew. *Chemical Engineering Journal* (2023) 457, 141153.

Scientific contribution: conceptualization, methodology, validation, investigation, data curation, writing – original draft, visualization.

- iii. **MOF@Cell: Anchoring a green metal-organic framework onto the surface of 3D printed biobased filters for mine effluent treatment**

Natalia Fijol, Andreas Mautner, Erik Svensson Grape, Zoltan Bacsik, A. Ken Inge and Aji P. Mathew. *Journal of Materials Chemistry A* (2023), 11, 12384-12394.

Scientific contribution: conceptualization, methodology, validation, investigation, data curation, writing – original draft, visualization.

- iv. **Accelerated ageing and long-term stability assessment of 3D printed, fully biobased water purification filters**

Natalia Fijol and Aji P. Mathew. *Polymer Testing*, Manuscript submitted

Scientific contribution: conceptualization, methodology, validation, investigation, data curation, writing – original draft, visualization.

- v. **Trash to treasure: 3D printing with waste-based polycotton filament for the production of water filters and commodity products**

Varvara Apostolopoulou-Kalkavoura*, Natalia Fijol*, Salvatore Lombardo, Maria-Ximena Ruiz-Caldas and Aji P. Mathew. In manuscript

*Indicates shared first authorship.

Scientific contribution: methodology, validation, investigation, data curation, writing – original draft, visualization.

Relevant publications **not** included in this thesis:

vi. 3D-printable biopolymer-based materials for water treatment applications: A review

Natalia Fijol, Andrea Aguilar Sanchez and Aji P. Mathew. *Chemical Engineering Journal* (2022) 430, 132964.

vii. Preclinical evaluation of 3D printed polylactic acid loaded with fish scale derived hydroxyapatite based composite scaffolds intended for alveolar bone regeneration

Nebu George Thomas, Mekha Grace Varghese, Yogesh Bharat Dalvi, Aji P. Mathew, Natalia Fijol, Binsi PK, Anand A. *Manuscript submitted*

viii. Biocompatible electroactive surfaces based on a glycolated polythiophene processed from a green solvent

Vasileios K. Oikonomou, Johannes Gladisch, Ilaria Abdel Aziz, Sophie Griggs, Hanne Biesmans, Natalia Fijol, Aji P. Mathew, Ian McCulloch, Magnus Berggren, Eleni Stavriniidou. *Manuscript submitted*

ix. MOF&Cell: 3D printed nanocellulose - green metal-organic framework hydrogels for water treatment applications

Jessica Erdmann, Natalia Fijol and Aji P. Mathew. *Manuscript in preparation*

Conferences

Conferences attended during the PhD studies:

- i. American Chemical Society (ACS), March 20-24th, 2022, San Diego, California, United States
Natalia Fijol, Andrea Aguilar-Sanchez and Aji P. Mathew

Oral presentation: 3D printed TEMPO oxidized cellulose nanofibers reinforced polylactic acid (PLA) filters for metal ions and microplastics removal from aqueous medium

- ii. New Zealand Institute of Chemistry (NZIC), November 21-24th, 2022, Auckland, New Zealand
Natalia Fijol, Erik Svensson Grape, A. Ken Inge and Aji P. Mathew

Oral presentation: 3D printed polylactic acid - based filters reinforced with cellulose nanofibers and surface functionalized with green metal-organic framework for water treatment

Awarded **The RSC New Zealand Branch Prize for Best PhD Oral Presentation at the NZIC 2022 Conference.**

- iii. 16th International conference on materials chemistry (MC16), July 3-6th, 2023, Dublin, Ireland
Natalia Fijol and Aji P. Mathew

Oral presentation: Sustainable water treatment solutions: 3D printed and biobased water purification filters

Contents

1. Introduction	1
1.1 Water pollution.....	1
1.2 Water treatment technologies of today	2
1.3 Biobased and recycled materials: the future of water treatment?.....	3
1.3.1 Polylactic acid	3
1.3.2 Hydroxyapatite	5
1.3.3 Cellulose	5
1.3.4 Chitin	7
1.3.5 Green metal-organic frameworks (MOFs)	8
1.3.6 Recycled textiles.....	8
1.4 Additive manufacturing (AM) – on-demand fabrication method	9
1.5 Preparation routes for the development of green and 3D printable composites.....	11
1.6 Accelerated ageing – the Arrhenius model	12
1.7 Scope of the thesis	13
2. Research methodology	15
2.1 Materials.....	15
2.2 Experimental – from the composite development to the filament extrusion.....	16
Hydroxyapatite (HAP) extraction.....	16
PLA - based biocomposite preparation	16
Textile - based composite preparation.....	16
Filament extrusion	17
2.3 3D printing – designs and parameters	17
2.4 MOF functionalization	20
2.5 Accelerated ageing	20
2.6 Characterization methods	21
Scanning Electron Microscopy (SEM).....	21
Thermogravimetric Analysis (TGA)	21
X-Ray Diffraction (XRD)	21
Fourier-transform Infrared Spectroscopy (FT-IR)	22
X-ray micro-computed tomography (μ-CT).....	22
Compression testing	22
Inductively Coupled Plasma Mass Spectrometry (ICP-MS).....	22

Surface zeta potential	23
X-ray photoelectron spectroscopy (XPS).....	23
Transmission Electron Microscopy (TEM).....	24
Dynamic Mechanical Thermal Analysis (DMTA).....	24
Conductometric Titration	24
2.7 Functionality of the 3D printed filters	24
Batch adsorption tests.....	24
Desorption and recyclability tests	26
Microplastics removal	27
Permeance and permeability measurements.....	27
3. Development of green composites for 3D printing	29
3.1 PLA - based composites	29
3.2 Textile - based composites	35
4. Performance optimization and evaluation of 3D printed water purification filters.....	37
4.1 Surface functionalization of the 3D printed biocomposite filters.....	37
4.2 Mechanical performance of the developed filters	38
4.3 Functionality of the 3D printed filters: water treatment applications.....	42
5. Estimating the lifespan of the filters via accelerated ageing experiments.....	47
6. Conclusions	51
7. Future outlook	52
Acknowledgments	54
References	57

List of abbreviations

AM	Additive manufacturing
UN	United Nations
WHO	World Health Organization
PLA	Polylactic acid
LA	Lactic acid
HAp	Hydroxyapatite
CNC	Cellulose nanocrystal
CNF	Cellulose nanofiber
TEMPO	2, 2, 6, 6 – tetramethylpiperidine-1-oxyl
TCNF	TEMPO-oxidized CNF
ChNC	Chitin nanocrystal
ChNF	Chitin nanofiber
MOF	Metal-organic framework
3D	Three-dimensional
CAD	Computer-aided design
STL	Standard triangle language
FDM	Fused-Deposition Modelling
PVA	Polyvinyl alcohol
PCL	Polycaprolactone
PEG	Polyethylene glycol
TIPS	Thermally Induced Phase Separation
PETG	Polyethylene terephthalate glycol
PET	Polyethylene terephthalate
RT	Room temperature
SEM	Scanning electron microscopy
TGA	Thermogravimetric analysis
XRD	X-ray diffraction
FT-IR	Fourier-transform infrared spectroscopy
μ -CT	X-ray micro-computed tomography
ICP-MS	Inductively coupled plasma mass spectrometry
XPS	X-ray photoelectron spectroscopy
SEC	Size exclusion chromatography
M_w	Molecular weight
MWD	Molecular weight distribution
TEM	Transmission electron microscopy
DMTA	Dynamic mechanical thermal analysis
Tan δ	Loss tangent
E'	Storage modulus
E''	Loss modulus
T_g	Glass transition temperature
SEM-EDX	SEM with Energy Dispersive X-Ray Analysis
NF	Nanofibers

1. Introduction

Water scarcity is a progressing concern, as global population's growth, urbanization, and climate change continue to strain the world's finite water resources. According to the United Nations reports¹, nearly a quarter of the world's population i.e. 1.6 billion people lack the necessary infrastructure to access potable water. This, combined with the extreme pollution of global water reservoirs with petroleum-based plastics, underscores the urgent need for sustainable water management practices and innovative solutions required to ensure access to clean water for all.

All of the above factors unite scientists in the search for green alternatives to non-biodegradable petroleum-based materials. The novel, desired materials need to be both as efficient and durable as synthetic materials, yet also biodegradable and environmentally friendly, with minimal impact on the planet. It is a big challenge to eliminate or even partially replace petroleum-based products, as many sectors of the industry remain highly dependent on this class of materials. According to a 2017 study², a total of 8.3 billion metric tons of virgin plastics have been manufactured since their emergence in the 1950s. Due to the poor recycling culture and non-biodegradability of petroleum-based materials, vast quantities of plastic waste accumulate in landfills, polluting not only the earth but also global water resources, aggravating the issue of water scarcity.

This thesis aims to develop fully biobased water purification filters by the means of additive manufacturing (AM) technology. This approach provides a cost-effective and on-demand solution to address water scarcity issues, while reducing the consumption of petroleum-based plastics by replacing them with 3D printable, sustainably sourced materials.

1.1 Water pollution

Water pollution is the contamination of water reservoirs with harmful substances of varying origins. The different sources of water pollution include industrial, agricultural and household sources³.

Industrial sources of water pollution include manufacturing, mining, and mineral processing – as well as oil and gas exploration and production industries. Industrial water pollutants include poisonous metal ions such as mercury, lead and cadmium; oils; microplastics; and other toxic chemicals such as industrial solvents or per - and polyfluoroalkyl substances (PFAS)³. Agricultural activities, such as crop production and livestock farming, can also contribute to water pollution. Agricultural pollutants include fertilizers, pesticides, and animal waste, which can contaminate surface and groundwater resources³. Moreover, regular household activities can contribute to water pollution by releasing chemicals such as

detergents, surfactants and soaps into the environment. Moreover, using household laundry machines has been shown to contribute to the release of microplastics into the environment⁴.

Water pollution threatens the well-being of whole ecosystems, including humans and wildlife. Contaminated water containing harmful chemicals, but also bacteria and viruses, has been recognized as a lead cause of various diseases including diarrhoea, cholera, typhoid fever, and hepatitis A¹. Moreover, prolonged exposure to contaminated water can lead to chronic health issues including cancer, developmental disorders and reproductive problems³. Therefore, the impact of water pollution on the environment cannot be ignored¹. Contaminated water leads to a decrease, or even extinction, of aquatic and land fauna and flora populations¹. Further bioaccumulation of toxic substances in animal tissues, disruption of natural food chains and reduced biodiversity within ecosystems are just a few more examples from a long list of negative consequences that water pollution has on the environment.

To address the growing problem of water pollution, many regulatory frameworks and policy initiatives have been proposed worldwide. In 2000, European Union's Water Framework Directive (WFD) was implemented in Europe. The WFD aims to protect and improve the quality of European waters by *'ensuring good qualitative and quantitative health, i.e. on reducing and removing pollution and on ensuring that there is enough water to support wildlife at the same time as human needs'*⁵. Apart from many other directives, the one by the United Nations (UN) is especially noteworthy. The UN has listed 'Clean water and sanitation' as one of its seventeen Sustainable Development Goals, highlighting the importance of *'availability and sustainable management of water and sanitation for all'*⁶. Moreover, the international guidelines for drinking water quality, published by the World Health Organization (WHO)⁷, outline the permissible concentration levels of numerous elements and chemical compounds. All of these combined, clearly indicate a high level of awareness regarding the water pollution problem among the legislators worldwide.

1.2 Water treatment technologies of today

The currently implemented water treatment techniques can be broadly classified into physical, chemical and biological methods. Physical methods, which rely on physical processes to remove contaminants from water, include techniques such as filtration⁸, sedimentation⁹, precipitation¹⁰, and distillation¹¹. Chemical methods of water treatment such as ion exchange¹², chlorination, or ozonation¹³, use chemical processes to eliminate contaminants from water. Adsorption is one of the most common techniques used for water purification, and it can be considered either a chemical or physical water treatment method, depending on the type of interactions between the adsorbent material used and the type of pollutant being removed. Lastly, biological methods of water treatment, such as the utilization of activated sludge¹⁴ or biofiltration¹⁵, rely fully on biological processes to purify contaminated water.

The implementation of water treatment technologies is often associated with several challenges that can affect their feasibility and effectiveness. These challenges include the cost of the technology, the energy consumption required for operation, and the maintenance requirements necessary to keep the technology running effectively. Moreover, commercially used filters and membranes often originate from either non-renewable or non-sustainable resources with the most common adsorbents including alumina¹⁶ and alumina-based adsorbents^{17–19}, silica²⁰ and silica-based materials^{21–23} as well as activated carbon^{24–26}. That means that at the end of their service-life, some of these might contribute to the non-biodegradable and non-recyclable waste accumulation and secondary environmental pollution issues. However, in the last two decades, the biobased filters and membranes developed using renewable materials such as cellulose^{27–31}, chitin^{32,33}, and polylactic acid (PLA)^{34,35} have gained scientific interest.

1.3 Biobased and recycled materials: the future of water treatment?

1.3.1 Polylactic acid

Polylactic acid (PLA) is a green alternative to petroleum-based plastics, as it can be obtained from renewable sources such as corn, rice, and sugarcane. PLA is a linear aliphatic polyester built out of lactic acid (LA) monomers, which are produced by converting plant-based sugars via either bacterial fermentation, using a strain of *Lactobacillus*, or chemical processes³⁶. LA comes in two different optical isomer forms i.e. *L* – and *D* – LA isomers (**Figure 1.1**). The LA produced by the chemical route is an optically inactive racemic mixture, while the LA obtained by bacterial fermentation yields an almost enantiomerically pure (99.5 %) *L* – LA isomer, which is optically active³⁶. The further polymerization of the LA monomers into PLA can be carried out either via direct condensation polymerization or by polymerization through lactide formation³⁶. The simplified scheme of the two processes is presented in **Figure 1.1**.

The lactide formation polymerization route is initiated by polycondensation of LA, followed by depolymerisation into the dehydrated cyclic lactide (3,4-dimethyl-1,4-dioxane-2,5-dione) and the ring-opening polymerization into high molecular weight (*M_w*) PLA chains. The cyclic lactide can be found in three different stereochemical configurations i.e. *D,D*–lactide, *L,L*–lactide and *D,L*–lactide. The stereochemistry of the final polymer product is determined by the ratio of different lactide isomers present during processing. The ring opening polymerization is the most commonly used method for the production of PLA, as direct polycondensation usually yields low *M_w* products and requires extra processing steps. While the direct polycondensation process requires solvent utilization under vacuum, the ring-opening polymerization of the cyclic lactide is solvent-free^{36,37}.

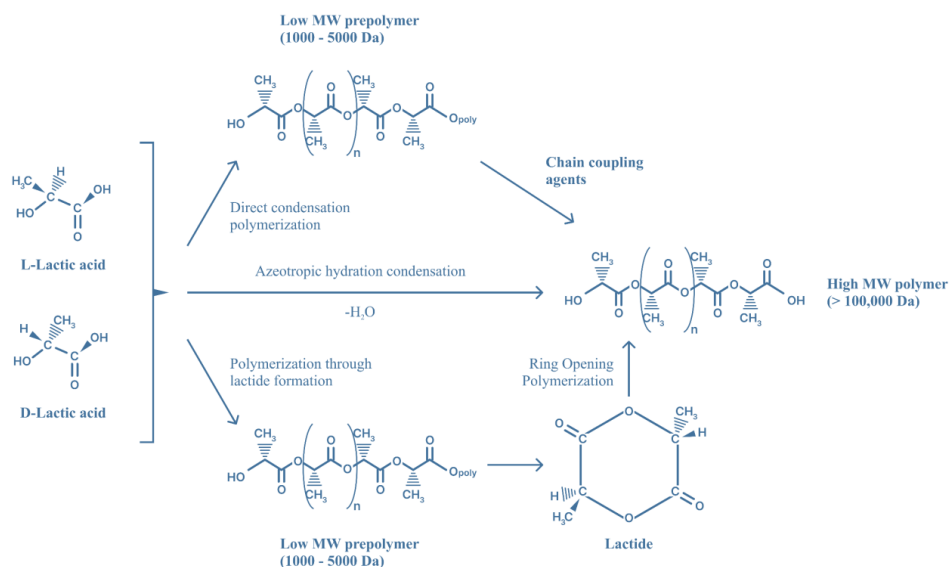


Figure 1.1 Reaction schemes to produce PLA as adapted from Muller et al.³⁷.

The advantages of PLA over synthetic plastics present themselves already at the manufacturing stage, as it was reported that production of PLA resin consumes between 25 and 55 % less fossil energy, compared to the energy required for the production of petroleum-based polymers³⁷. Due to its good thermal properties, PLA can be processed by a multitude of heat fabrication techniques such as injection³⁸ and blow moulding³⁹, extrusion⁴⁰, thermoforming⁴¹, and fiber spinning⁴². As it is derived from renewable sources, PLA is biodegradable, compostable, and recyclable³⁷. It has a rather slow degradation rate, so its compositing is usually conducted in controlled laboratory conditions³⁶. Moreover, it has been approved for use in biomedical applications due to its biocompatibility⁴³. PLA presents a good water vapour barrier, and even though it is insoluble in water, it can be dissolved in various solvents including i.a. chloroform, acetone, and dichloromethane³⁷. Nevertheless, due to its hydrophobicity and chemical inertness, PLA might be challenging to implement in composite processing applications. Other disadvantages of PLA include its low gas barrier properties, brittleness and low impact strength, which could all limit its potential applicability³⁶.

Recently, PLA and PLA-based materials have gained scientific popularity as materials suitable for implementation within water treatment applications. Functionalized PLA-materials in the form of e.g. electrospun fibers^{34,44}, membranes⁴⁵⁻⁴⁸, as well as 3D printed meshes⁴⁹⁻⁵¹ and filters^{35,52} have been used for oil-water separation^{34,44,45,49,51} as well as metal ions^{35,46-48} and dyes^{50,52} removal from contaminated water.

1.3.2 Hydroxyapatite

Hydroxyapatite (HAp) is a naturally occurring mineral that is a major component of vertebrate bones and teeth. Chemically, it is a calcium phosphate with a chemical formula $[\text{Ca}_{10}(\text{PO}_4)_6(\text{OH})_2]$. HAp has a Ca/P molar ratio of 1.67, and either a hexagonal or a monoclinic crystal structure, dependent on the orientation of the hydroxyl groups (OH)⁵³. At room temperature and a pH above 4.2, HAp is considered to be one of the most stable minerals among calcium phosphates⁵³. HAp crystals and nanocrystals are typically synthesized via solid-state reactions such as crystal growth under hydrothermal reaction, layer hydrolysis of other calcium phosphate salts and sol–gel crystallization^{54,55}. Moreover, HAp can be isolated from mineral rocks, plants, and biogenic products such as fish and chicken bones, egg shells and mussel shells⁵⁶. HAp is widely used in orthopaedics, dentistry, and tissue engineering due to its biocompatibility, osteoconductivity, and bone-bonding ability⁵³. In clinical applications, HAp can be used as a coating on medical implants to promote osteointegration, or as a bone substitute material to fill bone defects and stimulate bone regeneration⁵³.

Composites of HAp with PLA⁴⁶, polyvinyl alcohol⁵⁷, chitosan^{58,59}, polyacrylamide⁶⁰, polyurethane⁶¹, magnetic nanoparticles ($\text{Fe}_3\text{O}_4/\text{HAp}$)^{62,63} and magnetic nanoparticles-immobilized oxidized multiwall carbon nanotubes (mHAP-oMWCNTs)⁶⁴ in the form of coatings, powder, hydrogels and foams were previously studied for water treatment applications.

1.3.3 Cellulose

Cellulose is a linear polysaccharide formed by connecting repeating glucose units by covalent β -(1 \rightarrow 4) glycosidic bonds. It is the most abundant polymer on Earth, produced by nature at the annual rate of 10^{11-12} tonnes⁶⁵. Cellulose is the main component of the plant cell wall structure, so it can be extracted from wood, seeds, cotton, algae, and agricultural waste. Moreover, cellulose can be synthesized by some bacterial organisms (*Acetobacter*)⁶⁶, by eukaryotic species similar to fungi (*Oomycetes*)⁶⁷, and it is found in the plasma membrane of epidermal cells of the sea animal *Tunicates*⁶⁶.

Cellulose morphology is defined by the hierarchical organization of its fibrillar entities, which is schematically depicted in **Figure 1.2**. The intramolecular hydrogen bonds between adjacent cellulose molecules keep the overall molecular structure of the compound intact, and the additional van der Waals forces enable the organization of the cellulose chains into parallel stacking positions forming the elementary fibrils of width varying between 1.5 and 3.5 nm⁶⁶. These fibrils further aggregate forming larger microfibrils with a diameter between 5 and 50 nm, and a length of several microns⁶⁸. By a wide variety of chemical and mechanical treatments, it is possible to disintegrate cellulose pulp down into nanoscale particles presenting excellent mechanical stability, high specific surface area, and tuneable surface chemistry suitable for utilization in highly demanding applications^{66,68}. Cellulose nanomaterials

(CNMs) in the form of cellulose nanocrystals (CNC) and cellulose nanofibers (CNF)⁶⁸ have gained significant scientific interest in the field of materials science.

Unlike CNCs, which are obtained from cellulose sources by acid hydrolysis, the CNFs can be isolated by a variety of mechanical treatments including high-pressure homogenization, microfluidization, grinding, and electrospinning⁶⁸. CNCs are rigid, rod-shaped particles with dimensions between 3 – 70 nm in width and between 70 - 1000 nm in length, dependent on the source of extraction^{68–70}. CNFs consist of longer fibrils with lower crystallinity, with widths in the range between 5 – 500 nm⁷¹ and lengths of several micrometres⁶⁸.

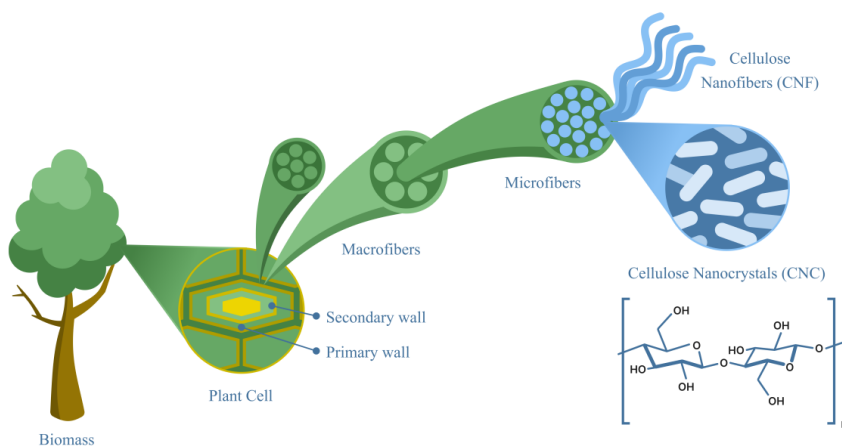


Figure 1.2. Schematic representation of the hierarchical structure of cellulose.

Due to their morphological structure and high aspect ratio, the CNFs are easy to process into functional nanomaterials including high gel-strength hydrogels and robust foams and films. Moreover, their surface chemistry allows for a variety of functionalization opportunities e.g. by TEMPO (2,2,6,6 – tetramethylpiperidine-1-oxyl) mediated oxidation using sodium hypochlorite and sodium bromide at ambient temperatures^{72,73}. During TEMPO-mediated oxidation, the primary hydroxyl groups on the surface of the CNFs are selectively oxidized to form carboxyl groups. This modification induces a negative surface charge on the fibers and increases the hydrophilic character of the CNFs, resulting in the formation of TEMPO-oxidized CNFs (TCNF)^{72,73}. TCNFs are characterized by their high aspect ratio and excellent mechanical properties⁷⁴. This alone makes them a promising material for a wide range of applications, however, the induction of negative charge on the surface of the fibers makes them particularly useful for water treatment applications, where they could be used for removal of positively charged contaminants from water^{75,76}.

The use of cellulose for water treatment applications is being continually explored. The functionalized cellulose-based nanomaterials in the form of coatings⁷⁷, membranes^{27,28}, beads^{75,78}, and foams^{79,80} have been reported as potential materials for oil and water separation applications^{79,80} as well as for the removal of metal ions^{27,75} and dyes^{27,78} from water.

1.3.4 Chitin

Chitin is the second most abundant biopolymer on Earth, found in the exoskeletons of crustaceans such as crabs and lobsters, as well as in the cell walls of fungi and the cuticles of insects⁸¹. It is composed of long linear chains of *N*-acetyl-2-amino-2-deoxy-D-glucose, which are linked together by β -(1 \rightarrow 4) glycosidic bonds, which means that the only difference between chitin and cellulose chemical structures is the chemical group attached to C2, which in case of cellulose is a hydroxyl group, while for chitin - an acetamide group⁸¹ (**Figure 1.3**). Just like cellulose, chitin is insoluble in water⁸². The main commercial source of chitin is crustaceans shell waste⁸³, however isolation of chitin is a complex process. Highly structured crystalline micro- and nanofibrils with strong intermolecular and intramolecular hydrogen bonding define the form of chitin macromolecules in crustaceans' shells. Shielding these micro- and nanofibrils in a protein and calcium carbonate matrix gives rise to chitin protein fibers that range in size from 50 to 300 nm^{84,85} (**Figure 1.3**). Their twisted or helicoidal stacking forms are known as the Bouligand structure⁸⁵ (**Figure 1.3**). The isolation of chitin nanostructures from these fibrils can be done using various approaches such as solvent hydrolysis⁸⁶, acid hydrolysis⁸⁷, mechanical processing⁸⁸, and TEMPO-mediated oxidation⁸⁹. The nanostructures include chitin nanocrystals (ChNC) with 6 – 60 nm in width and 100 – 800 nm in length and chitin nanofibers (ChNF) with 10 – 100 nm in width and lengths in the micrometre range⁸⁵. Apart from being biodegradable and biocompatible, nanochitin presents a wide range of desirable properties, including low density, high surface area, chemical reactivity as well as antimicrobial and antioxidant properties⁸⁵.

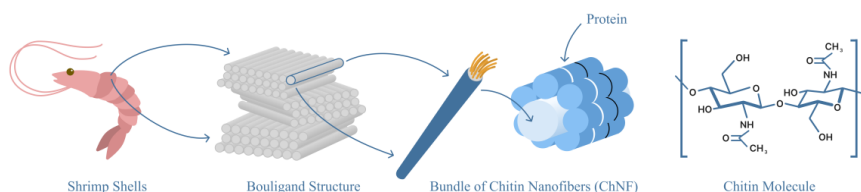


Figure 1.3. Schematic representation of the hierarchical structure of chitin.

Materials based on chitin and nanochitin are investigated for water treatment, as the exploration of biobased materials for this application advances. For instance, chitosan, which is a deacetylated form of chitin, is reported as suitable for the removal of i.a. metal ions^{90–94} and antibiotics⁹⁵ from water.

1.3.5 Green metal-organic frameworks (MOFs)

Metal-organic frameworks (MOFs) are a class of crystalline, porous materials composed of metal ions or clusters linked by organic ligands. Versatile properties of MOFs include high specific surface area, tuneable pore size and shape, and wide chemical functionality⁹⁶. The key advantage of MOFs is their tailored design and synthesis route, allowing them to be allocated within very specific and narrow applications including gas storage⁹⁷, separation⁹⁷, and catalysis⁹⁸. Within this work, a bioinspired microporous MOF, SU-101 is used⁹⁹. Chemically, SU-101 is a bismuth phenolate synthesized from non-hazardous materials including bismuth acetate and supplement-grade ellagic acid at ambient conditions⁹⁹. SU-101 has shown to be stable over a wide range of temperatures and pH⁹⁹, making it a great candidate for water treatment applications.

1.3.6 Recycled textiles

Disposed textiles pose a significant environmental challenge in today's world. With the rapid growth of the fashion industry and the increasing trend of fast fashion, the volume of textile waste being generated has reached alarming levels. It is estimated that in Europe and the US, between 65 – 85 % of textiles end up in landfills¹⁰⁰. That means that we lose tons of materials that could be suitable for recycling and repurposing. A popular fabric often used for the production of textiles worldwide is polycotton. Polycotton is a blend of polyester i.e. polyethylene terephthalate (PET) and cotton fibers¹⁰¹. The garments produced with the use of this material are more durable and strong, owing to the presence of synthetic fibers in the blend, while the presence of cotton fibers adds smoothness, softness, and breathability to the final garment¹⁰¹. Recycling polycotton is challenging and usually targets just one of the two components, by degrading¹⁰², dissolving¹⁰³, or depolymerizing¹⁰¹ the other. Another challenge is the fact that the fibers are often not possible to undergo re-spinning for the formation of new fibers¹⁰¹. This highlights the strong need of exploring new potential applications for these recycled materials. To the author's knowledge, there are currently no reports on using discarded garments for water treatment applications. However, pure and recycled PET^{104–106} as well as PET-based composite¹⁰⁷ have been shown to be an excellent match for processing via 3D printing. That opens up the novel possibility to use recycled and functionalized textiles for the creation of water purification filters using commercially available, desktop 3D printers.

1.4 Additive manufacturing (AM) – on-demand fabrication method

Additive manufacturing (AM), commonly referred to as three-dimensional (3D) printing, is a fabrication technique that relies on building a solid component in a layer-by-layer manner and with accordance to a 3D computer-aided design (CAD) model^{108,109}. The CAD model needs to be converted into standard triangle language (STL) file, and as such, it is optimized for 3D printing with the use of appropriate slicing computer software¹⁰⁹. 3D printing has been transforming the manufacturing industry since its invention in the 1980s, as it allows easy, speedy, and facile preparation of objects based on digital designs. Moreover, it enables the development of tailored parts with highly intricate designs, while consuming less energy, compared to conventionally used methods e.g. casting and injection moulding¹⁰⁹. Over the years, AM techniques have undergone significant advancements and found applications in diverse fields including prototyping, product development, aerospace, medicine, architecture, and many others¹⁰⁹. According to the American Society for Testing and Materials (ASTM) F2792-12 Additive Manufacturing standard¹¹⁰, the AM techniques can be classified into seven different categories (**Figure 1.4**). Within this thesis work, the AM technique of choice is Fused Deposition Modelling (FDM).

FDM relies on introducing a thermoplastic filament into a heated chamber, where it is melted into a viscous fluid. This fluid is further deposited onto the print bed in accordance with the CAD design (**Figure 1.5 a**). FDM offers many benefits compared to traditional manufacturing methods. Apart from its ability to create complex geometries and shapes, FDM is a cost-effective method that operates at a very high speed and generates lower material losses compared to traditional manufacturing techniques^{108,109}. Moreover, FDM allows the development of on-demand, high surface-finish quality prototypes, as it can operate using a wide range of printing materials, including high-performance thermoplastics, and relatively inexpensive desktop 3D printers¹¹¹. Additionally, the prototypes developed with the use of FDM require either none or minimal post-processing, which reduces the cost of tooling necessary to obtain high-quality end-use products¹⁰⁹. FDM can be regarded as a great manufacturing method for the preparation of water filtration and purification systems, as it enables the development of customized, multi-material parts of a variety of textures and finishes. That means that one desktop 3D printer can be used for the production of e.g., both, metal ion adsorbents and oil and water separators, dependent on the time-specific market requirement. Moreover, depending on the size of the printer, it is possible to print large-scale parts with very high accuracy and precision in terms of e.g. porosity architectures¹⁰⁹, which is of importance for the development of chemically functional sieving systems suitable for removal of suspended contaminants such as microplastics. Selected advantages of FDM technique are summarized in **Figure 1.5 b**.

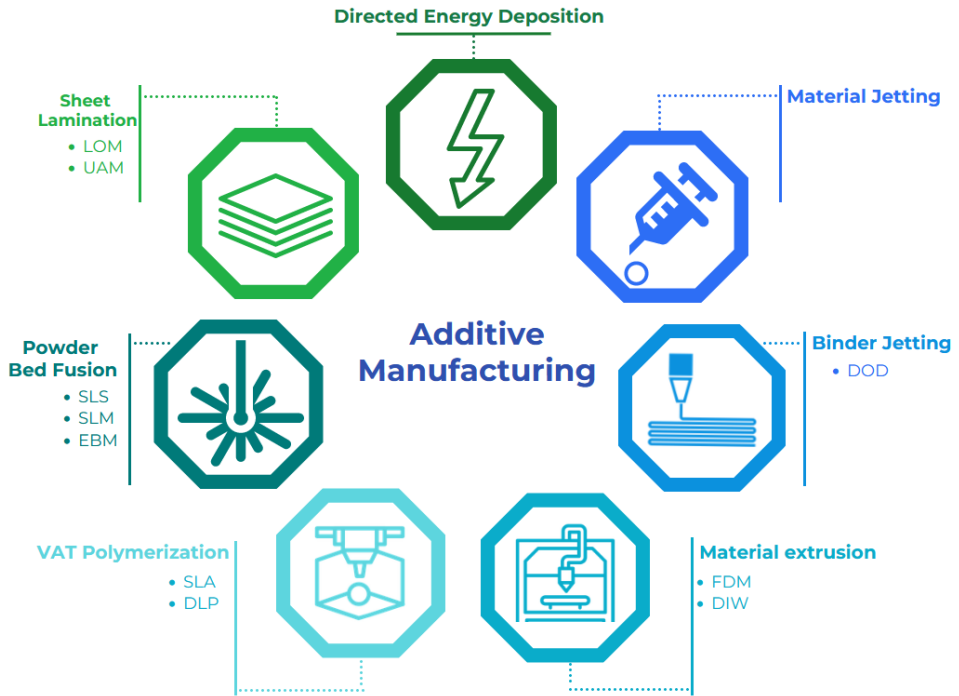


Figure 1.4. Classification of AM techniques according to the *ASTM F 2792-12 Additive Manufacturing* standard.

While AM techniques have revolutionized the manufacturing industry, several challenges remain. Among a few disadvantages of FDM, material limitations can be listed¹⁰⁹. The layer-by-layer manner of object fabrication relies strongly on the physical bonding and the chemical compatibility between the layers. That narrows down the thermoplastic materials suitable for use. Moreover, FDM presents lower resolution in comparison with other AM techniques, which can technically affect the accuracy of the final printed parts¹⁰⁹. Moreover, FDM-manufactured parts are prone to issues such as warping, curling and layer separation, which can critically decrease the quality of the final product. These issues, however, can often be solved by optimizing the print parameters during 3D printing. The FDM-produced parts sometimes present lower structural stability, leading to reduced strength and, when compared to parts produced by more conventional methods e.g. injection moulding¹⁰⁸. This can be explained by the fact that the FDM parts are limited in terms of their size and complexity due to the limitations of the FDM printing process, while the limited mechanical performance of the FDM-printed parts could be due to their anisotropic nature.

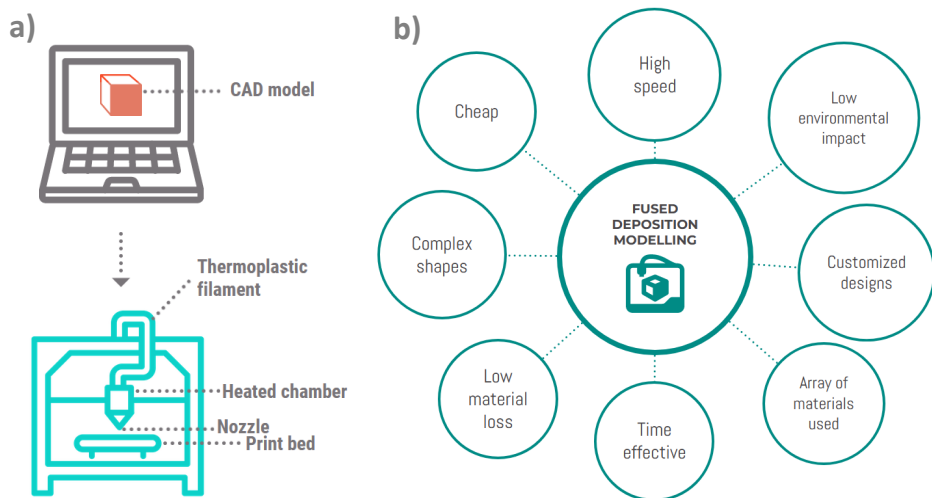


Figure 1.5. a) Schematic representation of the FDM procedure: from CAD model to 3D printing, b) selected advantages of FDM.

1.5 Preparation routes for the development of green and 3D printable composites

The most common processing methods used for the production of 3D printable composites reinforced with biobased particles include melt compounding e.g. melt mixing and extrusion¹¹², melt spinning¹¹³, compression moulding¹¹⁴, and solvent casting¹¹⁵. Among the biobased thermoplastic polymers used for the preparation of 3D printable composites, PLA, polyvinyl alcohol (PVA) and polycaprolactone (PCL) have gained the most scientific attention, as all of these materials are biobased, biodegradable, and easy to process during both, composite preparation, and 3D printing. The 3D printable PLA, PVA, and PCL - based composites reinforced with i.a. wood flour¹¹⁶, microcrystalline cellulose¹¹⁷, nanocellulose^{118,119}, hydroxyapatite^{120–122}, nanochitin¹²², and nanoclay¹²³ have been reported. However, the hydrophilic nature of various green reinforcing nanoparticles is one of the main obstacles in preparation of the biobased composite materials using hydrophobic polymeric matrices. To counteract this, hydrophilic nano-reinforcing species often undergo compatibilization and surface functionalization prior to composite processing¹⁰⁸.

The development of printable composites is often a very long and complicated process, involving many steps and a variety of chemicals. For instance, Wang et al.¹²⁴ reported the preparation route for the PLA-

based composite reinforced with a mixture of micro - and nanocellulose fibers intended for the production of 3D printing filament. Prior to heat processing, the cellulose fibers were treated with a silane coupling agent to improve their dispersion within the PLA, while at the same time, part of the PLA pellets were mixed with a plasticizer in the form of polyethylene glycol (PEG). The obtained materials were further dried, crushed into pellets, and twin-screw extruded. Even though the mechanical properties of the parts 3D printed with the developed filament were stable, they did not exceed the strength and stiffness values reported for pure PLA. Other studies also utilized direct mixing and extrusion to prepare composites with various fillers including ChNC¹¹⁹, microcrystalline cellulose¹¹⁷ and galactoglucomanan¹²⁵. Direct hot melt mixing and extrusion is another commonly used method for the preparation of biobased 3D printing filaments, using fillers such as wood flour¹¹⁶, blended cocoa shell waste¹²⁶, modified CNFs¹²⁷, cork¹²⁸, and lignin¹²⁹. Other scientific approaches focused on modifications and compatibilization of PLA with reinforcements. For instance, Petchwattana et al.¹³⁰ modified PLA with a core-shell rubber and added a silane coupling agent to improve adhesion between PLA and wood particles, while Guo et al.¹³¹ tested different toughening agents in wood-reinforced PLA composites and found that thermoplastic polyurethane significantly increased their strength.

Overall, the literature to date indicates that the combination of PLA and hydrophilic fillers in biocomposites has a high potential for the development of sustainable materials suitable for processing via 3D printing. However, there is still a lot of room for improvements, as optimization strategies for the dispersion of fillers to enhance their compatibility with various polymeric matrices including PLA are necessary to make the 3D printing of biobased composites scalable. Moreover, further improvement of composite development methods is needed to achieve consistent printability and mechanical performance of the 3D printed parts, so that they can be implemented in highly demanding applications. The current state of the literature on processing biopolymer-based and PLA materials by 3D printing for water treatment applications is discussed in detail in our recently published review¹³².

1.6 Accelerated ageing – the Arrhenius model

Polymers are often subjected to accelerated ageing procedures, which are aimed to assess the lifespan of the materials in their designated engineering applications. During ageing, a gradual deterioration of polymer properties occurs over time due to exposure to different environmental factors and/or chemical processes. Factors such as heat, light, oxygen, moisture, and mechanical stress can accelerate the ageing process^{133–136}. As polymers age, they may experience degradation, resulting in a loss of mechanical strength, stiffness, and flexibility¹³⁷. Additionally, chemical reactions such as oxidation, hydrolysis, and cross-linking¹³⁵ can alter the polymer's properties, leading to discoloration¹³⁴, brittleness, and reduced performance¹³³. Understanding the mechanisms and effects of polymer ageing is crucial for industries

that utilize polymers, as it helps in developing strategies to mitigate ageing and prolong the lifespan of polymer-based products¹³⁶.

The Arrhenius model is used for assessing the lifespan of polymers as it provides information on the combined effects of temperature and time. The model assumes that the degradation process follows an exponential relationship, where higher temperatures accelerate the reaction. Experimental measurements of the degradation rate at elevated temperatures are collected, and the logarithm of these rates is plotted against the reciprocal of the corresponding temperatures. A linear relationship is expected, and the slope of the line represents the activation energy. By extrapolating this line to lower temperatures, the degradation rate at the desired long-term operating conditions can be estimated. The Arrhenius model assumes that while the degradation mechanism does not change over time, the degradation rate is accelerated with an increase of exposure temperature^{138,139}.

1.7 Scope of the thesis

The research conducted in this thesis is motivated by the progressing climate change, resulting in water scarcity and pollution of global water reservoirs by hazardous substances. The primary objective of the experimental work was to develop green composites, based on either fully biobased materials or recycled waste materials, that can be processed using commercially available desktop 3D printers via FDM. The developed composites were intended to be used in the production of monolithic filters of various geometries and porosity architectures, suitable for implementation within the water treatment industry. Apart from being based on renewable materials including i.a. PLA, cellulose, and HAp or recycled textiles, the biocomposites were designed to be structurally stable and present excellent mechanical properties. This was done to ensure that the filters can withstand harsh environmental conditions, sustain high water flux, and effectively remove various types of contaminants based on their designated applications.

The initial stage of the experimental work involved the development of the composite preparation method that would ensure a homogenous dispersion of hydrophilic reinforcing species within the PLA matrix. To achieve this, a simple blending was employed, where the components were mixed at a slightly elevated temperature in the presence of a solvent. The blending process was followed by a thermally induced phase separation (TIPS) pelletization step and subsequent freeze-drying. This approach was implemented to develop composites of HAp/PLA, ChNF/PLA as well as TCNF/PLA composites (**Paper I** and **Paper II**). The obtained 3D printing filaments were used for the fabrication of water purification filters of various geometries (cubic, cylindrical and hourglass-shaped) and have shown to be suitable for removal of various metal ions (Cd^{2+} , Pb^{2+} , Cu^{2+}) as well as microplastics from water.

The surface functionalization capabilities of the developed filters were examined within the scope of **Paper III**. There, the TCNF/PLA filters were surface activated and functionalized with bioinspired MOF SU-101 in order to further expand the potential range of applications of the 3D printed filters. The functionalized filters have shown to be suitable for the selective removal of metal ions from mine effluent. Moreover, the 3D printed filters have demonstrated to withstand both activation, as well as recycling procedures, using harsh chemicals such as 10 M hydrochloric acid, proving the impeccable structural integrity of the 3D printed parts. Furthermore, the biodegradability and lifespan of the 3D printed filters was investigated in **Paper IV**. The filters were subjected to the accelerated ageing procedure in aqueous conditions and their mechanical properties were monitored over a nearly half-a-year period. The influence of the nanofillers on the hydrolytic degradation of the 3D printed filters was investigated, and the predicted service life for the TCNF/PLA and ChNF/PLA filters was estimated using the Arrhenius model.

Moreover, this thesis explores the possibility of using recycled materials for the development of 3D printing filaments suitable for the fabrication of i.a. water treatment systems. In **Paper V**, post-consumer polycotton-based textiles were TEMPO-oxidized and processed into 3D printing filaments. Apart from commodity applications, the parts 3D printed with the use thereof were shown to be able to remove dyes from contaminated water, hence implicating their potential for use within the water treatment industry.

2. Research methodology

2.1 Materials

The commercial 3D printing filaments used within the scope of this thesis included a transparent PLA filament (**Paper I**, **Paper II**, **Paper III** and **Paper IV**) ($\phi = 2.85$ mm, Ultimaker, Utrecht, Netherlands) and a transparent polyethylene terephthalate glycol (PETG) filament (**Paper V**) ($\phi = 2.85$ mm, Ultimaker, Utrecht, Netherlands). The raw materials used within this thesis work for the development of custom 3D printing filaments used in **Paper I**, **Paper II**, **Paper III** and **Paper IV** included transparent, extrusion grade polylactic acid (PLA) pellets (IngeoTM Biopolymer 4043D, Nature Works, provided by Add North 3D AB, Sweden) and 1,4-dioxane (anhydrous, 99.8%, Carlo Erba Reagents, Spain). The TEMPO (2,2,6,6-tetramethylpiperidine-1-oxyl radical)-mediated oxidized cellulose nanofibers (TCNF, 1.1 mmol/g of carboxyl groups) used in **Paper II**, **Paper III**, and **Paper IV** were provided by Swiss Federal Laboratories for Materials Science and Technology (EMPA, Switzerland). The dimensions of the nanofibers were determined by atomic force microscopy and were in the range of 3-5 nm in width and lengths in μm scale. Chitin nanofibers with fibrils diameter of 3 nm and lengths in nm - μm scale (ChNF, 2 wt. % in water suspension, with less than 5 wt. % of deacetylation degree) and a specific surface area of 200 m^2/g and polymerization degree of 300 used in **Paper II**, **Paper III**, and **Paper IV** were provided by BiNFi, Sugino Machine Limited, Japan. Post-consumer polycotton fabrics used in **Paper V** (50:50 cotton: polyethylene terephthalate (PET)) were provided by Wargön Innovation. Other materials used in **Paper V** included sodium hypochlorite (NaClO) (Merch), 2,2,6,6-tetramethyl-1-piperidinyloxy free radical (TEMPO, $\geq 98\%$, Alfa Aesar), sodium hydroxide (NaOH , P99.2%, Honeywell) and sodium bromide (NaBr , P99.5%, Sigma-Aldrich).

In **Paper I**, the chemicals used for the adsorption tests were lead nitrate ($\text{Pb}(\text{NO}_3)_2$, 98 %) and cadmium nitrate ($\text{Cd}(\text{NO}_3)_2$) (Sigma Aldrich, Germany). In **Paper II**, the reagent used for the adsorption study was copper (II) sulfate pentahydrate (99 %, Acros Organics, Belgium). The laundry water samples containing microplastics were donated by Mimby AB (Gothenburg, Sweden).

The raw materials used for further functionalization of the developed 3D prints in **Paper III** included SU-101 metal-organic framework prepared from ellagic acid (PureBulk Ltd., 90 % ellagic acid), and bismuth acetate (Alfa Aesar, 99 %). Hydrochloric acid (HCl , 37 %, VWR International, Germany) and nitric acid (65 %, VWR International, France) were used for the desorption of metal ions and vial preparation prior sample collection, respectively. The IVL Swedish Environmental Institute (Stockholm, Sweden) kindly donated the mine effluent. Methylene blue (MB) (Sigma-Aldrich) was used for the dye adsorption study in **Paper III** and **Paper V**.

2.2 Experimental – from the composite development to the filament extrusion

Hydroxyapatite (HAp) extraction In **Paper I**, HAp was extracted using a standardised laboratory protocol. Briefly, fish scales were collected from fresh water fish (*Catla catla*) and the extraneous matter and pigments were removed by scrubbing and repeated washing under running tap water. The cleaned scales were initially deproteinized by hydrolysis using enzyme alkalase (0.5 % of the protein content of scale (w/w) for 6 h at 55 °C). The decollagenised scales were separated by filtration and dried at 100 °C in a hot air oven for 6 h. Afterwards, the dried fish scales were sintered at 450 °C for 2 h followed by the second stage of sintering at 900 °C for different durations to yield a fine powder of HAp. The obtained HAp powder was stored in an airtight container at ambient temperature.

PLA - based biocomposite preparation The same experimental procedure was employed for the development of three different biocomposites i.e. HAp/PLA, TCNF/PLA, and ChNF/PLA (**Paper I** and **Paper II**). In both cases, a 10 % PLA suspension was prepared by dissolving transparent PLA pellets in 1,4 – dioxane by overnight magnetic stirring at room temperature (RT). The reinforcing particles in the form of HAp powder (**Paper I**) and either TCNF (1.5 wt. % in water suspension) or ChNF (2 wt. % in water suspension) gel (**Paper II**) were added to the PLA suspension and stirred for 2 h. The obtained biocomposite suspension (15 wt. % HAp/PLA as well as 5 wt. % TCNF/PLA and ChNF/PLA, respectively) was added dropwise into liquid nitrogen forming composite pellets in the process of Thermally Induced Phase Separation (TIPS). The pellets were further freeze-dried for 48 h.

Textile - based composite preparation In **Paper V**, eight different coloured polycotton fabrics were cut into small squares, mixed and fed into a 5 L beaker. The textile material was placed in water, reaching a cellulose concentration of 2 wt. %. It was further subjected to TEMPO-mediated oxidation, as described in the literature⁷⁴, using 0.1 mmol of TEMPO, 0.1 g of NaBr, and 10 mmol of NaClO per gram of cellulose. The pH was kept at 10 using a 2 M NaOH solution. After 4 h, the oxidized material was washed to remove the excess reagents in several filtration/washing cycles with deionized water until the conductivity was less than 10 µS/cm. The purified oxidized material was then diluted again to a cellulose concentration of 2 wt. % and was dispersed for 20 minutes using a High-Shear Dispermix (Ystral GmbH, Germany). The obtained dispersion was casted to films with a thickness of 1-2 cm. The films were overnight dried at 60 °C and then cut into small square pellets (1 × 1 cm) using a commercial paper guillotine.

Filament extrusion All of the PLA - based freeze-dried biocomposite pellets as well as the cut textile - based pellets were single-screw extruded at a feed temperature of 220 °C and screw speed of 40 rpm into 3D printing filaments with a diameter of 2.85 mm by AddNorth (Ölsremma, Sweden). During the extrusion process the biocomposite pellets were mixed with small quantities of pure PLA, while the textile – based pellets were mixed with small quantities of PETG pellets, to make the extrusion process smoother.

2.3 3D printing – designs and parameters

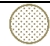










Within the scope of this thesis, there were two commercial desktop 3D printers used i.e. Ultimaker S5 and Ultimaker 2+ Connect (Ultimaker BV, The Netherlands). All of the developed and tested models (presented in **Table 1**) were based on commercially available computer-aided design (CAD) models. The dimensions of the models as well as their pore architectures were adjusted with the use of CURA slicing software prior generating the G-code file necessary for being processed by the printer.

In **Paper I**, there were two different 3D printing filaments used: HAp/PLA filament as well as the reference PLA filament (custom extruded from the same batch of PLA pellets, which were used for the preparation of the biocomposite filament). The general printing parameters used were: nozzle diameter of 400 µm, layer thickness of 150 µm, and print bed temperature of 90 °C. The nozzle temperature was set to 210 °C and 230 °C for the reference, and biocomposite filament, respectively. The print speed was set to 40 mm/s and 50 mm/s for the reference and biocomposite filament, respectively.

Overall, three different structures were printed and these included discs ($r = 6$ mm and thickness of 3 mm) and two cubic filters ($20 \times 20 \times 20$ mm) with varying porosity architectures. The printing parameters for the discs were: Infill density: 75%, Infill line distance: 0.5 mm, Printing speed: 30 mm/s. The printing parameters for the gradient porosity cube were: Infill density: 40%, Infill line distance: 0.8 mm, Gradual infill steps: 2, Gradual infill height: 7 mm, Print speed: 45 mm/s. The printing parameters used for the uniformly porous model were: Infill density: 40%, Infill line distance: 0.8 mm, Print speed: 45 mm/s.

In **Paper II**, four different models were 3D printed and these were based on cylindrical and hourglass-shaped CAD models. The general printing parameters used for both the biocomposite and reference commercial PLA filaments were: nozzle diameter 400 µm, print bed temperature 60 °C, printing speed 35-55 mm/s, layer thickness 150 µm, shell thickness 500 µm. The nozzle temperature was set to 200 °C and 220 °C for the PLA, and biocomposite systems, respectively.

Table 1. Overview of main model designs developed within the scope of this thesis.

Proj.	Model	Dimensions (mm)	Porosity structure	Pore size (mm)	Material	Application
I		6 × 3	Uniform	0.5	HAp/PLA and PLA	Adsorption of Cd ²⁺ and Pb ²⁺ ions
		20 × 20 × 20	Uniform	0.8		
		10 × 10 × 10	Three-level gradient	0.8		
				1.6		
				3.2		
II		40 × 40 × 40	Uniform	1.5	TCNF/PLA, ChNF/PLA and PLA	Adsorption of Cu ²⁺ ions Microplastics separation from laundry effluent
			Three-level gradient	2.0		
				4.0		
				8.0		
		20 × 20 × 20	Uniform	1.5		
		10 × 10 × 10				
			3.0			
	III		15 × 15 × 5	Uniform		
IV			60 × 13 × 1.5	Non-porous	N/A	TCNF/PLA, ChNF/PLA and PLA
	25.4 × 12.7 × 12.7*	Uniform	1.5			
V		20 × 20 × 20	Uniform	1	Polycotton-based composite and PETG	MB removal
				2		
				3		

*Standardized dimensions of compression models. The compression models of these dimensions, but varying pore architectures, corresponding to the filter's specific porosities were tested in **Paper II-V**.

Four different models were printed and tested for each composite system and reference PLA. These included (i) uniform porosity and (ii) three-level gradient porosity cylindrical filters, as well as the (iii) uniform porosity and (iv) two-level gradient porosity hourglass-shaped filters, moreover two different compressive designs were printed out (with corresponding uniform and two-level gradient porosity structure and standardized dimensions of 25.4 × 12.7 × 12.7 mm). The printing dimensions of the samples varied depending on the experiment of choice (i.e. 40 × 40 × 40 mm, 20 × 20 × 20 mm, and 10 × 10 × 10 mm), however the porous structure (size, geometry) and proportions were kept consistent. The printing parameters for cylindrical filters were: infill density: 10%, infill line distance: 1.5 mm,

infill pattern: grid, wall thickness: 0.5 mm, printing speed: 45 mm/s. The printing parameters for hourglass-shaped filters were: infill density: 10%, infill line distance: 1.5 mm, infill pattern: lines, wall thickness: 0.2 mm, printing speed: 55 mm/s. The printing parameters for the uniform compression models were: infill density: 10%, infill line distance: 1.0 mm, infill pattern: grid, wall thickness: 0.5 mm, printing speed: 45 mm/s. The printing parameters for the two-level gradient compression models were: infill density: 10%, infill line distance: 1.5 mm, infill pattern: grid, wall thickness: 0.5 mm, gradual infill steps: 1, step height: 12.7 mm, printing speed: 45 mm/s.

In **Paper III**, there were two different models printed out and these included: (i) cuboid models ($15 \times 15 \times 5$ mm), which were used for the optimization of the anchoring procedure as well as for the batch adsorption studies, and (ii) cuboid models (in standardized dimensions of $25.4 \times 12.7 \times 12.7$ mm), which were used for the compression tests. The printing parameters used for all the models i.e. TCNF/PLA biocomposite filaments as well as the reference, commercial PLA filaments were: nozzle diameter 400 μ m, print bed temperature 60 $^{\circ}$ C, printing speed 45 mm/s, layer thickness 150 μ m, shell thickness 500 μ m, infill density: 10%, infill line distance: 1.5 mm, infill pattern: grid, wall thickness: 0.5 mm, printing speed: 45 mm/s. The nozzle temperature was set to 200 $^{\circ}$ C and 215 $^{\circ}$ C for the PLA, and TCNF/PLA filaments, respectively.

In **Paper IV**, there were two different models printed out, i.e. (i) cuboid models in standardized size ($25.4 \times 12.7 \times 12.7$ mm) used for compression testing and (ii) a flat rectangular model ($60 \times 13 \times 1.5$ mm) used for dynamic-mechanical thermal analysis (DMTA) experiments. The printing parameters used for all of the used filaments were: nozzle diameter 400 μ m, print bed temperature 60 $^{\circ}$ C, printing speed 45 mm/s, layer thickness 150 μ m, shell thickness 500 μ m, wall thickness 0.5 mm, printing speed: 45 mm/s. The nozzle temperature was set to 200 $^{\circ}$ C and 215 $^{\circ}$ C for the PLA and biocomposite filaments, respectively.

In **Paper V**, there were several different models printed out. These included: (i) cuboid models in standardized size ($25.4 \times 12.7 \times 12.7$ mm) used for compression testing, and (ii) cubic filter models for adsorption study ($20 \times 20 \times 20$ mm) with varying pore structures, i.e. 1 mm, 2 mm, and 3 mm. The printing parameters used for both, the custom made as well as commercial, reference PETG filaments were: nozzle diameter 600 μ m, print bed temperature 90 $^{\circ}$ C, printing speed 25 mm/s, layer thickness 150 μ m, shell thickness 500 μ m, infill density: between 20 % and 95 % (dependent on the model), infill distance: between 0.1 – 3 mm (dependent on the model). The printing temperature was set to 250 $^{\circ}$ C for both filaments used.

2.4 MOF functionalization

In **Paper III**, 3D printed cuboid prototypes ($15 \times 15 \times 5$ mm) were surface functionalized with SU-101 MOF. The anchoring procedure included activation of the PLA matrix with either a 5 h acid bath (10 M HCl) or UV-ozone treatment for 10 min (UV/Ozone ProCleaner™, Bioforce Nanosciences, USA). The activated samples were then immersed in 1% SU-101 suspension and stirred for 12 h at 45 °C. Then, the samples were rinsed with deionized water to remove excess of unattached MOF, followed by oven drying at 70 °C for 1 h, and subsequent air drying for 24 h.

2.5 Accelerated ageing

The ageing procedure reported in **Paper IV**, aimed to simulate the degradation processes of reference PLA as well as reinforced TCNF/PLA and ChNF/PLA 3D printed filters to assess the duration of their service life. The ageing procedure was conducted by immersing 3D printed models in 5 L of deionized water of varying temperatures i.e. RT (18-20 °C), 30 °C, 40 °C, and 50 °C under constant stirring of 250 rpm for a varying period as presented in **Table 2**. There was a total of 12 separate ageing beakers prepared (4 for each material and each temperature point). At each time point, five and two models of specific dimensions suitable for analysis by compression testing and DMTA, respectively, were removed from each beaker and further analysed.

Table 2. Time points of the ageing study

Batch	Ageing period
A	Start
B	3 weeks (504 h)
C	7 weeks (1176 h)
D	15 weeks (2520 h)
E	19 weeks (3192 h)

Taking Young's modulus values as the end-point-criterion, the thermal endurance profile of all the samples was calculated and the lifespan was estimated using the Arrhenius model. With the use of Arrhenius equation, the performance of polymers during short-term tests conducted at elevated temperatures could be mathematically translated into the long-term performance at ambient temperature. Combining this with the kinetic equation, which describes the change of a given property in time, yields a rate that can be used for the estimation of service life. The Arrhenius relationship is:

$$K = Ae^{-E_a/RT} \quad (1)$$

Thus,

$$\ln K(T) = \frac{-E_a}{RT} + C \quad (2)$$

Where $K(T)$ is the rate constant, E_a is the activation energy, R is the gas constant, T is the absolute temperature and C is a constant¹³⁸. The Arrhenius model is accurate when a straight line is obtained by plotting the logarithm of the degradation rate against the reciprocal of test temperatures¹³⁹.

2.6 Characterization methods

Scanning Electron Microscopy (SEM) The morphology of the biocomposite pellets, 3D printing filaments as well as the pore structure of the 3D printed filters, was investigated with the use of a JEOL JSM-7000F Analytical Scanning Electron Microscope (JEOL Ltd, Japan) (**Paper I** and **Paper II**) and a Hitachi TM3000, Tabletop Microscope (Hitachi Ltd, Japan) (**Paper I** and **Paper III**). The samples were analysed at an accelerating voltage between 2 kV and 15 kV in both secondary electron and back-scattered electron modes. All the samples were prepared for the microscope examination by sputtering with a thin layer of gold (for 60 s, at 10 mA and from a 30 mm distance). The pore sizes of 3D printed models were measured based on each porosity level cross-section from the obtained SEM image using *ImageJ* software¹⁴⁰.

Thermogravimetric Analysis (TGA) The thermal decomposition of the materials in the form of biocomposite pellets, custom extruded biocomposite filaments, and reference commercial filaments, as well as 3D printed parts was analysed with the use of an STA 449 F1 Jupiter (Netzsch Instruments, Germany) (**Paper I**) and Discovery TGA (TA Instruments Inc., United States) (**Paper II, III, IV and V**). The samples were weighted to fractions of between 10-25 mg, and placed in either high-temperature platinum holders (**Paper II, III, IV and V**) or ceramic cups (**Paper I**). The samples were heated from 30 °C up to 1350 °C at a heating rate of 10 °C/min under air flow of 40 mL/min (**Paper I**); from 30 °C up to 550 °C at a heating rate of 10 °C/min under nitrogen flow of 20 mL/min (**Paper II, Paper III**), from 30 °C up to 500 °C at a heating rate of 20 °C/min under airflow of 20 mL/min (**Paper IV**) and from 30 °C up to 700 °C at a heating rate of 15 °C/min under airflow of 20 mL/min (**Paper V**).

X-Ray Diffraction (XRD) The crystallinity of the materials was assessed by XRD. The samples were tested in the form of pellets (**Paper I**), casted films (**Paper II**), as well as in the form of powder (SU-101), and 3D printed pieces (**Paper III**). The instrument used was a PANalytical X'Pert PRO MRD

City (Malvern Instruments, UK) (Cu $K\alpha_{1,2}$, $\lambda_1 = 1.5406 \text{ \AA}$, $\lambda_2 = 1.5444 \text{ \AA}$) using a Bragg–Brentano geometry.

Fourier-transform Infrared Spectroscopy (FT-IR) The developed biocomposite pellets, filaments, and filters (**Paper I**, **Paper II**, **Paper III**, **Paper V**) were examined using IR (610 IR FT-IR spectrometer, Varian Inc., CA, USA) equipped with a Specac Golden Gate single reflection attenuated total reflection (ATR) accessory with a diamond ATR element (Specac, UK). Sixteen scans between 4000 cm^{-1} and 400 cm^{-1} were averaged for each spectrum at intervals of 1 cm^{-1} .

X-ray micro-computed tomography (μ -CT) The pore structure and the dispersion of the HAp filler in the PLA matrix in the uniform and gradient filters (**Paper I**) were evaluated with the use of a 3D X-ray microscope (Zeiss Xradia Versa XRM520). The tomographic data acquisition involved 1601 projections of 1024×1024 pixels, acquired over 360° sample rotation with the X-ray source set to 60 kV and 5 W. Two data sets were acquired with different sample-to-detector distances and reconstructed, with the Zeiss Reconstructor software, to yield 3D image volumes with cubic voxels of widths $24 \text{ }\mu\text{m}$ and $8 \text{ }\mu\text{m}$. The acquisition used 1 s and 1.7 s exposure time per image, respectively. The $24 \text{ }\mu\text{m}$ images covered the full sample diameter and the $8 \text{ }\mu\text{m}$ images covered an internal cylindrical field of view of about 8 mm diameter.

Compression testing Compressive tests were performed according to the Standard Test Method D695-15 on cuboid specimens ($12.7 \times 12.7 \times 25.4 \text{ mm}$) (**Paper II**, **Paper III**, **Paper IV**, **Paper V**). Five specimens were tested for each type of material and porosity structure. Samples were conditioned prior to the analysis for 48 h in a conditioning chamber at 23°C and 51 % relative humidity. A 10 kN load cell and a compression rate of 1 mm/min , until 60 % deformation was reached, were applied. Tests were performed by applying the force perpendicular to the printing direction on an Instron 5960 dual-column universal test frame (Instron Corporation, USA) in a controlled environment (23°C and 51 % relative humidity). The apparent compressive elastic modulus was calculated from the slope of the linear elastic section of the stress-strain curves, without considering the plateau and the densification regime. The energy dissipation, i.e. toughness of the samples, was calculated considering the area under the stress-strain curve.

Inductively Coupled Plasma Mass Spectrometry (ICP-MS) The adsorption properties of MOF@Cell and MOF@PLA filters were analyzed by ICP-MS (**Paper III**). The specimens were conserved with HNO_3 to a concentration of 1 % and analyzed by ICP-MS according to a method based on SS-EN ISO 17294-2 2016 and SS-EN 14902:2005. The analysis was performed in KED mode with

collisional gas on ICP-MS (ICAP-Q, Thermo Scientific) with an internal standard of germanium, iridium, rhodium, and indium in order to correct matrix effects in the analysis.

Surface zeta potential The surface charge of the 3D printed PLA, TCNF/PLA and ChNF/PLA parts (**Paper II**) as well as MOF@Cell and MOF@PLA filters (**Paper III**) was investigated by recording the ζ -potential in dependence of the pH value with a SurPASS electrokinetic analyzer (Anton Paar, Graz, Austria). The specimens were mounted into an adjustable gap cell with double-sided tape at a gap width of 130 μm . A KCl solution (1 mmol L⁻¹) was used as an electrolyte and the pH value was controlled by titrating HCl and KOH (0.05 mol L⁻¹). The ζ -potential was calculated from the recorded streaming current.

X-ray photoelectron spectroscopy (XPS) XPS analysis for the HAp/PLA filters after adsorption (**Paper I**), and for the PLA and TCNF/PLA filters before and after functionalization by acid and ozone treatment (**Paper III**) was conducted using Thermo Fischer (K-alpha, monochromated, Al K α radiation, 1486.6 eV) (**Paper I**) and Axis Ultra DLD electron spectrometer (Kratos Analytical Ltd, UK) (K-alpha, monochromated, Al K α radiation) (**Paper III**) with a pass energy of 160 eV, an analysis area of 300 μm x 700 μm , an energy step size of 1 eV for the survey spectrum (5 scans). The high-resolution spectra (step size 0.1 eV) of the single elements were acquired with 3-10 scans at pass energies of 20 eV.

Size exclusion chromatography (SEC) In **Paper III**, the analysis of the molecular weight (Mw) and the molecular weight distribution (MWD) of the reference as well as acid- and ozone-activated samples was performed with SEC (Malvern Instruments, Malvern, UK). The separation was carried out on a double, 5 μm PLgel, MIXED-D column. Chloroform was used as the eluent. The flow rate was 0.5 mL/min and the experiment was carried out at 35 °C. In **Paper IV**, the analysis of the molecular weight (Mw) and the molecular weight distribution of the reference PLA and TCNF/PLA samples, as well as of the selected samples aged at 50 °C was performed with Viscotek TDA302 and GPCmax (Malvern Instruments, Malvern, UK). The samples in the form of crushed 3D printed pellets were prepared by dissolution in 0.05 M potassium trifluoroacetate/ hexafluoroisopropanol (KTFA/HFIP) at a concentration of approximately 10 mg/mL, under gentle rocking at room temperature. The samples were further filtered through a 0.22 μm Polytetrafluoroethylene (PTFE) syringe filter before injection. Separation was performed with 0.05 M KTFA in HFIP as the eluent at 30 °C and a flow rate of 0.7 mL/min. Polymethylmethacrylate (PMMA) standards were used for calibration. A Refractive Index (RI) detector, Right Angle and Low Angle Light Scattering (RALS/LALS) detector, and Four-Capillary Differential Viscometer were used for polymer detection.

Transmission Electron Microscopy (TEM) The morphology of the HAp powder (**Paper I**) and TCNF/PLA filters (**Paper II**) was assessed using a JEM-2100F from JEOL operated at 200 kV using a Gatan Ultrascan camera with an exposure time of 1 s. The TCNF solution (0.001%) was drop-casted onto a glow-discharged carbon-coated copper grid (EMS CF150-Cu-UL). The characterisation of the final 3D printed TCNF/PLA filter, an internal part of the filter was first sectioned into 100 nm thickness using a Leica Ultracut UCT with a 45 ° diamond knife from Diatome and later transferred the same type of grid.

Dynamic Mechanical Thermal Analysis (DMTA) Viscoelastic measurements of aged PLA, TCNF/PLA and ChNF/PLA (**Paper IV**) samples were conducted on Dynamic Mechanical Analyzer DMA 850 (TA instruments, United States). The samples ($60 \times 13 \times 1.5$ mm) were tested in an oscillation temperature ramp mode with preload of 0.1 N using a 35 mm dual cantilever clamp. Two samples per each material and temperature point were tested. The experimental parameters were: a constant frequency of oscillation of 1 Hz and a prescribed amplitude of 20 μ m. The temperature was ramped from 25 °C to 150 °C at a rate of 3 °C/min. The values of loss tangent ($\tan \delta$), storage modulus (E'), and loss modulus (E'') versus temperature and frequency were obtained. The glass transition temperature values (T_g) for all the samples were obtained from E' onset point.

Conductometric Titration In **Paper V**, the charge density of the TEMPO - oxidized polycotton textiles was estimated by four conductometric titrations. Polycotton suspensions with a concentration of cellulose at 0.25 wt. % were prepared for the titrations. Before the titration, a few drops of 5 M HCl were added to the polycotton suspension to reach a pH of 2.5 and ensure the protonation of the available carboxyl groups. The suspensions were titrated with 0.1 M NaOH (Titripur®) as titrant while the conductivity was recorded 30 seconds after the addition of 0.1-0.2 ml of the titrant until reaching pH>10. The charge density was calculated into mmol of COO⁻/kg after performing linear regressions in the three distinct regions corresponding to the neutralization of the free hydroxyl groups, the neutralization of the carboxyl groups, and the excess NaOH.

2.7 Functionality of the 3D printed filters

Batch adsorption tests

The adsorption experiments were performed by immersing the 3D printed parts in the form of circular discs (**Paper I**), uniformly porous hourglass-shaped filters (**Paper II**), and cubic filters (**Paper III** and **Paper V**) in model contaminants solutions.

In **Paper I**, the HAp/PLA as well as reference PLA samples were immersed in $\text{Pb}(\text{NO}_3)_2$ and $\text{Cd}(\text{NO}_3)_2$ solutions of varying concentrations (5 mg, 10 mg, 50 mg, and 100 mg) and stirred at 500 rpm and at room temperature (18 – 20 °C) for 12 h. The concentration of Cd^{2+} and Pb^{2+} ions in the supernatant was determined using Inductively Coupled Plasma Atomic Emission Spectroscopy (ICP-OES). The adsorption capacity (q_e) (mg/g), and adsorption efficiency (%) were calculated as follows:

$$\text{Adsorption capacity} = \frac{C_0 - C_e}{m} \times V \quad (3)$$

$$\text{Adsorption efficiency} = \frac{C_0 - C_e}{C_0} \times 100 \quad (4)$$

Where C_0 and C_e (mg/L) are the initial and equilibrium concentration in aqueous solution, respectively, m (g) is the mass of the adsorbent and V is the volume (L) of the solution containing solute.

Further selectivity of adsorption towards metal ions was measured by immersing the 3D printed discs in 300 mL solution of ($\text{Co}(\text{NO}_3)_2$, $\text{Cu}(\text{NO}_3)_2$, $\text{Pb}(\text{NO}_3)_2$, $\text{Cd}(\text{NO}_3)_2$, $\text{Zn}(\text{NO}_3)_2$, AlCl_3 , and FeCl_3 (50 ppm for each element). The adsorbent was soaked for 12 h before using SEM with Energy Dispersive X-Ray Analysis (SEM-EDX) analysis to determine the remaining metal ions content. Selectivity was calculated using the following equation:

$$\text{Selectivity (\%)} = \frac{[\text{Metal Concentration, wt.\%}]}{[\text{Total Metal Concentration, wt.\%}]} \times 100 \quad (5)$$

In **Paper II**, the TCNF/PLA, ChNF/PLA, and reference PLA hourglass-shaped filters were immersed in 80 mL of either 1 mM or 10 mM CuSO_4 solution. The experiments were carried out at RT (18 – 20 °C), pH range between 6.0 and 7.5 and under magnetic stirring (450 rpm). The filtrate samples with volumes of approximately 15 mL were collected after 0.5 h, 1 h, 3 h, 6 h, and 8 h. The metal concentration in the collected aliquots was assessed with the Ultraviolet-visible (UV-Vis) spectrophotometer (Genesys™, 40/50, ThermoFisher) using the colorimetric method (λ_{max} =810 nm). The adsorbed copper ions were desorbed from the filters with a hydrochloric acid treatment (immersion of the filters in 80 mL of 10 M HCl), followed by immersion in deionized water at room temperature and overnight air-drying. Adsorption-desorption experiments were repeated three times on the set of three filters for each material to assess the recyclability potential of the filters. The adsorption capacity (q_e , mg/g) and adsorption efficiency (%) were calculated with accordance to Equations 3 and 4, respectively.

In **Paper III**, the adsorption tests were conducted using mine wastewater effluent collected at Håkansboda mine in Sweden. The metal ion adsorption capabilities of MOF@Cell, MOF@PLA as well as control PLA filters were assessed by immersing the filters in 150 mL of wastewater effluent. The adsorption tests were conducted under continuous magnetic stirring (450 rpm) and RT (18 – 20 °C). The pH of the effluent water was measured to be in the range between 7.4 – 7.8 and it was not controlled or modified within the duration of the adsorption experiment to assess the performance of filters under realistic conditions. The filtrate samples with a volume of approximately 25 mL were collected after 1 h and 24 h into 2 vol. % of nitric acid (HNO₃, 65%, VWR International, France) washed and overnight-soaked vials. The metal concentration in the collected aliquots was assessed by the ICP-MS measurements.

In **Paper V**, the adsorption tests were performed by immersing the 3D printed filters in MB solutions of varying concentrations, ranging from 0.001 g/L to 1.4 g/L. The adsorption experiments were conducted under continuous magnetic stirring at RT overnight. The concentration of free MB was determined before and after adsorption from the absorbance at 664 nm. The amount of adsorbed MB (μmol/g) was plotted as a function of free MB concentration (mM). The Langmuir model was applied to describe the data, and it can be expressed from the following equation:

$$q_e = \frac{q_{max}K_L C_e}{1 + (C_e * K_L)} \quad (6)$$

where q_e is the amount of adsorbed molecule normalized by the total amount of adsorbent, usually expressed in mg g⁻¹ or mmol g⁻¹, q_{max} is the maximum adsorption capacity, C_e is the concentration of the adsorbate at the equilibrium¹⁴¹. K_L and q_{max} can be determined from non-linear square fitting a double-reciprocal plot.

Desorption and recyclability tests

There were several different desorption procedures conducted within the experimental scope of this thesis. In **Paper II**, the Cu²⁺ ions adsorbed onto filters were desorbed by immersion in 1 M HCl for 5 h followed by an overnight bath in deionized water. In **Paper III**, the metal ions adsorbed onto the filter's surface were desorbed by immersing the filters in 20 % NH₄Cl solution at room temperature (18 – 20 °C) and stirred at 450 rpm for 3 h. After that, the filters were further treated with 10 M HCl for 15 min to both, remove any remaining metal ions and re-activate the filter's surface before the following MOF re-anchoring procedure. To further assess the recyclability potential of the filters, they were tested for the removal of MB from water. The same filters, which were used for metal ions adsorption study were tested for dye removal (after triple ion desorption and MOF re-anchoring procedure). The filters were

immersed in 80 mL of MB solution (conc. 10 mg/L) at RT (18 – 20 °C) and stirred at 400 rpm. Aliquots of 20 mL were removed for analysis after 0.25 h, 0.5 h, 1 h and 24 h. The removal efficiency was assessed with the UV-Vis spectrophotometer (Genesys™, 40/50, ThermoFisher) using the colorimetric method ($\lambda^{\max} = 664$ nm). In **Paper V**, desorption experiments were performed by immersing the filters in subsequent solutions of MB of decreasing concentrations and water, and the concentration of MB was determined using the colorimetric method ($\lambda^{\max} = 664$ nm).

Microplastics removal

In **Paper II**, the developed TCNF/PLA and ChNF/PLA filters were tested for the separation of microplastics from laundry effluent. The initial liquid sample contained bigger pieces of debris, therefore before proceeding with the separation experiments, the sample was sieved through a 1 mm mesh to ensure that all of the dispersed particles met the specification of microplastics stated in ISO/TR 21960:2020, i.e. that their diameter was equal or below 1 mm. 100 mL of sieved liquid was then poured into a previously weighed, clean, and oven-dried beaker, and placed in a furnace at 100 °C to evaporate the water. The separation experiments were conducted on uniformly porous TCNF/PLA, ChNF/PLA and reference PLA filters of both geometries i.e. on the hourglass-shaped and cylindrical filters. The separation efficiency was measured by gravimetric method. 50 mL of microplastics solution was pushed through each filter with the use of a syringe, followed by a thorough rinse with deionized water for 1 min. The filtrate solution was collected in an oven-dried pre-weighed beaker and placed in the furnace at 100 °C to evaporate water. The remaining debris was weighted and related to the weight of the starting microplastics content. To ensure experimental reproducibility, five experimental runs for each design and material were carried out.

Permeance and permeability measurements

The water permeance through the 3D printed cubic (**Paper I**) as well as cylindrical and hourglass-shaped (**Paper II**) filters was tested using two different in-house-constructed setups in the dead-end filtration mode. The experiments were carried out at RT (18 – 20 °C) and a water temperature of 20 °C at a constant flow-rate of 1500 cm³/min. The permeance of the samples was assessed by measuring the exact time (t) needed for 2 L of water (V) to pass through the filter with a cross-sectional area (A) (Eq. (7)). The pressure difference between filter's inlet and outlet was measured. The experiments were repeated five times for each filter design and material. The permeance was determined using the following equation:

$$Permeance = \frac{V}{t \times A \times p} \quad (7)$$

Additionally, for **Paper I**, the permeability (k) values were calculated from Darcy's equation (Eq. (8)), where μ is water viscosity, A is the filter's cross-sectional area, q is the measured fluid flow rate, l is filter's height and Δp is the difference between measured inlet and outlet pressure.

$$k = -\frac{\mu q}{A \frac{\Delta p}{l}} \quad (8)$$

3.Development of green composites for 3D printing

3.1 PLA - based composites

The incorporation of reinforcing, biobased nanoparticles into polymeric matrices presents a promising avenue for enhancing i.e. the mechanical and functional properties of the material, while simultaneously promoting sustainability. However, the dispersion of species such as HAp, CNFs or ChNFs poses significant challenges due to inherent incompatibility between these hydrophilic nanoparticles and hydrophobic polymers such as PLA. In order to overcome these challenges, various strategies were explored and reported in the literature. Taking nanocellulose as the example, the most commonly reported approach is the surface functionalization thereof, which involves chemical modification of the surface of nanofibers (NFs) to enhance their compatibility with hydrophobic polymers. This is often carried out via chemical reactions such as acylation or esterification⁶⁸. These treatments promote better dispersion of the NFs in the hydrophobic polymer matrix by introduction of hydrophobic groups onto the NFs surface. Other popular approaches include using compatibilization agents such as silane coupling¹²⁴ agents or block copolymers¹⁴², which lead to the creation of strong and stabilized interface between the NFs and the polymer matrix. Additionally, various processing techniques have been explored for their potential to improve the dispersion of hydrophilic reinforcements in the polymers; these include e.g. melt blending, extrusion, and high shear mixing⁶⁸. Optimization of processing parameters, such as temperature, shear rate, processing time etc. can play a crucial role in breaking up the NFs agglomerates facilitating more homogenous distribution thereof within the polymer matrix.

For the development of the PLA-based composites studied within **Paper I – Paper IV**, an extra processing step between the physical blending of components in the presence of solvent and the heat extrusion was implemented. The step was the pelletization step, namely Thermally Induced Phase Separation (TIPS), which is commonly used for fabrication of porous materials with controlled porosity and morphology¹⁴³. However, within the scope of this thesis, it was used to obtain a homogenous dispersion of the filler in the PLA matrix at the very early stages of the composite development i.e. at biocomposite pelletization step. The TIPS technique takes advantage of the thermodynamic behaviour of polymer solutions or blends to induce phase separation upon temperature changes¹⁴³. In **Paper I**¹⁴⁴ and **Paper II**¹⁴⁵, a homogeneous polymer suspension was prepared by dissolving commercial PLA pellets in a 1,4-dioxane solvent. This was followed by the addition of the nanospecies, i.e. HAp powder (**Paper I**) and either TCNF or ChNF gels (**Paper II**) resulting in either 15 wt. % or 5 wt. % composite suspension, as reported in **Paper I** and **Paper II**, respectively. Upon cooling the composite suspension

during TIPS, the system underwent a phase separation process, which resulted in the formation of polymer-rich and solvent-rich phases. Subsequent solvent removal by freeze-drying led to the formation of lightweight porous pellets, which could have been further processed into 3D printing filaments using a conventional method of single-screw extrusion. The overview of the experimental procedure is presented in **Figure 3.1**. While the obtained HAp/PLA filament was quite rough to the touch and presented a few issues during printing such as nozzle clogging and uneven flow (which were solved by during-print optimization of the printing parameters), the TCNF/PLA and ChNF/PLA filters matched the commercial PLA filament in terms of their texture and ease of processing, and differed only by colour and odour.

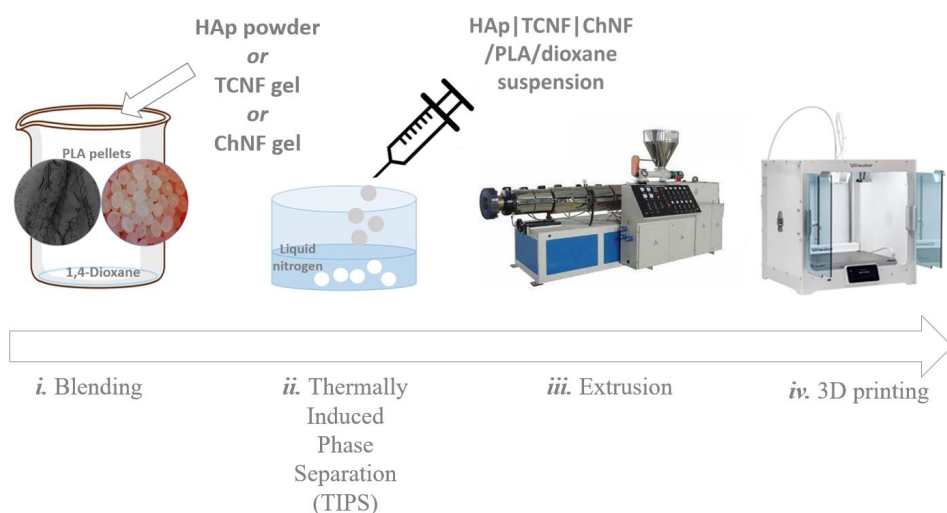


Figure 3.1. Simplified overview of the composite development process: from components blending to 3D printing filament.

The morphology, the dispersion of the nanoparticles within the PLA matrix, the integrated and designed porosity systems as well as other crucial parameters were controlled within each experimental step (i.e. starting materials → composite pellets → composite filaments → composite 3D printed filters) using a variety of characterization methods such as SEM, TEM, TGA and μ -CT. The overview of the development of PLA-based composites is summarized in **Figure 3.2**.

In **Paper I**, the TEM analysis allowed size determination of the HAp particles used within the work, and it has revealed irregular particles in a size range between 50 – 200 nm (**Figure 3.3 a**). The obtained high-resolution TEM (HR-TEM) image proved the crystalline character of the used fish-scale extracted HAp with a lattice plane of 0.28 nm corresponding to Miller index (211). The TEM analysis of the

starting materials, composite pellets and 3D printed filters, as reported in **Paper II**, revealed that the starting TCNF fibers are polydisperse with varying thickness between 7 – 30 nm and lengths in micrometre scale. However, it was not possible to observe any inhomogeneity in the TEM images obtained for the TCNF/PLA pellets and 3D prints, potentially indicating a consistent dispersion of NFs within the PLA matrix (**Figure 3.3 b**). Moreover, the SEM measurements allowed to further analyse the dispersion of the fillers in the PLA matrix in pellets, filaments and 3D prints. Furthermore, with the use of the SEM, the analysis of the pore shrinkage induced by 3D printing was conducted.

In **Paper I**, it was observed that with each experimental step the HAp particle size decreases, as measured using *ImageJ* software from the obtained SEM images. Starting from 46 μm for the HAp powder, through 16 μm for the freeze-dried composite pellet, to 11 μm for the HAp/PLA filament. The SEM images have proven that, while the distribution and dispersion of HAp in the PLA is improved with each progressing experimental step, the HAp particles do not reach the nanometre scale and so, they should be considered a micro-addition to the developed PLA-based composite system. Moreover, the SEM served as a method to examine the 3D printed filters in terms of their porosity architectures, consistency of the pore sizes and channel interconnectivity. The channel interconnectivity and the geometry of the pores were perfectly maintained (**Figure 3.3 c**). The SEM, however, confirmed the actual pore sizes differed from the programmed ones. For the uniform porosity filter, the drop in the final pore diameter, compared to the designed one, was 36 %. For the gradient porosity filters the drop of the pore size oscillated around 43 %, and 19 % for the small and medium pores, respectively, while the size of biggest pores remained unaffected. Additionally, the distribution and dispersion of the HAp filler within the 3D printed uniformly porous filters was assessed using $\mu\text{-CT}$. The obtained cross-section images revealed that HAp is distributed homogeneously in the outer walls of the 3D filter as well as around the pores (**Figure 3.3 d**). Moreover, while the 3D printed HAp/PLA filters looked impeccable to the naked eye, the $\mu\text{-CT}$ scans reveal micro-interruptions in the printed pattern, indicating the possible need for further optimization of printing parameters.

Similar experiments were performed on the TCNF/PLA and ChNF/PLA composite pellets and filaments, which were developed as a part of work reported in **Paper II**. Notably, the captured SEM images of filament cross-section (**Figure 3.2**) exhibited a complete absence of any inhomogeneity, clusters, or agglomerates of fibers, indicating the successful nano-dispersion of both TCNFs and ChNFs within the PLA matrix. Consequently, SEM analysis primarily focused on assessing the pore and channel interconnectivity of the 3D printed filters, as well as investigating the pore shrinkage observed during the 3D printing process, as previously noted in the case of the HAp/PLA 3D printed filters. Within the work reported in **Paper II**, the shrinkage of the material also resulted in deviations of the actual pore sizes from the programmed ones. The reference PLA filters exhibited minimal shrinkage.

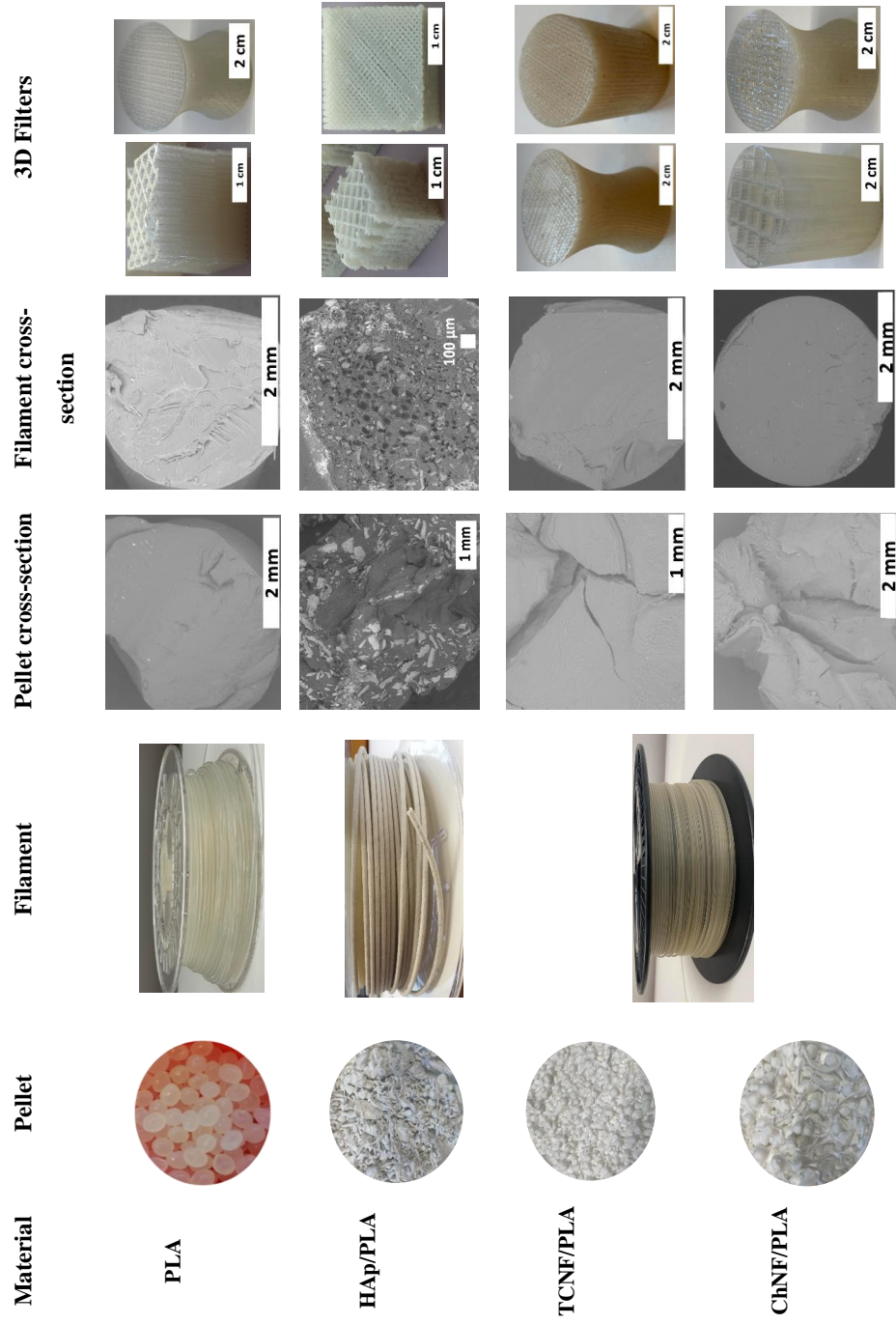


Figure 3.2. Processing overview for the PLA-based composites: from pellet development to the 3D printed filters.

They maintained the intended porosity architecture, both in the case of the big pores of the gradient cylinder and small pores of the gradient hourglass-shaped filter (**Figure 3.3 e**).

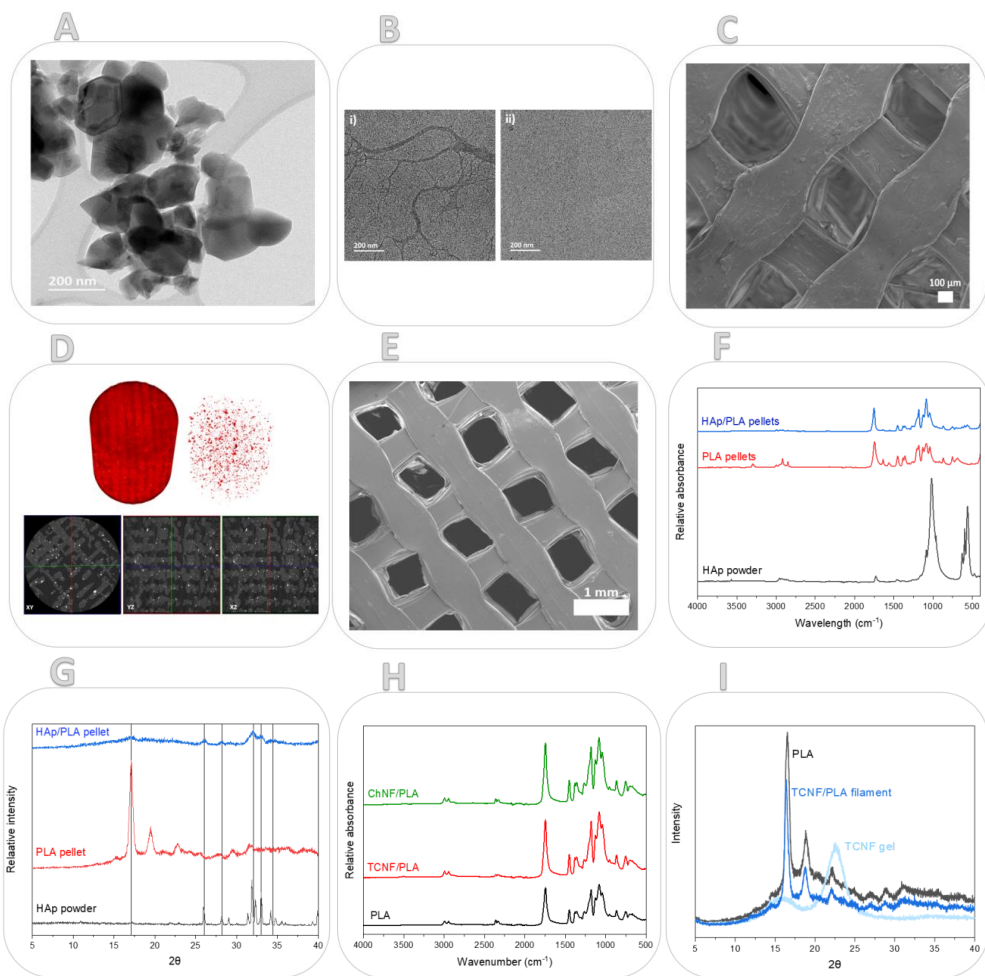


Figure 3.3 (a) TEM micrograph showing the HAp powder particles, b) (i) TCNF starting material and (ii) a section of the TCNF/PLA 3D printed filter; c) SEM of the porosity structure of the uniformly porous HAp/PLA cube; d) 3D rendering of the 8 mm μ CT volume plus a rendering showing just the HAp in the biofilter as well as μ CT representative cross-sections of the 3D printed biofilters showing the dispersion of HAp in the PLA; e) SEM of the porosity structure of the uniformly porous cylindrical TCNF/PLA filter; f) IR spectra and g) diffraction patterns of the starting materials and PLA/HAp; h) IR spectra of the PLA, TCNF/PLA and ChNF/PLA pellets; i) diffraction patterns of TCNF/PLA filament and corresponding starting materials.

For all the other models and porosity cross-sections, PLA was also affected by the 3D printing, and the reduction in pore size ranged from 8 % to 26 %, for gradient and uniform cylindrical and hourglass-shaped filters. Biocomposite samples showed more significant pore shrinkage, with pore size reductions for the uniformly porous cylindrical filters being 27 % and 42 % for the TCNF/PLA and ChNF/PLA filters, respectively. Notably, the pore size reduction was more pronounced for the ChNF/PLA filters, irrespective of their design. While the reduction of the pores during 3D printing is a common phenomenon caused by the temperature variations between the freshly extruded melt and cooled extruded layers, the addition of specific NFs as a reinforcement clearly amplifies it. As it was hypothesized in **Paper II**, it is believed that the addition of high aspect-ratio species such as TCNF and ChNF to the PLA changes the polymer chain orientation during printing, leading to more pronounced shrinkage of the pores in the 3D printed filters. The obtained results could suggest that the ChNF had higher aspect ratio compared to the used TCNF. Another plausible explanation for this phenomenon is the impact of the viscosity of the biocomposite filaments during the melting stage of the 3D printing process, since the addition of TCNF and ChNF nanofibers changes the viscosity of the PLA filament. This, combined with higher printing temperature necessary for processing the biocomposite filaments and subsequent easier extrusion, leads to thicker walls and smaller pore sizes in the biocomposite - based filters.

Moreover, FT-IR analysis was employed to assess the presence of different functional groups in all three developed PLA-based composite systems. In both, **Paper I** and **Paper II**, the obtained IR spectrum of pristine PLA exhibits bands associated with ester functional groups, such as C-O and C=O stretching vibrations at 1080 cm^{-1} and 1180 cm^{-1} , as well as, at 1640 cm^{-1} and 1740 cm^{-1} , respectively. Bands corresponding to the C-H bending vibrations were observed at 1350 cm^{-1} , 1450 cm^{-1} and 1560 cm^{-1} and bands corresponding to C-H stretching vibrations at 2913 cm^{-1} . In **Paper I**, the successful development of the composite system was confirmed by TGA, XRD and FT-IR analysis. With the use of TGA it was possible to assess the weight content of HAp in the filament, as at $1000\text{ }^{\circ}\text{C}$, when all of the PLA was decomposed, there was still residual 15 – 18 wt. % of the HAp powder left in the system. Moreover, the crystallinity of the developed HAp/PLA composite was assessed using XRD and it was shown that crystal peaks of both starting materials i.e. PLA and HAp have translated into diffraction pattern of the composite, indicating the development of composite (**Figure 3.3 g**). In the IR spectra, apart from the bands corresponding to the pristine PLA, there are a few new bands observable on the IR spectrum of the HAp/PLA system. These originate from the HAp powder and are observable at 566 cm^{-1} , 600 cm^{-1} and 630 cm^{-1} , and correspond to the P-O bending vibrations of phosphate groups (**Figure 3.3 f**). In **Paper II**, however, while it was observed that the spectral features of pristine PLA translated into the IR spectra of both the composite systems, no new bands were detected. This could be caused by the fact that the expected C-H stretching vibrations, observable on both ChNF and TCNF gels in the region

between 900 and 1200 cm^{-1} , overlap with the more intense PLA bands of the composite system (**Figure 3.3 h**), as the nano-reinforcement contents are within a maximum of 5 wt. %.

The thermal stability of the TCNF/PLA and ChNF/PLA freeze-dried pellets, filaments, and 3D printed filters was evaluated and compared to PLA reference using TGA. The addition of TCNF and ChNF had varying effects on the thermal stability of PLA - based composites. The results showed that the degradation temperature of the composite pellets was lower than that of the PLA reference, but the difference decreased after the extrusion step and further minimized after 3D printing. The gradual improvement in thermal stability with each step indicates the importance of heat-treatment processes. The increase in crystallinity during heat treatment may be the explanation of the higher degradation temperature of printed parts compared to pellets and filaments¹⁴⁶. Furthermore, XRD analysis was carried out to assess the crystallinity of the developed composite pellets and filaments, compared to the starting materials, (PLA pellets as well as TCNF and ChNF gels in the form of casted films). The PLA pellets as well as TCNF/PLA and ChNF/PLA 3D printing filaments displayed similar crystal structures, characterized by sharp peaks at $2\theta = 17^\circ$, 19° , and 22° . However, specific crystalline peaks observed in the TCNF gel diffractogram at $2\theta = 23^\circ$ and a broad peak at $2\theta = 16^\circ$, as well as in the ChNF gel diffractogram at $2\theta = 10^\circ$ and 20° , were absent in the filament spectra (**Figure 3.3 i**).

3.2 Textile - based composites

In **Paper V**, the polycotton textile waste, consisting of a 50:50 blend of cotton and PET, was directly used as feedstock for TEMPO-mediated oxidation without pre-treatment, using the adjusted protocol previously used on the wood pulp¹⁴⁷. The reaction was followed by a filtration step, aimed to remove the excess of solvents. The TEMPO-mediated oxidation enabled partial fibrillation of the oxidized polycotton, and the resulting mixture was dried in the form of casted films, which were further cut into small pellets and single-screw extruded into a 3D printing filament. FT-IR analysis confirmed the presence of carboxyl groups in the oxidized polycotton, as indicated by an additional peak in the range of 1602 - 1633 cm^{-1} . This peak corresponds to the stretching vibration of carboxyl sodium salts (COONa) introduced during TEMPO-mediated oxidation. The charge density of the oxidized polycotton was estimated to be $1221 \pm 82 \text{ mmol COO}^-/\text{kg}$ of cellulose, indicating presence of highly charged cellulose fibers.

The extruded filament contained approximately 80 wt. % of the oxidized textile waste, with the remaining component being pure PETG. The filament was very smooth to the touch, and presented no problems during the printing process, matching the commercially available PETG 3D printing filaments in terms of its texture and flexibility. The SEM images captured on the filament cross-section, however,

revealed some residual porosity present in the filament. While this is not something that affected the printability of the material, it could have affected the mechanical performance of the 3D printed parts by potentially leading to micro-interruptions in the print pattern. That, however, could only be detectable by techniques such as μ -CT, which were not conducted within this study. The obtained IR spectrum of the extruded 3D printing filament does not exhibit neither the broad peak at $3270 - 3340 \text{ cm}^{-1}$ associated with the stretching vibration of hydroxyl groups in cellulose molecules nor the peak at $1602 - 1633 \text{ cm}^{-1}$, related to the stretching vibration of carboxyl sodium salts (COONa). The extrusion process, conducted at 230°C , could result in partial cellulose degradation, as suggested by previous studies on the heat treatment and decomposition of TCNF and TCNF - based materials¹⁴⁸, which could lead to cellulose dehydration and decarboxylation, leading to formation of sodium carbonate. It is, however, difficult to assess whether it is precisely what is happening in the system, as the expected peak of sodium carbonate would appear around $1400 - 1415 \text{ cm}^{-1}$, hence overlapping with the present ester peak of PET (Figure 3.4. a). The obtained TGA results (Figure 3.4 b) show that the tested pellets exhibited earlier onset of degradation when compared to the starting materials, due to the fibrillation and presence of carbonyl groups on the surface of oxidized fibrils. However, the onset temperature of degradation for both the filament and 3D printed parts was delayed, compared to both, the pellets and the starting material.

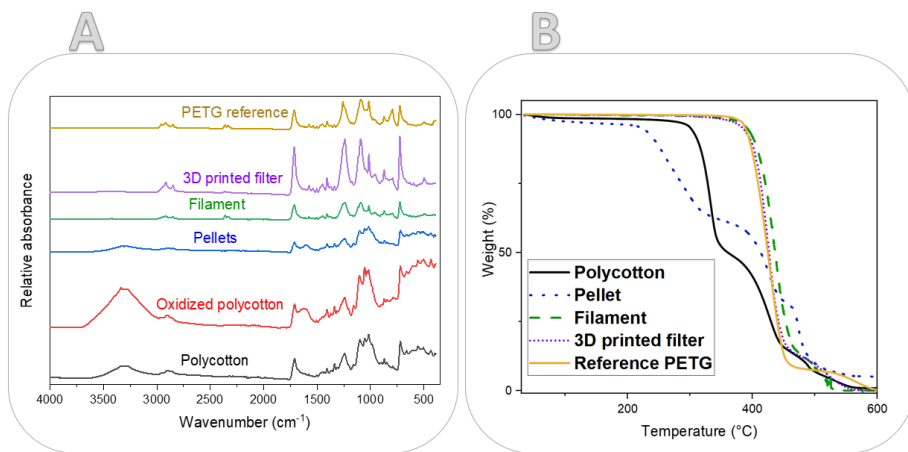


Figure 3.4 a) IR spectra of the polycotton, oxidized polycotton, pellets and filament and 3D printed filters, b) TGA curves obtained for the same materials.

4. Performance optimization and evaluation of 3D printed water purification filters

4.1 Surface functionalization of the 3D printed biocomposite filters

In **Paper III**¹⁴⁹, the TCNF/PLA filters (developed in **Paper II**) were further surface functionalized in order to enhance their potential for removal of wider range of contaminants from water, creating ‘MOF@Cell’ systems. The filters were subjected to two different activation mechanisms i.e. either acid or ozone (O₃) treatment. The adsorbent in the form of a green metal-organic framework (MOF) – SU-101 was further anchored onto the activated surface. The main objective of activating the surface of the PLA-based filters was to break the ester linkages of the polymer, either by acid hydrolysis or photooxidation reaction, leading to exposure of different functional groups i.e. hydroxyl and carboxyl groups on the surface of PLA, facilitating the further adsorption and anchoring of the SU-101 adsorbent onto the filters surface. The higher concentration of negative charges on the surface of the filters was verified through the measurement of the filter's zeta potential. It was shown that at the experimental pH values (around pH 7.4 - 7.8), the zeta potential of the acid and O₃-activated filters deviates from that of the PLA reference filter, displaying more negative values (**Figure 4.1 a**). This difference is especially significant in the case of the acid-activated filters.

The activated TCNF/PLA and reference PLA filters were subsequently immersed in a 1 % suspension of SU-101 in water and the deposition thereof over the filters’ surfaces was examined by i.a. SEM and SEM-EDX mapping, targeting the main element of SU-101 - Bi. It was observed, that both the O₃-induced photooxidation reaction, as well as the acid hydrolysis, promoted the homogenous deposition of SU-101 over the filters’ surfaces. The interaction between SU-101 and the filter surface occurs through various mechanisms, as hypothesized in **Paper III**¹⁴⁹. While the SU-101 itself lacks charge, the primary expected mechanism would involve physical interactions such as van der Waals forces. However, considering the presence of exposed hydroxyl and carbonyl groups on the hydrolysed and photooxidized matrix surfaces, adsorptive connections cannot be completely ruled out. Additionally, both acid and O₃ treatments result in the roughening of the matrix surfaces, creating nano- and micro-pores that could entrap SU-101 molecules on the surfaces of the filters.

The successful deposition of the SU-101 was confirmed by the visible colour change of the functionalized filters, as shown in **Figure 4.1 b**, for both the reference PLA and TCNF/PLA filters. The

obtained SEM images were used to locate the SU-101 deposits over the filters surface (Figure 4.1 b). The SEM-EDX analysis presented in Figure 4.1 b, confirms the homogenous distribution of MOF over the filters surface, while highlighting the importance of subjecting the filters to an activation mechanism prior anchoring. It can be observed that both types of activation processes increase the deposited load of SU-101, what results in a homogeneous distribution of the MOF over the surfaces of the filters.'

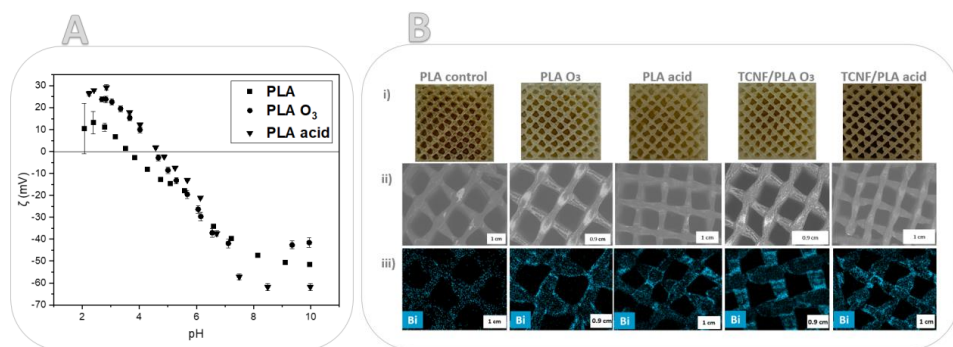


Figure 4.1 a) zeta potential of acid and O₃ – activated samples compared to the reference PLA filter b) (i) Overview of the functionalized filter's surface, (ii) corresponding SEM images, (iii) elemental mapping confirming homogenous deposition of SU-101 MOF over the filters surface (*Reprinted with permission from*¹⁴⁹).

The character of the SU-101 deposition over the filters surfaces was further studied with the use of FT-IR, XRD and XPS. While no solid conclusions about the nature of interactions between the surface and the MOF can be drawn from the collected IR spectra, the obtained PXRD diffraction patterns confirm the presence of MOF on the 3D printed parts, indicating a higher load of MOF over the O₃-activated substrates and conversion of MOF into BiOCl in the acid-activated filters. The successful anchoring of MOF was also indicated by the XPS measurements, allowing the estimation of the amount of SU-101 attached. Pure SU-101 exhibits a surface Bi content of 7.7 at %, while Bi contents at the activated filters surfaces were 0.8, 2.8, 1.8 and 1.7 at % for PLA (O₃), PLA (acid), TCNF/PLA (O₃) and TCNF/PLA (acid), respectively.

4.2 Mechanical performance of the developed filters

The mechanical performance of the filters developed within **Paper II - Paper V**, was verified using the specimens with standardized dimensions of 12.7 x 12.7 x 25.4 mm. The compression tests on the developed filters of varying porosity, corresponding to the porosity architectures of the filters studied

within each work, were carried out with accordance to the ASTM D695-15 standard. The mechanical properties of the specimens tested within **Paper IV** are discussed separately in **Chapter 5**.

The tested 3D printed filters included TCNF/PLA and ChNF/PLA filters and reference PLA filters (**Paper II**); MOF-functionalized TCNF/PLA and PLA filters and reference PLA and TCNF/PLA filters (**Paper III**); as well as textile-based composite filters and the reference PETG filters (**Paper V**). All of the specimen were subjected to uniaxial compression tests obtaining stress-strain curves, which enabled determination of the apparent compressive elastic modulus from the elastic region of the curves as well as energy dissipation i.e. toughness calculated based on the area under the stress-strain curves.

In **Paper II**, the impact of both: addition of nanofibers and the porosity structure on the mechanical performance of the PLA was studied. Two different porosity architectures were examined i.e. uniform and gradient porosity structures. When comparing filters with uniform porosity to those with gradient porosity, significant differences in their behaviour were observed. The collapse of the uniformly porous structure started in the middle of the filter and spread along the z-axis under the applied pressure. The calculated apparent compressive elastic modulus for the uniformly porous TCNF/PLA samples was 3% higher (981.9 ± 4.6 MPa) than for PLA (949.9 ± 2.8 MPa), while for ChNF/PLA (886.6 ± 37.1 MPa) it was 7% lower. However, the gradient porosity structures exhibited a more pronounced enhancement in mechanical properties. For both TCNF/PLA and ChNF/PLA, the larger pore section was initially affected, followed by the bending of the smaller pore section. As a result, the apparent compressive elastic modulus values were 13 % and 28 % higher for TCNF/PLA (622.7 ± 1.6 MPa) and ChNF/PLA (702.9 ± 5.4 MPa), respectively, compared to the reference PLA (550.7 ± 2.8 MPa). This suggests that not only the addition of reinforcing nanospecies, but also the type of the porosity architecture has an impact on the stiffness of the 3D printed filters. The representative stress-strain curves of the tested specimens are presented in **Figure 4.2 a**.

Toughness data showed that the addition of both types of nanofibers significantly improves the energy dissipation of the PLA filters. This phenomenon was again more pronounced for the gradient porosity structures, where the average toughness for TCNF/PLA and ChNF/PLA filters was 4.4 ± 0.2 J/cm³ and 8.4 ± 0.9 J/cm³, respectively, when compared to 3.9 ± 0.3 J/cm³ for the reference PLA filters.

Overall, it was demonstrated that the addition of both TCNF and ChNF has a positive impact on the mechanical properties of the PLA-based filters, making them suitable for applications in the water treatment industry, where the filters would be expected to operate under high water pressure. The improved mechanical properties can be attributed to the combined effect of customized pore architecture and the overall design of the 3D printed filters, as well as the uniform dispersion of reinforcing NFs within the composite matrix.

The effect of subjecting the filters to acid and O₃ treatments, as well as the impact of their further functionalization with SU-101 on the mechanical properties of the 3D printed TCNF/PLA and PLA filters was investigated in **Paper III**. The results obtained within this work support the findings previously reported in **Paper II**, as it was once again concluded that the addition of TCNF improves both Young's modulus and toughness values of the PLA filters. The overall Young's modulus values obtained for the specimens within this work are higher than those reported previously, and it can be linked to the different porosity design of the filters. The calculated Young's modulus values for the unmodified TCNF/PLA and PLA filters are 1262.4 ± 128 MPa and 1159.8 ± 102 MPa, respectively.

However, the main objective of the compressive tests conducted within **Paper III** was to establish how the two different activation mechanisms, i.e. acid and O₃ treatments, affect the mechanical properties of the filters. The representative stress-strain curves of the tested specimens are presented in **Figure 4.2 b**. The acid treatment has led to a slight reduction of Young's modulus values when compared to the reference materials, and so, for the acid-activated MOF@PLA it was 1089.4 ± 57 MPa while for the MOF@TCNF/PLA aka MOF@Cell it was 1184.7 ± 89 MPa. Therefore, it can be concluded that acid treatment does not impose a significant change on the mechanical performance of the filters, it does however stress out the importance of using the TCNF as the reinforcement, as ultimately the TCNF/PLA and MOF@Cell filters present enhanced mechanical properties compared to both the unmodified PLA and MOF@PLA filters. However, the photooxidation reaction induced by O₃ treatment affects the mechanical properties of the filters in a more pronounced manner, with the Young's modulus drop of 13 % and 7 %, for the MOF@PLA and MOF@Cell filters, respectively, when compared to their corresponding reference filters. Regrettably, the toughness values and their standard deviations obtained within this work were too similar, indicating a lack of significant variation and provide very limited information, hence they did not substantially contribute to the interpretation of the results.

Overall, the compiled results demonstrated that the activation mechanism applied to the surface of the filters prior to anchoring the SU-101 adsorbent does not exert a substantial influence on the mechanical properties of MOF@Cell filters. This shows the potential of the developed TCNF/PLA filters to sustain additional chemical and/or physical surface treatments prior to use in real-life water treatment applications. Moreover, the results demonstrate the versatility of the developed filters, as they can easily be surface functionalized to accommodate an array of adsorbents suitable for removal of specific contaminants, and all that without compromising the mechanical integrity of the filters.

In **Paper V**, the mechanical properties of the textile-based composite filters were assessed and compared to the performance of the reference PETG filters. Both, the influence of PET and polycotton compositing, as well as the influence of the porosity architectures, on mechanical properties of filters

was studied. The drop in Young's modulus values between non-porous (NP) reference specimens and NP composite specimens was over 50 % (i.e. 1186 ± 132 MPa for PETG filters vs. 574 ± 38 MPa for composite NP filters). The incorporation of pores into the designed structures have deepened these differences, reaching nearly 60 % drop in Young's modulus values for the composite filters (350 ± 39 MPa for porous composite specimens vs. 815 ± 112 MPa for porous reference PETG specimens) (**Figure 4.2 c**). However, by taking density of the developed models into consideration and calculating the specific modulus, the differences between the composite and reference specimens were less pronounced. The drop in specific modulus values was approximately 37 % for NP filters ($1.02 \text{ m}^2\text{s}^{-2}$ for PETG vs. $0.64 \text{ m}^2\text{s}^{-2}$ for composites), and approximately 45 % for porous filters ($0.51 \text{ m}^2\text{s}^{-2}$ for composites vs. $0.93 \text{ m}^2\text{s}^{-2}$ for PETG).

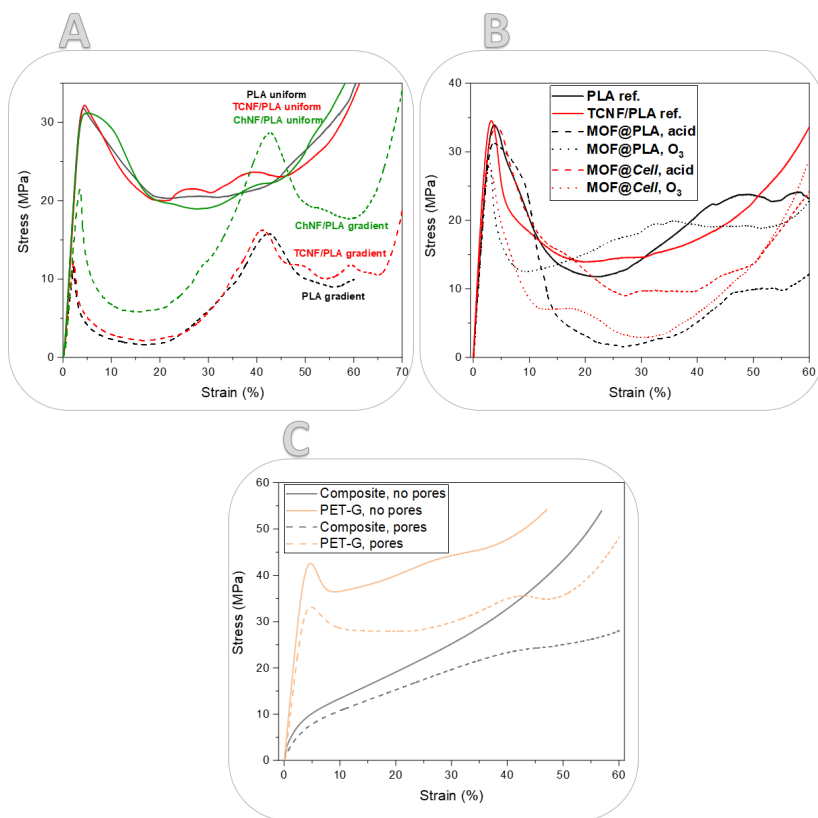


Figure 4.2 Representative stress-strain curves of the filters studied within a) **Paper II**, b) **Paper III**, c) **Paper V**.

While the Young's modulus values of both materials were equally affected by the pore incorporation, the porosity had little influence on the toughness of PETG specimens, which remained stable (oscillating around $18.7 \pm 0.4 \text{ J/cm}^3$ for NP samples and $18.3 \pm 0.8 \text{ J/cm}^3$ for porous samples). However, the

toughness of composite samples was affected by incorporation of pores, with obtained values of $15.7 \pm 0.6 \text{ J/cm}^3$ for NP specimens and $10.6 \pm 0.5 \text{ J/cm}^3$ for porous specimens.

We hypothesize that the decrease of mechanical performance of textile-based composites can be attributed to i.a. fillers and stress concentrations, leading to micro- and nanocracks development. Moreover, the textile-based composites were processed at higher temperature than PLA-based composites (i.e. at 250°C) and this could also contribute to increased brittleness and reduced mechanical properties of the printed filters.

4.3 Functionality of the 3D printed filters: water treatment applications

The 3D printed filters developed in **Paper I – III** and **Paper V** were tested for removal of various contaminants from water including metal ions, microplastics and dyes.

In **Paper I**, the HAp/PLA – based, 3D printed discs were tested for removal of metal ions from separate model solutions containing either Pb^{2+} or Cd^{2+} ions. The adsorption efficiency reached 45 % and 40 %, for the removal of Cd^{2+} and Pb^{2+} , respectively. In **Paper I**, it was hypothesized that the adsorption of Cd^{2+} ions occurred via a two-step surface complexation mechanism, whereas Pb^{2+} ions were adsorbed via coprecipitation. The chemical character of adsorption of metal ions onto the HAp/PLA structures was indicated by the XPS measurements, where the peaks at binding energy of 531.3 eV and 531.1 eV were observed after adsorption of Cd and Pb ions, respectively. These peaks suggest an interaction between the metal ions and the oxygen present on the surface of the filters. Moreover, the flux and permeability of the 3D printed cubic filters was tested with the in-house constructed setup and it was shown that the flux reached approximately 1.8 and $2.0 \text{ M Lm}^{-2}\text{h}^{-1}\text{bar}^{-1}$ for the uniform and gradient porosity structures, respectively. Moreover, the calculated permeability of the uniform and gradient cubic filters was $3.58 \times 10^{-10} \text{ m}^2$ and $4.77 \times 10^{-10} \text{ m}^2$, respectively. The calculated values prove a very high throughput character of the developed filters, making them suitable for applications within the water treatment industry.

In **Paper II**, the developed TCNF/PLA and ChNF/PLA hourglass-shaped filters with uniform porosity were tested for removal of two different contaminants i.e. Cu^{2+} ions from model solutions of 250 mL and two different concentrations (1 mM and 10 mM) via batch adsorption study, as well as for microplastics separation from an actual laundry effluent. The recyclability potential of the filters was tested by desorbing the adsorbed Cu^{2+} ions using acid in a series of adsorption-desorption experiments. In total, three consecutive adsorption-desorption cycles were carried out on the filters. Within the first adsorption cycle in 1 mM solution, the highest adsorption efficiency was achieved by ChNF/PLA filters

(51 %), followed by TCNF/PLA (47 %) filters, what compared to a removal efficiency of 11 % reached by the reference PLA filters, highlights the role of NFs in the adsorption process.

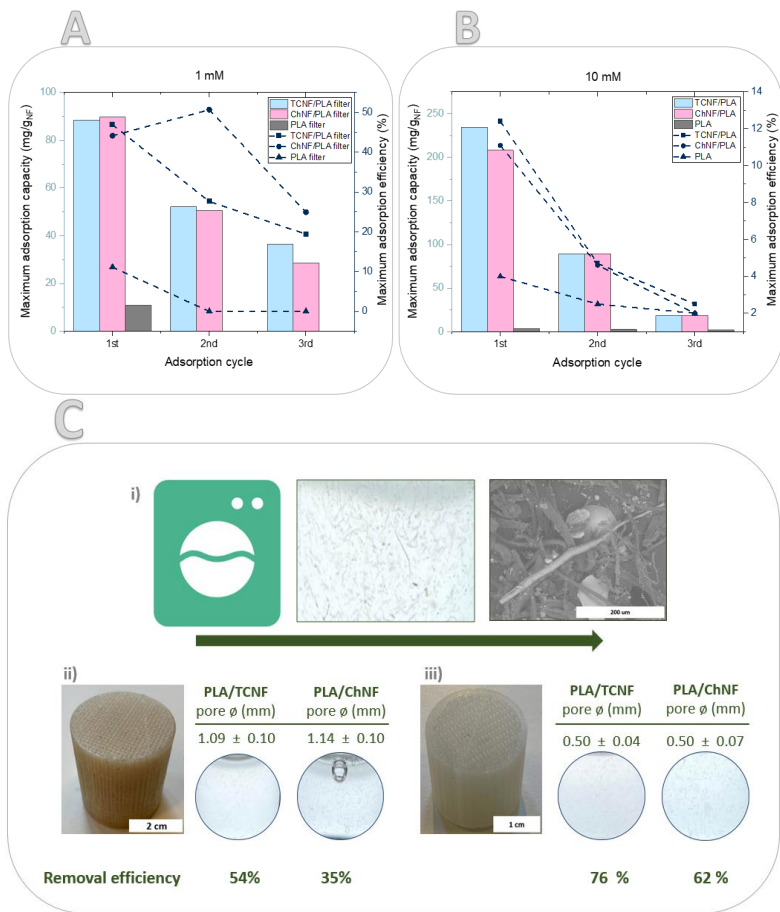


Figure 4.3 Adsorption capacity and efficiency of the filters as tested in a) 1 mM and b) 10 mM copper sulfate solutions at pH = 6–7.5, c) (i) Microplastics solution collected from laundry, SEM image of the particles, and average pore diameter and microplastics removal efficiency of (ii) filters with programmed pore size of 1 mm and (iii) programmed pore size of 0.5 mm (*Adapted and Reprinted with permission from*¹⁴⁵).

Similarly, higher maximum adsorption capacities were recorded for the biocomposite filters, reaching 88 mg/g_{NF} and 90 mg/g_{NF} for ChNF/PLA and TCNF/PLA filters, respectively, whereas the reference PLA filter had a adsorption capacity of 10 mg/g. Furthermore, the adsorption capacity increased as the initial concentration of the metal solution increased to 10 mM. At this concentration, the ChNF/PLA

and TCNF/PLA filters achieved adsorption capacities of 208 mg/g_{NF} (10.4 mg/g_{filter}) and 234 mg/g_{NF} (12.6 mg/g_{filter}), respectively. In comparison, the reference PLA filter had a much lower adsorption capacity of 4 mg/g. These findings emphasize the potential of the developed 3D filters for effectively removing Cu²⁺ ions from aqueous media (**Figure 4.3 a-b**). The results also indicate that the NFs not only reinforce the bulk of the filaments and filters, but also play a functional role on the filters surfaces.

However, it is important to acknowledge the contribution of PLA in the adsorption process. Although the adsorption capacities are presented per gram of NFs, the presence of PLA enhances the adsorption process. Previous literature extensively discussed both the adsorption mechanism and adsorption kinetics of different metal ions onto cellulose^{73,75,150,151} - and chitin³⁰ - based materials. The mechanism of adsorption of Cu²⁺ ions onto ChNF/PLA filters can be linked to the formation of complexes with amino groups of ChNFs, while the adsorption onto the TCNF/PLA filters can be associated to the formation of electrostatic interactions between the metal ions and carboxyl groups present on the surface of the fibers¹⁵². As the removal efficiencies and capacities recorded for the filters decrease with each adsorption-desorption cycle, the same filters, used for removal of Cu²⁺ ions, were repurposed for use as separators of bigger suspended contaminants from water. The potential recyclability application tested was the separation of microplastics debris from laundry effluent, taking advantage of the filters' tuned porosity architecture. Within this work, it was determined that each wash cycle releases up to 12 grams of microplastics to the environment. However, by employing the ChNF/PLA and TCNF/PLA - based 3D printed filters with 1 mm pores, up to 35 % and 40 %, respectively, of the contaminants can be successfully retained. Moreover, decreasing the filter's pore size in half, results in increased removal efficiencies of approximately 75 % and 60 % for TCNF/PLA and ChNF/PLA filters, respectively (**Figure 4.3 c**). We hypothesize that size exclusion is one mechanism of separation, while creation of physical bonds between the contaminants and NFs present on the surface of the filters is another component, as a preference for adsorption with the use of TCNF-reinforced filters can be observed. However, future studies are needed to systematically evaluate the mechanisms and interactions involved in this process.

While the as-printed TCNF/PLA filters have successfully demonstrated to be feasible for removal of Cu²⁺ ions and microplastics from water, their subsequent surface-functionalization with a green SU-101 MOF aimed to further widen their applicability potential. As reported in **Paper III**, the MOF@PLA and MOF@TCNF/PLA (*aka* MOF@Cell) filters have shown to be suitable for removal of various toxic metal ions from an actual mine effluent. Analysis of the mine effluent revealed the presence of various metal ions, including V, Cr, Cd, Mn, Co, Ni, Cu, Zn, and As. SEM-EDX mapping confirmed the adsorption of these metal ions onto the filter surfaces, with Cd, Pb, and As indicating higher adsorption affinity, based on the more pronounced presence of these metals on the surface of the filters (**Figure 4.4 a**). The removal efficiencies for Cd²⁺, Pb²⁺, As³⁺, Mn²⁺, and Zn²⁺ were quantitatively analyzed using

ICP-MS and the results of Pb^{2+} adsorption are presented in **Figure 4.4 b**. The filters showed highest affinity for removal of Mn^{2+} ions from effluent, reducing their concentration well below the allowed levels for drinking water i.e. below $50 \mu\text{g/L}$ ¹⁵³, while they were least effective in removal of As^{3+} ions from the contaminated water. Chelation is a plausible mechanism of adsorption, as the phenolate groups on the MOF surface can coordinate with metal ions, releasing water molecules from the metal ion's hydration shell. The reversible nature of adsorption is demonstrated through successful desorption experiments. Moreover, the integrated porosity of the SU-101 MOF and the nanopores formed through hydrolysis of PLA during acid treatment contribute to enhanced adsorption capacity, which can be linked to increased surface area.

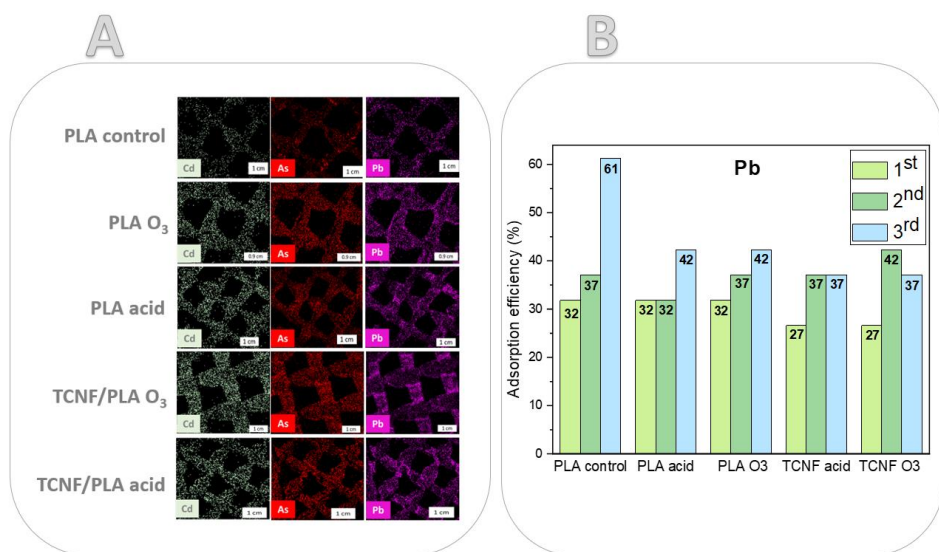


Figure 4.4 a) SEM-EDX images for all of the 3D printed filters with elemental mapping for cadmium (Cd), arsenic (As) and (Pb), b) adsorption efficiency for removal of Pb ions after 24 h immersion during three adsorption cycles as measured by ICP-MS (*Reprinted with permission from*¹⁴⁹).

While MOFs are usually tested as adsorbents towards one and very specific type of contaminant such as e.g. pharmaceutical pollutants¹⁵⁴, within this work we aimed to demonstrate the wide potential of the SU-101 for removal of various types of pollutants. Therefore, after three cycles of adsorption and desorption, the filters underwent a final re-anchoring procedure. The same filters, which were used three times for the adsorption of metal ions from mine effluent, were then tested for adsorption of MB. The filters showed removal efficiencies of 52 % and 53 % for acid and O₃ - activated MOF@PLA filters, while MOF@Cell filters had slightly lower efficiencies of 43 % and 38 %, respectively. We hypothesize that the adsorption of MB onto the filters primarily occurred through interactions between SU-101 and MB, such as electrostatic interaction, hydrogen bonding, and π - π stacking.

Moreover, MB was also used as a model pollutant to study the adsorption properties of textile-based composite filters developed in **Paper V**, and compared to PETG filters. The addition of polycotton greatly increase the adsorption properties, as the maximum adsorption capacity increased from 0.02 mg/g for the pure PET filter through 0.3 mg/g for the textile-based filament, to 1 mg/g for the 3D printed textile-containing filters. This enhanced adsorption capacity could be linked to the presence of sodium carbonate in the filters. However, conductivity measurements showed that the filament present a very little amount of titratable carboxylic groups, of around 1 $\mu\text{mol/g}$, and this little amount could be the reason of the low adsorption capacity compared to the other filters prepared in this work. Desorption experiments performed on both textile-based composite filters and pure PETG filters demonstrated the recyclability of the filters, which can be cleaned by simple water washing. In addition, experiments on textile-based composite filters showed that porosity is a crucial factor for adsorption, as non-porous textile-based filters showed very little MB adsorption. We aim to study the adsorption of metal ions and other pollutants, to better investigate the potential of these textile-based filter for water remediation applications. Overall, the enhanced adsorption capacity of the filters prepared, compared to the PETG filters, demonstrate the potential of these filters in water remediation application, as the adsorption capacity could be further enhanced by specific surface modifications or by increasing the porosity and thus the surface area.

5. Estimating the lifespan of the filters via accelerated ageing experiments

Using materials in highly demanding medical and engineering applications requires the careful consideration of their long-term mechanical performance and durability. The ageing behavior of pure and reinforced plastics often exhibits significant differences, and that is why within **Paper IV** the degradation behaviour of PLA, and PLA-based biocomposites reinforced with either TCNF or ChNF, was investigated in the series of accelerated ageing experiments in water. Cuboid and flat rectangular, 3D printed models of three varying compositions (PLA, TCNF/PLA and ChNF/PLA) were subjected to tests at various temperatures (RT, 30 °C, 40 °C and 50 °C) for a total of 19 weeks. At various time points, the thermomechanical properties of the filters were assessed using compression testing, DMTA and TGA.

The study investigated the effects of composition, ageing period, and ageing temperature on Young's modulus and toughness values. It was revealed that the drop of the Young's modulus values is more significant for the biocomposite filters, when compared to pristine PLA filters. The Young's modulus values of the latter being stable even after 19 weeks of ageing at RT being 1385 ± 43 MPa, while the biocomposite systems have recorded a drop of 26 % (TCNF/PLA) and 33 % (ChNF/PLA) for their Young's modulus values after ageing in the same conditions for the same amount of time (**Figure 5.1**). Moreover, the T_g values of the aged samples decreased due to water absorption, with a notable drop of approximately 10 °C observed for the biocomposite materials after just 3 weeks of ageing. The storage modulus (E') of the reinforced samples was higher than that of pure PLA, indicating improved mechanical stability in dry conditions. However, pure PLA filters exhibited better resistance to ageing in aqueous environments, while the reinforced filters showed significant deterioration in E' values. Prolonged ageing led to a considerable decrease in E' for all samples. Moisture absorption, chemical degradation of both the PLA and NFs, loss of the interfacial adhesion between the NFs and the matrix, and oxidation were potential factors contributing to the reduced mechanical performance.

The lifespan of the 3D printed filters during prolonged moisture exposure was predicted using the Arrhenius model (See **Equation 1** and **2**). The experiment lasted for 19 weeks, corresponding to 3192 hours of aging. Young's modulus was chosen as the tested property, and relative values were assigned based on the non-aged specimens. The maximum decrease in YM was observed in filters aged at 50 °C, with all filters reaching the endpoint criterion of a 50% drop in YM within the duration of the experiment.

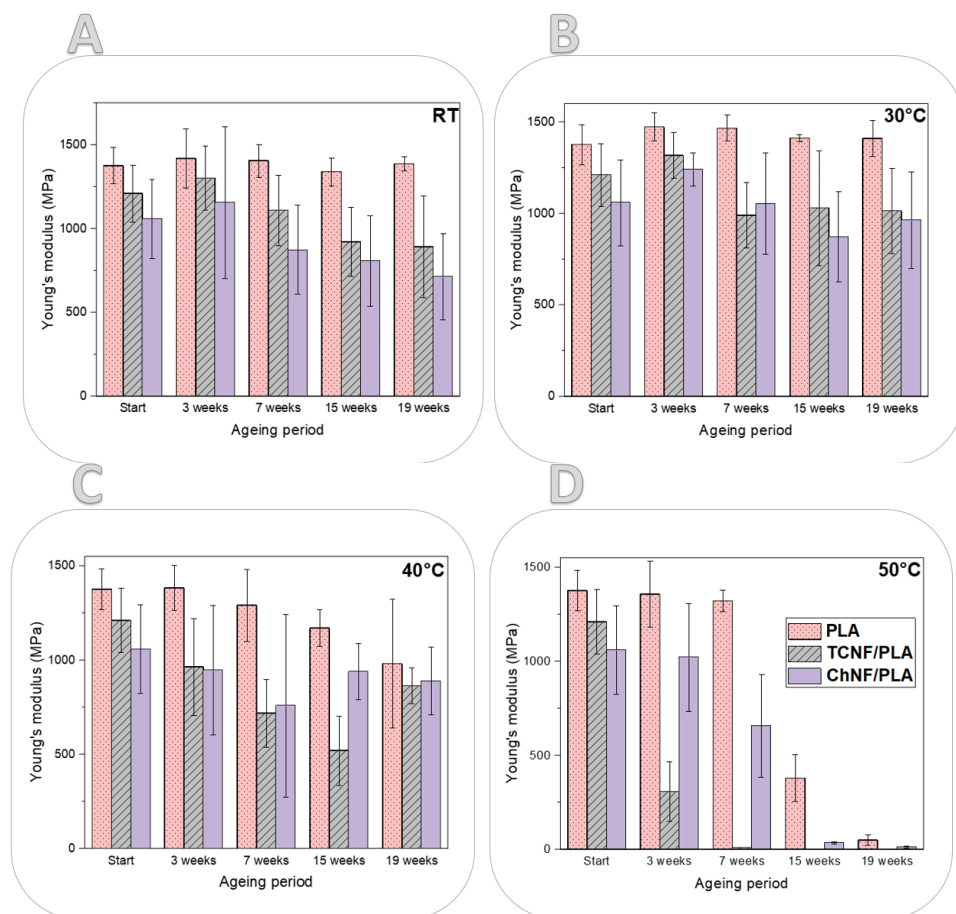


Figure 5.1 Average Young's modulus (MPa) values obtained for PLA, TCNF/PLA and ChNF/PLA filters aged for varying amount of time at a) RT, b) 30 °C, c) 40 °C, and d) 50 °C, adapted from submitted **Paper IV**.

The PLA, TCNF/PLA, and ChNF/PLA filters took approximately 2050 hours (85 days), 480 hours (19 days), and 1300 hours (54 days), respectively, to reach the endpoint (**Figure 5.2**). For filters aged at lower temperatures, the endpoint criterion had to be extrapolated based on the experimental results. Based on the obtained results, the PLA filters can be used for effluent treatment at RT for over 3.5 years, while for the TCNF/PLA and ChNF/PLA filters it was up to 8 and 5 months, respectively before losing 50 % of their mechanical capacity. According to the Arrhenius model, the rate constant of material aging is assumed to follow a straightforward exponential relationship with temperature. When predicting the

lifespan of plastics using the Arrhenius model, higher aging temperatures led to a decrease in predicted lifespan.

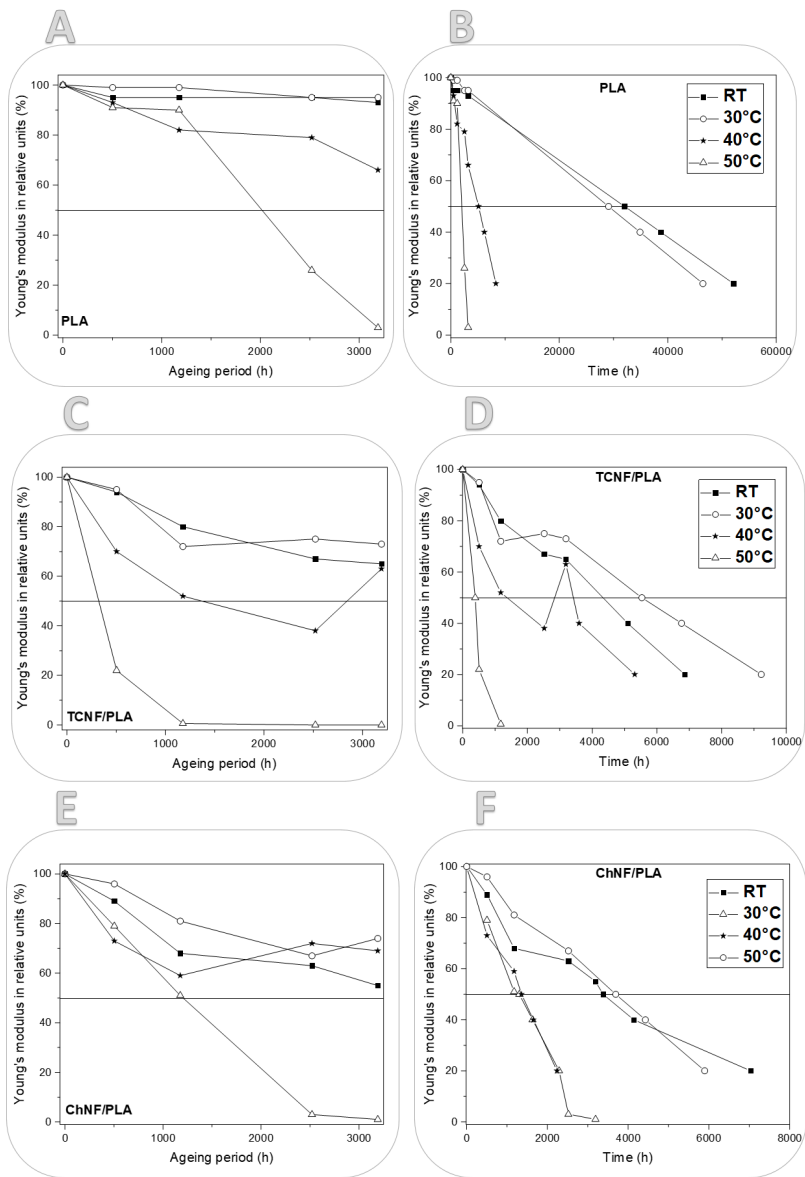


Figure 5.2 Young’s modulus values within the experiment duration and lifespan projection using Arrhenius model for a,b) PLA, c,d) TCNF/PLA and e,f) ChNF/PLA filters, adapted from the submitted Paper IV.

This is observed in unmodified PLA filters, where RT-aged filters have the longest expected lifespan, and 50 °C - aged filters have the shortest. However, if the opposite is observed i.e. material follows non-Arrhenius behaviour, it could indicate the presence of other mechanisms, such as moisture absorption, changes in T_g , crosslinking, or impurities from processing.

It is important to exercise caution when interpreting the lifespan prediction results, as the extrapolation of experimental data cannot account for all degradation mechanisms beyond the test span and prolonged water exposure. However, these results provide a good estimation of the service life of the 3D printed filters intended for water treatment applications.

6. Conclusions

This thesis reports the development of four green composite systems suitable for processing by the means of FDM into water purification filters. The obtained results highlight both, the possibilities and the challenges associated with the design of novel, 3D printable, and most importantly, green materials for the development of sustainable water treatment systems.

By combining physical blending with TIPS method as a pelletization step, three different PLA - based composites were developed, and these included HAp/PLA, TCNF/PLA and ChNF/PLA systems. All of these presented excellent printability potential and were successfully processed into monolithic water purification filters of various geometries and porosity architectures. The 3D printed filters have shown great mechanical stability and permeance and have shown to be suitable for removal of different metal ions (Cd^{2+} and Pb^{2+} for HAp/PLA) and (Cu^{2+} for TCNF/PLA and ChNF/PLA) from water and microplastics from laundry effluent. Moreover, the accelerated ageing study revealed that TCNF/PLA and ChNF/PLA filters are suitable for use for up to 8 and 5 months, respectively, at RT water, while maintaining at least 50 % of their original Young's modulus value i.e. 1210 ± 170 MPa for the TCNF/PLA filters and 1059 ± 235 for the ChNF/PLA filters.

Moreover, the developed TCNF/PLA filters were successfully surface functionalized with a green MOF – SU-101, creating robust MOF@Cell filters. The functionalization process improved the adsorption properties of the filters, which have been proven to be suitable for removal of wider range of metal ions from an actual mine effluent. Moreover, within this work the recyclability potential of the filters and mechanical stability of the 3D printed matrices was demonstrated, as the filters underwent three adsorption-desorption cycles with maintaining their functional and structural performance. Moreover, the MOF – functionalized filters have been shown to be suitable for removal of MB from water.

Lastly, the use of polycotton textile waste for 3D printing and utilization of the developed filters for removal of MB from water was explored. It was demonstrated that TEMPO- mediated oxidation carried out on the textile introduces negative charge on the surface of the filament and consequently on the surface of 3D printed filters, making them promising materials for removal of cationic molecules from contaminated water, as shown by MB adsorption experiments.

7. Future outlook

Four years of PhD studies are certainly not enough to explore and analyse all the possibilities associated with the development of ‘sustainable water treatment’ systems using a combination of green materials and 3D printing. While I can only hope that this thesis makes a small contribution to the field, I can already identify several key areas that would benefit from further exploration and improvement.

1. **Composite preparation:** While the implemented TIPS pelletization method have shown to improve dispersion of the nanoparticles in the PLA matrix, it is a rather time-consuming method, which currently lacks scalability potential. It would be advantageous to investigate alternative approaches that result in equally well-dispersed hydrophilic nanospecies in hydrophobic composite matrices.
2. **Tailored design and functionality:** Further research should aim to expand the range of filter designs, pore sizes, and surface functionalities to address more specific water treatment challenges. This could involve incorporating specialized compounds to e.g. enhance pollutant removal efficiency or antimicrobial properties. Moreover, preparation of 3D printing filaments with actuating materials would be a great way to obtain selective water purification filters sensitive to e.g. pH, temperature or salinity changes.
3. **Lifecycle Assessment and Environmental Impact:** As sustainability is a primary objective, future studies should conduct comprehensive lifecycle assessments to evaluate the environmental impact of the developed 3D printed, green composite-based water purification filters.
4. **Integration of smart technologies:** The integration of smart technologies into the 3D printed biobased water purification filters could enhance the monitoring, control, and maintenance of the system. Real-time data collection, sensor integration, and automated feedback mechanisms can enhance performance of the filters, and enable predictive maintenance. Further research in this area can lead to intelligent and autonomous water treatment systems that operate efficiently and effectively.
5. **Scalability potential:** Future studies should focus on optimizing manufacturing processes, exploring cost-effective and sustainable feedstock options, and addressing regulatory and certification requirements to enable large-scale production and adoption of green composite-based filters manufactured with the use of FDM.

In conclusion, the future of sustainable water treatment technologies based on biobased materials and 3D printing holds a great promise. Through ongoing research and emergence of novel technologies, advancements in material performance, design customization, scalability, and enhancement of manufacturing processes are anticipated.

Acknowledgments

Firstly, I would like to thank my supervisor – Aji. Thank you very much for giving me the opportunity to conduct the PhD studies under your supervision. I joined your group as a master thesis student and it was you, who first made me believe that I can continue as a PhD student. You have a special way of making us, students, feel like *partners*. I have always felt encouraged by you to try new methods in the lab. Your openness to discussion, kindness and trust you bestowed in me as an independent scientist is something I am extremely grateful for. None of my work, however, would be conducted without funding from Knut and Alice Wallenberg Foundation (Wallenberg Wood Science Center). I am very happy and honoured that I was able to be a part of the WWSC network! Moreover, to my past and current groupmates – thank you! I could not imagine being a part of a kinder and a more helpful group of people! Thank you Charlotte Boegård for helping me fulfil my dream of studying in Sweden. Without your help and support during my bachelor years, I would not be here today.

To all the people, who have contributed to this thesis work with their expertise and collaborated with me on the research papers – thank you! I would like to acknowledge Dr. Hani Nasser Abdelhamid, Dr. Binsi Pillai, Dr. Stephen A. Hall, Dr. Nebu Thomas, Dr. Andreas Mautner, Dr. Jakob Redlinger-Pohn, Dr. Zoltán Bacsik and Dr. A. Ken Inge. Special thanks to my collaborators/groupmates/friends, so Dr. Andrea, Dr. Vera, Dr. Salvatore, Dr. Erik, and soon to be Dr. Ximena – thank you for your support, help and fruitful discussions. It was such a pleasure working with all of you! Moreover, I would like to thank Dr. Anumol Ashok, Dr. Tom Willhammar, Mathias Nero, Dr. Jing Li, Prof. Andrey Shchukarev and Prof. Ulrica Edlund for conducting additional experiments presented within this thesis. Thanks to AddNorth for extrusion of all of the filaments used within this thesis!

I would also like to thank all the people of MMK for creating a great working environment. All of the professors, researchers and administration staff were always very kind, welcoming and helpful. Special thanks to my co-supervisor Lennart. I would like to thank Kjell, Mirva, Jakob, Ken, Zoltán and Jekabs for their patience in helping me master new instruments and techniques, as well as help me design some of the experimental setups. You never made me feel like asking too many questions was a problem – thank you for that!

To my old office-mates, Andrea and Dimi – PhDeeing together with you during the global pandemic made this crazy time so much easier. I love you guys and I will always cherish the memories we shared during the long office hours and of course during the California’22 trip! To Ximena, my current office mate and a friend, thank you for always being helpful and brightening many gloomy days with a good

joke! I always appreciate a good laugh shared with you and I absolutely admire your passion for science. You are a great scientist – there is a very bright future in the academia awaiting you! Thank you so much Vera for being a great friend and a colleague – you are a walking inspiration and a definition of a superwoman! I am absolutely positive that you will meet the Swedish king at least once more in your life, during the acceptance of your Nobel prize perhaps? Salvatore – I wish you have joined our group much earlier! You are a great scientist and a fun guy to hang out with! To my azizamis Atefeh, Sadaf and Elnaz – you guys make me suspect that there is something in the Iranian water that turns people into the absolutely kindest and sweetest sort! It is always such a pleasure hanging out with you! To all the fellow PhD students and post-docs at MMK – thank you! Lunchtime shared together with all of you was something that I was always looking forward to. Apart from all the previously mentioned people, I would like to acknowledge Houssine, Jessica, Jędrzej, Jianhong, Xia, Martin, Joy, Matilda, Fengyang, Alberto, Ievgen, Alexandros, Unnimaya, Maja-Stina, Kanglei, Ehsan, Blanca, Luis, Shiqi, Kosta, Pierre, Jinrong, Moh, Miao, Agnes, Jian, and the fifth-floorers Fredrik, Erik, Laura P. and Laura S. Special thanks to the lunchmates and fellow PhD council 2021 members: Carina, Irina, Misha, Molly and Roja. Many, many, many more people made my time at MMK unforgettable - thank you all! Outside of MMK, I met a bunch of fantastic and inspiring PhD students from all over Sweden thanks to being a part of the WWSC network – special thanks to my favourite Swedish girl – Dr. Linnea (now my newest office mate!) and my favourite Moldovan girl – Dr. Iuliana! You guys made the WWSC meetings so much more fun and special!

To all of the outside-academia friends and family, thank you! Viola and Ola– thank you for your friendship. Even if some of you are on the other side of the world, I know I can always count on you. My sisters and their families – love you and thank you! Dagmara – my 11 years older spiritual (and physically identical) twin sister – without you, I would definitely not be here today. Thank you for everything. Asia – thank you for your constant support and love throughout the years. It means the world to me to be able to reach out to you whenever I need help. Olek and Wojtek – men, who came to my life when I was just 12 and 14 years old, respectively, and became my brothers-in-law. However, over the years, the ‘in-law’ part has vanished. You had bigger impact on my life than you know. Thank you for everything. To Ola, Leon and Ania, my nieces and nephew, please continue being the sweetest and smartest kids on the planet. Remember that the sky is the limit and you can achieve whatever you set your minds to! I am such a proud auntie seeing you mould into these little fantastic, joyful and curious individuals. Love you so much my kiddos! To my Stockholm-based outside academia friends – thank you for keeping me sane! Special shout out to Anna – my opera nights date and the loveliest person on the planet.

Drozdzy Rodzice, z całego serca dziękuję Wam za wszystko. Bez Was, Mamo i Tato, nie dałabym rady ukończyć studiów w Szwecji. Gdyby nie Wy, nie byłoby mnie na świecie, a więc świat, nie tylko nie

doświadczyłby tej przepotężnej siły humoru, której utożsamieniem jestem, ale przede wszystkim współczesna nauka byłaby uboższa o moje przełomowe odkrycia w dziedzinie wykorzystania biomateriałów do produkcji filtrów do oczyszczania wody przy użyciu technologii druku 3D. Także, ta rozprawa doktorska to zdecydowanie nasza wspólna praca! Jestem Wam bardzo wdzięczna za to, że zawsze mogłam na Was liczyć. Wasze wsparcie było nieocenione i bez niego nie osiągnęłabym swoich celów.

Last, but definitely not least – my biggest supporter, cheerleader and love – Charis. Thank you for being my rock through all these years, from bachelor, through master, and now the PhD studies. I would have never been able to do all of this without you. I am very lucky to have a man like you by my side. Honorary mention to our furever-puppy, Mando, for filling our house with joy by constantly expressing his unconditional love.

References

- (1) *The United Nations world water development report 2020: water and climate change - UNESCO Digital Library*. <https://unesdoc.unesco.org/ark:/48223/pf0000372985.locale=en> (accessed 2021-03-30).
- (2) Geyer, R.; Jambeck, J. R.; Law, K. L. Production, Use, and Fate of All Plastics Ever Made. *Science Advances* **2017**, *3* (7), e1700782. <https://doi.org/10.1126/sciadv.1700782>.
- (3) Schwarzenbach, R. P.; Egli, T.; Hofstetter, T. B.; Von Gunten, U.; Wehrli, B. Global Water Pollution and Human Health. *Annu. Rev. Environ. Resour.* **2010**, *35* (1), 109–136. <https://doi.org/10.1146/annurev-environ-100809-125342>.
- (4) Galvão, A.; Aleixo, M.; De Pablo, H.; Lopes, C.; Raimundo, J. Microplastics in Wastewater: Microfiber Emissions from Common Household Laundry. *Environ Sci Pollut Res* **2020**, *27* (21), 26643–26649. <https://doi.org/10.1007/s11356-020-08765-6>.
- (5) *Water Framework Directive*. https://environment.ec.europa.eu/topics/water/water-framework-directive_en (accessed 2023-05-04).
- (6) *THE 17 GOALS / Sustainable Development*. <https://sdgs.un.org/goals> (accessed 2023-05-04).
- (7) *Guidelines for drinking-water quality, 4th edition, incorporating the 1st addendum*. <https://www.who.int/publications-detail-redirect/9789241549950> (accessed 2023-06-07).
- (8) Borbély, G.; Nagy, E. Removal of Zinc and Nickel Ions by Complexation–Membrane Filtration Process from Industrial Wastewater. *Desalination* **2009**, *240* (1), 218–226. <https://doi.org/10.1016/j.desal.2007.11.073>.
- (9) Bakkaloglu, I.; Butter, T. J.; Evison, L. M.; Holland, F. S.; Hancockt, I. C. Screening of Various Types Biomass for Removal and Recovery of Heavy Metals (ZN, CU, NI) by Biosorption, Sedimentation and Desorption. *Water Science and Technology* **1998**, *38* (6), 269–277. [https://doi.org/10.1016/S0273-1223\(98\)00587-3](https://doi.org/10.1016/S0273-1223(98)00587-3).
- (10) Kim, J.; Yoon, S.; Choi, M.; Min, K. J.; Park, K. Y.; Chon, K.; Bae, S. Metal Ion Recovery from Electrodialysis-Concentrated Plating Wastewater via Pilot-Scale Sequential Electrowinning/Chemical Precipitation. *Journal of Cleaner Production* **2022**, *330*, 129879. <https://doi.org/10.1016/j.jclepro.2021.129879>.
- (11) Gryta, M.; Tomaszewska, M.; Karakulski, K. Wastewater Treatment by Membrane Distillation. *Desalination* **2006**, *198* (1), 67–73. <https://doi.org/10.1016/j.desal.2006.09.010>.
- (12) Ćurković, L.; Cerjan-Stefanović, Š.; Filipan, T. Metal Ion Exchange by Natural and Modified Zeolites. *Water Research* **1997**, *31* (6), 1379–1382. [https://doi.org/10.1016/S0043-1354\(96\)00411-3](https://doi.org/10.1016/S0043-1354(96)00411-3).
- (13) Zheng, J.; Su, C.; Zhou, J.; Xu, L.; Qian, Y.; Chen, H. Effects and Mechanisms of Ultraviolet, Chlorination, and Ozone Disinfection on Antibiotic Resistance Genes in Secondary Effluents of Municipal Wastewater Treatment Plants. *Chemical Engineering Journal* **2017**, *317*, 309–316. <https://doi.org/10.1016/j.cej.2017.02.076>.
- (14) Waqas, S.; Bilal, M. R.; Man, Z.; Wibisono, Y.; Jaafar, J.; Indra Mahlia, T. M.; Khan, A. L.; Aslam, M. Recent Progress in Integrated Fixed-Film Activated Sludge Process for Wastewater Treatment: A Review. *Journal of Environmental Management* **2020**, *268*, 110718. <https://doi.org/10.1016/j.jenvman.2020.110718>.
- (15) Tomar, P.; Suthar, S. Urban Wastewater Treatment Using Vermi-Biofiltration System. *Desalination* **2011**, *282*, 95–103. <https://doi.org/10.1016/j.desal.2011.09.007>.
- (16) Thavamani, S. S.; Rajkumar, R. Removal of Cr(VI), Cu(II), Pb(II) and Ni(II) from Aqueous Solutions by Adsorption on Alumina. **2013**, *3*, 5.
- (17) Wang, R.; Zhang, W.; Zhang, L.; Hua, T.; Tang, G.; Peng, X.; Hao, M.; Zuo, Q. Adsorption Characteristics of Cu(II) and Zn(II) by Nano-Alumina Material Synthesized by the Sol-Gel Method in Batch Mode. *Environ Sci Pollut Res* **2019**, *26* (2), 1595–1605. <https://doi.org/10.1007/s11356-018-3453-5>.
- (18) Deravanesiyan, M.; Beheshti, M.; Malekpour, A. Alumina Nanoparticles Immobilization onto the NaX Zeolite and the Removal of Cr (III) and Co (II) Ions from Aqueous Solutions. *Journal*

- of Industrial and Engineering Chemistry **2015**, *21*, 580–586.
<https://doi.org/10.1016/j.jiec.2014.03.023>.
- (19) Mahapatra, A.; Mishra, B. G.; Hota, G. Electrospun Fe₂O₃–Al₂O₃ Nanocomposite Fibers as Efficient Adsorbent for Removal of Heavy Metal Ions from Aqueous Solution. *Journal of Hazardous Materials* **2013**, *258–259*, 116–123. <https://doi.org/10.1016/j.jhazmat.2013.04.045>.
 - (20) Guibal, E.; Lorenzelli, R.; Vincent, T.; Cloirec, P. L. Application of Silica Gel to Metal Ion Sorption: Static and Dynamic Removal of Uranyl Ions. *Environmental Technology* **1995**, *16* (2), 101–114. <https://doi.org/10.1080/09593331608616251>.
 - (21) FISCHER, R. J.; PANG, D.; BEATTY, S. T.; ROSENBERG, E. Silica-Polyamine Composite Materials for Heavy Metal Ion Removal, Recovery, and Recycling. II. Metal Ion Separations from Mine Wastewater and Soft Metal Ion Extraction Efficiency*. *Separation Science and Technology* **1999**, *34* (16), 3125–3137. <https://doi.org/10.1081/SS-100100826>.
 - (22) Burke, A. M.; Hanrahan, J. P.; Healy, D. A.; Sodeau, J. R.; Holmes, J. D.; Morris, M. A. Large Pore Bi-Functionalised Mesoporous Silica for Metal Ion Pollution Treatment. *Journal of Hazardous Materials* **2009**, *164* (1), 229–234. <https://doi.org/10.1016/j.jhazmat.2008.07.146>.
 - (23) Hu, H.; Wang, Z.; Pan, L. Synthesis of Monodisperse Fe₃O₄@silica Core–Shell Microspheres and Their Application for Removal of Heavy Metal Ions from Water. *Journal of Alloys and Compounds* **2010**, *492* (1), 656–661. <https://doi.org/10.1016/j.jallcom.2009.11.204>.
 - (24) Gupta, V. K.; Suhas. Application of Low-Cost Adsorbents for Dye Removal – A Review. *Journal of Environmental Management* **2009**, *90* (8), 2313–2342. <https://doi.org/10.1016/j.jenvman.2008.11.017>.
 - (25) Kadirvelu, K.; Namasivayam, C. Activated Carbon from Coconut Coirpith as Metal Adsorbent: Adsorption of Cd(II) from Aqueous Solution. *Advances in Environmental Research* **2003**, *7* (2), 471–478. [https://doi.org/10.1016/S1093-0191\(02\)00018-7](https://doi.org/10.1016/S1093-0191(02)00018-7).
 - (26) Kadirvelu, K.; Thamaraiselvi, K.; Namasivayam, C. Adsorption of Nickel(II) from Aqueous Solution onto Activated Carbon Prepared from Coirpith. *Separation and Purification Technology* **2001**, *24* (3), 497–505. [https://doi.org/10.1016/S1383-5866\(01\)00149-6](https://doi.org/10.1016/S1383-5866(01)00149-6).
 - (27) Georgouvelas, D.; Abdelhamid, H. N.; Li, J.; Edlund, U.; Mathew, A. P. All-Cellulose Functional Membranes for Water Treatment: Adsorption of Metal Ions and Catalytic Decolorization of Dyes. *Carbohydrate Polymers* **2021**, *264*, 118044. <https://doi.org/10.1016/j.carbpol.2021.118044>.
 - (28) Jalvo, B.; Aguilar-Sanchez, A.; Ruiz-Caldas, M.-X.; Mathew, A. P. Water Filtration Membranes Based on Non-Woven Cellulose Fabrics: Effect of Nanopolysaccharide Coatings on Selective Particle Rejection, Antifouling, and Antibacterial Properties. *Nanomaterials* **2021**, *11* (7), 1752. <https://doi.org/10.3390/nano11071752>.
 - (29) Aguilar-Sanchez, A.; Jalvo, B.; Mautner, A.; Nameer, S.; Pöhler, T.; Tammelin, T.; Mathew, A. P. Waterborne Nanocellulose Coatings for Improving the Antifouling and Antibacterial Properties of Polyethersulfone Membranes. *Journal of Membrane Science* **2021**, *620*, 118842. <https://doi.org/10.1016/j.memsci.2020.118842>.
 - (30) Liu, P.; Sehaqui, H.; Tingaut, P.; Wichser, A.; Oksman, K.; Mathew, A. P. Cellulose and Chitin Nanomaterials for Capturing Silver Ions (Ag⁺) from Water via Surface Adsorption. *Cellulose* **2014**, *21* (1), 449–461. <https://doi.org/10.1007/s10570-013-0139-5>.
 - (31) Liu, P.; Oksman, K.; Mathew, A. P. Surface Adsorption and Self-Assembly of Cu(II) Ions on TEMPO-Oxidized Cellulose Nanofibers in Aqueous Media. *Journal of Colloid and Interface Science* **2016**, *464*, 175–182. <https://doi.org/10.1016/j.jcis.2015.11.033>.
 - (32) Davila-Rodriguez, J. L.; Escobar-Barrios, V. A.; Shirai, K.; Rangel-Mendez, J. R. Synthesis of a Chitin-Based Biocomposite for Water Treatment: Optimization for Fluoride Removal. *Journal of Fluorine Chemistry* **2009**, *130* (8), 718–726. <https://doi.org/10.1016/j.jfluchem.2009.05.012>.
 - (33) Gopi, S.; Balakrishnan, P.; Divya, C.; Valic, S.; Bajsic, E. G.; Pius, A.; Thomas, S. Facile Synthesis of Chitin Nanocrystals Decorated on 3D Cellulose Aerogels as a New Multi-Functional Material for Waste Water Treatment with Enhanced Anti-Bacterial and Anti-Oxidant Properties. *New J. Chem.* **2017**, *41* (21), 12746–12755. <https://doi.org/10.1039/C7NJ02392H>.
 - (34) Shi, J.; Zhang, L.; Xiao, P.; Huang, Y.; Chen, P.; Wang, X.; Gu, J.; Zhang, J.; Chen, T. Biodegradable PLA Nonwoven Fabric with Controllable Wettability for Efficient Water

- Purification and Photocatalysis Degradation. *ACS Sustainable Chem. Eng.* **2018**, 6 (2), 2445–2452. <https://doi.org/10.1021/acssuschemeng.7b03897>.
- (35) Kim, K.; Ratri, M. C.; Choe, G.; Nam, M.; Cho, D.; Shin, K. Three-Dimensional, Printed Water-Filtration System for Economical, on-Site Arsenic Removal. *PLOS ONE* **2020**, 15 (4), e0231475. <https://doi.org/10.1371/journal.pone.0231475>.
 - (36) Rasal, R. M.; Janorkar, A. V.; Hirt, D. E. Poly(Lactic Acid) Modifications. *Progress in Polymer Science* **2010**, 35 (3), 338–356. <https://doi.org/10.1016/j.progpolymsci.2009.12.003>.
 - (37) Muller, J.; González-Martínez, C.; Chiralt, A. Combination of Poly(Lactic) Acid and Starch for Biodegradable Food Packaging. *Materials* **2017**, 10 (8), 952. <https://doi.org/10.3390/ma10080952>.
 - (38) Gao, P.; Kundu, A.; Coulter, J. Vibration-Assisted Injection Molding: An Efficient Process for Enhanced Crystallinity Development and Mechanical Characteristics for Poly Lactic Acid. *Int J Adv Manuf Technol* **2022**, 121 (5), 3111–3124. <https://doi.org/10.1007/s00170-022-09522-4>.
 - (39) Aversa, C.; Barletta, M.; Gisario, A.; Prati, R.; Vesco, S. Injection-Stretch Blow Molding of Poly (Lactic Acid)/Polybutylene Succinate Blends for the Manufacturing of Bottles. *Journal of Applied Polymer Science* **2022**, 139 (4), 51557. <https://doi.org/10.1002/app.51557>.
 - (40) Lacambra-Andreu, X.; Morelle, X. P.; Maazouz, A.; Chenal, J.-M.; Lamnawar, K. Rheological Investigation and Modeling of Healing Properties during Extrusion-Based 3D Printing of Poly(Lactic-Acid). *Rheol Acta* **2023**, 62 (1), 31–44. <https://doi.org/10.1007/s00397-022-01377-6>.
 - (41) Goument, C.; Gerges, T.; Lombard, P.; Lakhdar, H.; Arli, M.; Gilmus, V. M.; Lambert, S. A.; Allard, B.; Charmeau, J.-Y.; Cabrera, M. In-Mold Electronics on Poly(Lactic Acid): Towards a More Sustainable Mass Production of Plastronic Devices. *Int J Adv Manuf Technol* **2023**, 125 (5), 2643–2660. <https://doi.org/10.1007/s00170-023-10878-4>.
 - (42) Guo, S.; Zhou, Z.; Yu, S.; Chen, Z.; Xiang, H.; Zhu, M. The Synergistic Effect of Heterogeneous Nucleation and Stress-Induced Crystallization on Supramolecular Structure and Performances of Poly(Lactic Acid) Melt-Spun Fibers. *International Journal of Biological Macromolecules* **2023**, 226, 1579–1587. <https://doi.org/10.1016/j.ijbiomac.2022.11.270>.
 - (43) Athanasiou, K. A.; Niederauer, G. G.; Agrawal, C. M. Sterilization, Toxicity, Biocompatibility and Clinical Applications of Polylactic Acid/ Polyglycolic Acid Copolymers. *Biomaterials* **1996**, 17 (2), 93–102. [https://doi.org/10.1016/0142-9612\(96\)85754-1](https://doi.org/10.1016/0142-9612(96)85754-1).
 - (44) Nugraha, M. W.; Wirzal, M. D. H.; Ali, F.; Roza, L.; Sambudi, N. S. Electrospun Polylactic Acid/ Tungsten Oxide/ Amino-Functionalized Carbon Quantum Dots (PLA/WO₃/N-CQDs) Fibers for Oil/Water Separation and Photocatalytic Decolorization. *Journal of Environmental Chemical Engineering* **2021**, 9 (5), 106033. <https://doi.org/10.1016/j.jece.2021.106033>.
 - (45) Su, Y.; Zhao, Y.; Zheng, W.; Yu, H.; Liu, Y.; Xu, L. Asymmetric Sc-PLA Membrane with Multi-Scale Microstructures: Wettability, Antifouling, and Oil–Water Separation. *ACS Appl. Mater. Interfaces* **2020**, 12 (49), 55520–55526. <https://doi.org/10.1021/acsmi.0c17545>.
 - (46) Shokri, E.; Khangahi, B.; Esmizadeh, E.; Etemadi, H. Biopolymer-Based Adsorptive Membrane for Simultaneous Removal of Cationic and Anionic Heavy Metals from Water. *Int. J. Environ. Sci. Technol.* **2022**, 19 (5), 4167–4180. <https://doi.org/10.1007/s13762-021-03592-9>.
 - (47) Zia, Q.; Tabassum, M.; Lu, Z.; Khawar, M. T.; Song, J.; Gong, H.; Meng, J.; Li, Z.; Li, J. Porous Poly(L–Lactic Acid)/Chitosan Nanofibres for Copper Ion Adsorption. *Carbohydrate Polymers* **2020**, 227, 115343. <https://doi.org/10.1016/j.carbpol.2019.115343>.
 - (48) Zia, Q.; Tabassum, M.; Meng, J.; Xin, Z.; Gong, H.; Li, J. Polydopamine-Assisted Grafting of Chitosan on Porous Poly (L-Lactic Acid) Electrospun Membranes for Adsorption of Heavy Metal Ions. *International Journal of Biological Macromolecules* **2021**, 167, 1479–1490. <https://doi.org/10.1016/j.ijbiomac.2020.11.101>.
 - (49) Yan, C.; Ma, S.; Ji, Z.; Guo, Y.; Liu, Z.; Zhang, X.; Wang, X. 3D Printing of an Oil/Water Mixture Separator with In Situ Demulsification and Separation. *Polymers* **2019**, 11 (5), 774. <https://doi.org/10.3390/polym11050774>.
 - (50) Shi, Z.; Xu, C.; Chen, F.; Wang, Y.; Li, L.; Meng, Q.; Zhang, R. Renewable Metal–Organic-Frameworks-Coated 3D Printing Film for Removal of Malachite Green. *RSC Advances* **2017**, 7 (79), 49947–49952. <https://doi.org/10.1039/C7RA10912A>.

- (51) Xing, R.; Huang, R.; Qi, W.; Su, R.; He, Z. Three-Dimensionally Printed Bioinspired Superhydrophobic PLA Membrane for Oil-Water Separation. *AIChE Journal* **2018**, *64* (10), 3700–3708. <https://doi.org/10.1002/aic.16347>.
- (52) Park, S.-S.; Lee, Y.-S.; Lee, S.-W.; Repo, E.; Kim, T.-H.; Park, Y.; Hwang, Y. Facile Surface Treatment of 3D-Printed PLA Filter for Enhanced Graphene Oxide Doping and Effective Removal of Cationic Dyes. *Polymers* **2023**, *15* (2), 269. <https://doi.org/10.3390/polym15020269>.
- (53) Anita Lett, J.; Sagadevan, S.; Fatimah, I.; Hoque, M. E.; Lokanathan, Y.; Léonard, E.; Alshahateet, S. F.; Schirhagl, R.; Oh, W. C. Recent Advances in Natural Polymer-Based Hydroxyapatite Scaffolds: Properties and Applications. *European Polymer Journal* **2021**, *148*, 110360. <https://doi.org/10.1016/j.eurpolymj.2021.110360>.
- (54) Dorozhkin, S. V. Bioceramics of Calcium Orthophosphates. *Biomaterials* **2010**, *31* (7), 1465–1485. <https://doi.org/10.1016/j.biomaterials.2009.11.050>.
- (55) Venkatesan, J.; Qian, Z. J.; Ryu, B.; Thomas, N. V.; Kim, S. K. A Comparative Study of Thermal Calcination and an Alkaline Hydrolysis Method in the Isolation of Hydroxyapatite from Thunnus Obesus Bone. *Biomed. Mater.* **2011**, *6* (3), 035003. <https://doi.org/10.1088/1748-6041/6/3/035003>.
- (56) Ibrahim, M.; Labaki, M.; Giraudon, J.-M.; Lamonier, J.-F. Hydroxyapatite, a Multifunctional Material for Air, Water and Soil Pollution Control: A Review. *Journal of Hazardous Materials* **2020**, *383*, 121139. <https://doi.org/10.1016/j.jhazmat.2019.121139>.
- (57) Abd El-aziz, A. M.; El-Maghraby, A.; Taha, N. A. Comparison between Polyvinyl Alcohol (PVA) Nanofiber and Polyvinyl Alcohol (PVA) Nanofiber/Hydroxyapatite (HA) for Removal of Zn²⁺ Ions from Wastewater. *Arabian Journal of Chemistry* **2017**, *10* (8), 1052–1060. <https://doi.org/10.1016/j.arabjc.2016.09.025>.
- (58) Trung, T. S.; Minh, N. C.; Cuong, H. N.; Phuong, P. T. D.; Dat, P. A.; Nam, P. V.; Hoa, N. V. Valorization of Fish and Shrimp Wastes to Nano-Hydroxyapatite/Chitosan Biocomposite for Wastewater Treatment. *Journal of Science: Advanced Materials and Devices* **2022**, *7* (4), 100485. <https://doi.org/10.1016/j.jsamd.2022.100485>.
- (59) Hsu, H.-C.; Chung, Y.-C.; Wu, S.-C.; Ho, Y.-C.; Chang, H.-H.; Ho, W.-F. Preparation of Chitosan/Hydroxyapatite Composite Coating Obtained from Crab Shells on Hierarchical Micro/Nano-Textured Ti Surface. *Surface and Coatings Technology* **2022**, *437*, 128364. <https://doi.org/10.1016/j.surfcoat.2022.128364>.
- (60) Jang, S. H.; Jeong, Y. G.; Min, B. G.; Lyoo, W. S.; Lee, S. C. Preparation and Lead Ion Removal Property of Hydroxyapatite/Polyacrylamide Composite Hydrogels. *Journal of Hazardous Materials* **2008**, *159* (2), 294–299. <https://doi.org/10.1016/j.jhazmat.2008.02.018>.
- (61) Jang, S. H.; Min, B. G.; Jeong, Y. G.; Lyoo, W. S.; Lee, S. C. Removal of Lead Ions in Aqueous Solution by Hydroxyapatite/Polyurethane Composite Foams. *Journal of Hazardous Materials* **2008**, *152* (3), 1285–1292. <https://doi.org/10.1016/j.jhazmat.2007.08.003>.
- (62) Dong, L.; Zhu, Z.; Qiu, Y.; Zhao, J. Removal of Lead from Aqueous Solution by Hydroxyapatite/Magnetite Composite Adsorbent. *Chemical Engineering Journal* **2010**, *165* (3), 827–834. <https://doi.org/10.1016/j.cej.2010.10.027>.
- (63) Feng, Y.; Gong, J.-L.; Zeng, G.-M.; Niu, Q.-Y.; Zhang, H.-Y.; Niu, C.-G.; Deng, J.-H.; Yan, M. Adsorption of Cd (II) and Zn (II) from Aqueous Solutions Using Magnetic Hydroxyapatite Nanoparticles as Adsorbents. *Chemical Engineering Journal* **2010**, *162* (2), 487–494. <https://doi.org/10.1016/j.cej.2010.05.049>.
- (64) Wang, Y.; Hu, L.; Zhang, G.; Yan, T.; Yan, L.; Wei, Q.; Du, B. Removal of Pb(II) and Methylene Blue from Aqueous Solution by Magnetic Hydroxyapatite-Immobilized Oxidized Multi-Walled Carbon Nanotubes. *Journal of Colloid and Interface Science* **2017**, *494*, 380–388. <https://doi.org/10.1016/j.jcis.2017.01.105>.
- (65) Introduction. In *Comprehensive Cellulose Chemistry*; John Wiley & Sons, Ltd, 1998; pp 1–7. <https://doi.org/10.1002/3527601929.ch1>.
- (66) Klemm, D.; Heublein, B.; Fink, H.-P.; Bohn, A. Cellulose: Fascinating Biopolymer and Sustainable Raw Material. *Angewandte Chemie International Edition* **2005**, *44* (22), 3358–3393. <https://doi.org/10.1002/anie.200460587>.

- (67) Mérida, H.; Sandoval-Sierra, J. V.; Diéguez-Uribeondo, J.; Bulone, V. Analyses of Extracellular Carbohydrates in Oomycetes Unveil the Existence of Three Different Cell Wall Types. *Eukaryotic Cell* **2013**, *12* (2), 194–203. <https://doi.org/10.1128/ec.00288-12>.
- (68) Klemm, D.; Kramer, F.; Moritz, S.; Lindström, T.; Ankerfors, M.; Gray, D.; Dorris, A. Nanocelluloses: A New Family of Nature-Based Materials. *Angewandte Chemie International Edition* **2011**, *50* (24), 5438–5466. <https://doi.org/10.1002/anie.201001273>.
- (69) Lombardo, S.; Villares, A. Engineered Multilayer Microcapsules Based on Polysaccharides Nanomaterials. *Molecules* **2020**, *25* (19), 4420. <https://doi.org/10.3390/molecules25194420>.
- (70) Lagerwall, J. P. F.; Schütz, C.; Salajkova, M.; Noh, J.; Hyun Park, J.; Scalia, G.; Bergström, L. Cellulose Nanocrystal-Based Materials: From Liquid Crystal Self-Assembly and Glass Formation to Multifunctional Thin Films. *NPG Asia Mater* **2014**, *6* (1), e80–e80. <https://doi.org/10.1038/am.2013.69>.
- (71) Siddiqui, N.; Mills, R. H.; Gardner, D. J.; Bousfield, D. Production and Characterization of Cellulose Nanofibers from Wood Pulp. *Journal of Adhesion Science and Technology* **2011**, *25* (6–7), 709–721. <https://doi.org/10.1163/016942410X525975>.
- (72) Saito, T.; Hirota, M.; Tamura, N.; Kimura, S.; Fukuzumi, H.; Heux, L.; Isogai, A. Individualization of Nano-Sized Plant Cellulose Fibrils by Direct Surface Carboxylation Using TEMPO Catalyst under Neutral Conditions. *Biomacromolecules* **2009**, *10* (7), 1992–1996. <https://doi.org/10.1021/bm900414t>.
- (73) Saito, T.; Isogai, A. Ion-Exchange Behavior of Carboxylate Groups in Fibrous Cellulose Oxidized by the TEMPO-Mediated System. *Carbohydrate Polymers* **2005**, *61* (2), 183–190. <https://doi.org/10.1016/j.carbpol.2005.04.009>.
- (74) Isogai, A.; Saito, T.; Fukuzumi, H. TEMPO-Oxidized Cellulose Nanofibers. *Nanoscale* **2011**, *3* (1), 71–85. <https://doi.org/10.1039/C0NR00583E>.
- (75) Fiol, N.; Vásquez, M. G.; Pereira, M.; Tarrés, Q.; Mutjé, P.; Delgado-Aguilar, M. TEMPO-Oxidized Cellulose Nanofibers as Potential Cu(II) Adsorbent for Wastewater Treatment. *Cellulose* **2019**, *26* (2), 903–916. <https://doi.org/10.1007/s10570-018-2106-7>.
- (76) Lombardo, S.; Thielemans, W. Thermodynamics of Adsorption on Nanocellulose Surfaces. *Cellulose* **2019**, *26* (1), 249–279. <https://doi.org/10.1007/s10570-018-02239-2>.
- (77) Aguilar-Sanchez, A.; Jalvo, B.; Mautner, A.; Nameer, S.; Pöhler, T.; Tammelin, T.; Mathew, A. P. Waterborne Nanocellulose Coatings for Improving the Antifouling and Antibacterial Properties of Polyethersulfone Membranes. *Journal of Membrane Science* **2021**, *620*, 118842. <https://doi.org/10.1016/j.memsci.2020.118842>.
- (78) Xue, J.; Zhu, E.; Zhu, H.; Liu, D.; Cai, H.; Xiong, C.; Yang, Q.; Shi, Z. Dye Adsorption Performance of Nanocellulose Beads with Different Carboxyl Group Content. *Cellulose* **2023**, *30* (3), 1623–1636. <https://doi.org/10.1007/s10570-022-04964-1>.
- (79) Antonini, C.; Wu, T.; Zimmermann, T.; Kherbeche, A.; Thoraval, M.-J.; Nyström, G.; Geiger, T. Ultra-Porous Nanocellulose Foams: A Facile and Scalable Fabrication Approach. *Nanomaterials* **2019**, *9* (8), 1142. <https://doi.org/10.3390/nano9081142>.
- (80) Wang, Y.; Ni, Q.; Geng, B.; Wu, X.; Shan, G.; Feng, J.; Zhou, G.; Wu, Q.; Du, M. Facile Preparation of Ni Foam/Bacterial Nanocellulose Composite for Oil/Water Separation. *Fibers Polym* **2023**, *24* (4), 1441–1452. <https://doi.org/10.1007/s12221-023-00152-5>.
- (81) Shamshina, J. L.; Berton, P.; Rogers, R. D. Advances in Functional Chitin Materials: A Review. *ACS Sustainable Chem. Eng.* **2019**, *7* (7), 6444–6457. <https://doi.org/10.1021/acssuschemeng.8b06372>.
- (82) Peniche, C.; Argüelles-Monal, W.; Goycoolea, F. M. Chapter 25 - Chitin and Chitosan: Major Sources, Properties and Applications. In *Monomers, Polymers and Composites from Renewable Resources*; Belgacem, M. N., Gandini, A., Eds.; Elsevier: Amsterdam, 2008; pp 517–542. <https://doi.org/10.1016/B978-0-08-045316-3.00025-9>.
- (83) Yan, N.; Chen, X. Sustainability: Don't Waste Seafood Waste. *Nature* **2015**, *524* (7564), 155–157. <https://doi.org/10.1038/524155a>.
- (84) Das, S.; Roy, D.; Sen, R. Chapter Two - Utilization of Chitinous Wastes for the Production of Chitinase. In *Advances in Food and Nutrition Research*; Kim, S.-K., Toldrá, F., Eds.; Marine Enzymes Biotechnology: Production and Industrial Applications, Part I - Production of

- Enzymes; Academic Press, 2016; Vol. 78, pp 27–46.
<https://doi.org/10.1016/bs.afnr.2016.04.001>.
- (85) Ngasotter, S.; Sampath, L.; Xavier, K. A. M. Nanochitin: An Update Review on Advances in Preparation Methods and Food Applications. *Carbohydrate Polymers* **2022**, *291*, 119627. <https://doi.org/10.1016/j.carbpol.2022.119627>.
 - (86) Hong, S.; Yuan, Y.; Yang, Q.; Chen, L.; Deng, J.; Chen, W.; Lian, H.; Mota-Morales, J. D.; Liimatainen, H. Choline Chloride-Zinc Chloride Deep Eutectic Solvent Mediated Preparation of Partial O-Acetylation of Chitin Nanocrystal in One Step Reaction. *Carbohydrate Polymers* **2019**, *220*, 211–218. <https://doi.org/10.1016/j.carbpol.2019.05.075>.
 - (87) Marchessault, R. H.; Morehead, F. F.; Walter, N. M. Liquid Crystal Systems from Fibrillar Polysaccharides. *Nature* **1959**, *184* (4686), 632–633. <https://doi.org/10.1038/184632a0>.
 - (88) Ifuku, S.; Saimoto, H. Chitin Nanofibers: Preparations, Modifications, and Applications. *Nanoscale* **2012**, *4* (11), 3308–3318. <https://doi.org/10.1039/C2NR30383C>.
 - (89) Fan, Y.; Saito, T.; Isogai, A. Chitin Nanocrystals Prepared by TEMPO-Mediated Oxidation of α -Chitin. *Biomacromolecules* **2008**, *9* (1), 192–198. <https://doi.org/10.1021/bm700966g>.
 - (90) Zhang, D.; Xiao, J.; Guo, Q.; Yang, J. 3D-Printed Highly Porous and Reusable Chitosan Monoliths for Cu(II) Removal. *J Mater Sci* **2019**, *54* (8), 6728–6741. <https://doi.org/10.1007/s10853-019-03332-y>.
 - (91) Appuhamillage, G. A.; Berry, D. R.; Benjamin, C. E.; Luzuriaga, M. A.; Reagan, J. C.; Gassensmith, J. J.; Smaldone, R. A. A Biopolymer-Based 3D Printable Hydrogel for Toxic Metal Adsorption from Water. *Polymer International* **2019**, *68* (5), 964–971. <https://doi.org/10.1002/pi.5787>.
 - (92) Rani Sethy, T.; Biswal, T.; Kumar Sahoo, P. An Indigenous Tool for the Adsorption of Rare Earth Metal Ions from the Spent Magnet E-Waste: An Eco-Friendly Chitosan Biopolymer Nanocomposite Hydrogel. *Separation and Purification Technology* **2023**, *309*, 122935. <https://doi.org/10.1016/j.seppur.2022.122935>.
 - (93) Lin, Z.; Yang, Y.; Liang, Z.; Zeng, L.; Zhang, A. Preparation of Chitosan/Calcium Alginate/Bentonite Composite Hydrogel and Its Heavy Metal Ions Adsorption Properties. *Polymers* **2021**, *13* (11), 1891. <https://doi.org/10.3390/polym13111891>.
 - (94) Karimi, F.; Ayati, A.; Tanhaei, B.; Sanati, A. L.; Afshar, S.; Kardan, A.; Dabirifar, Z.; Karaman, C. Removal of Metal Ions Using a New Magnetic Chitosan Nano-Bio-Adsorbent; A Powerful Approach in Water Treatment. *Environmental Research* **2022**, *203*, 111753. <https://doi.org/10.1016/j.envres.2021.111753>.
 - (95) Bergamonti, L.; Bergonzi, C.; Graiff, C.; Lottici, P. P.; Bettini, R.; Elviri, L. 3D Printed Chitosan Scaffolds: A New TiO₂ Support for the Photocatalytic Degradation of Amoxicillin in Water. *Water Research* **2019**, *163*, 114841. <https://doi.org/10.1016/j.watres.2019.07.008>.
 - (96) Qian, Y.; Zhang, F.; Pang, H. A Review of MOFs and Their Composites-Based Photocatalysts: Synthesis and Applications. *Advanced Functional Materials* **2021**, *31* (37), 2104231. <https://doi.org/10.1002/adfm.202104231>.
 - (97) Li, H.; Li, L.; Lin, R.-B.; Zhou, W.; Zhang, Z.; Xiang, S.; Chen, B. Porous Metal-Organic Frameworks for Gas Storage and Separation: Status and Challenges. *EnergyChem* **2019**, *1* (1), 100006. <https://doi.org/10.1016/j.enchem.2019.100006>.
 - (98) Pascanu, V.; González Miera, G.; Inge, A. K.; Martín-Matute, B. Metal–Organic Frameworks as Catalysts for Organic Synthesis: A Critical Perspective. *J. Am. Chem. Soc.* **2019**, *141* (18), 7223–7234. <https://doi.org/10.1021/jacs.9b00733>.
 - (99) Grape, E. S.; Flores, J. G.; Hidalgo, T.; Martínez-Ahumada, E.; Gutiérrez-Alejandre, A.; Hautier, A.; Williams, D. R.; O’Keefe, M.; Öhrström, L.; Willhammar, T.; Horcajada, P.; Ibarra, I. A.; Inge, A. K. A Robust and Biocompatible Bismuth Ellagate MOF Synthesized Under Green Ambient Conditions. *J. Am. Chem. Soc.* **2020**, *142* (39), 16795–16804. <https://doi.org/10.1021/jacs.0c07525>.
 - (100) Ruiz-Caldas, M.-X.; Carlsson, J.; Sadiktsis, I.; Jaworski, A.; Nilsson, U.; Mathew, A. P. Cellulose Nanocrystals from Postconsumer Cotton and Blended Fabrics: A Study on Their Properties, Chemical Composition, and Process Efficiency. *ACS Sustainable Chem. Eng.* **2022**, *10* (11), 3787–3798. <https://doi.org/10.1021/acssuschemeng.2c00797>.

- (101) Palme, A.; Peterson, A.; de la Motte, H.; Theliander, H.; Brelid, H. Development of an Efficient Route for Combined Recycling of PET and Cotton from Mixed Fabrics. *Textiles and Clothing Sustainability* **2017**, *3* (1), 4. <https://doi.org/10.1186/s40689-017-0026-9>.
- (102) Ouchi, A.; Toida, T.; Kumaresan, S.; Ando, W.; Kato, J. A New Methodology to Recycle Polyester from Fabric Blends with Cellulose. *Cellulose* **2010**, *17* (1), 215–222. <https://doi.org/10.1007/s10570-009-9358-1>.
- (103) Silva, R. D.; Wang, X.; Byrne, N. Recycling Textiles: The Use of Ionic Liquids in the Separation of Cotton Polyester Blends. *RSC Adv.* **2014**, *4* (55), 29094–29098. <https://doi.org/10.1039/C4RA04306E>.
- (104) Skibicki, S.; Pultorak, M.; Kaszynska, M. Evaluation of Material Modification Using PET in 3D Concrete Printing Technology. *IOP Conf. Ser.: Mater. Sci. Eng.* **2021**, *1044* (1), 012002. <https://doi.org/10.1088/1757-899X/1044/1/012002>.
- (105) Schneevogt, H.; Stelzner, K.; Yilmaz, B.; Abali, B. E.; Klunker, A.; Völlmecke, C. Sustainability in Additive Manufacturing: Exploring the Mechanical Potential of Recycled PET Filaments. *Composites and Advanced Materials* **2021**, *30*, 263498332110000. <https://doi.org/10.1177/26349833211000063>.
- (106) Ferrari, F.; Esposito Corcione, C.; Montagna, F.; Maffezzoli, A. 3D Printing of Polymer Waste for Improving People's Awareness about Marine Litter. *Polymers* **2020**, *12* (8), 1738. <https://doi.org/10.3390/polym12081738>.
- (107) Idrees, M.; Jeelani, S.; Rangari, V. Three-Dimensional-Printed Sustainable Biochar-Recycled PET Composites. *ACS Sustainable Chem. Eng.* **2018**, *6* (11), 13940–13948. <https://doi.org/10.1021/acssuschemeng.8b02283>.
- (108) Mazzanti, V.; Malagutti, L.; Mollica, F. FDM 3D Printing of Polymers Containing Natural Fillers: A Review of Their Mechanical Properties. *Polymers* **2019**, *11* (7), 1094. <https://doi.org/10.3390/polym11071094>.
- (109) Gibson, I.; Rosen, D.; Stucker, B.; Khorasani, M. *Additive Manufacturing Technologies*; Springer International Publishing: Cham, 2021. <https://doi.org/10.1007/978-3-030-56127-7>.
- (110) *Standard Terminology for Additive Manufacturing Technologies*,. <https://www.astm.org/f2792-12.html> (accessed 2023-06-07).
- (111) Mallikarjuna, B.; Bhargav, P.; Hiremath, S.; Jayachristiyan, K. G.; Jayanth, N. A Review on the Melt Extrusion-Based Fused Deposition Modeling (FDM): Background, Materials, Process Parameters and Military Applications. *Int J Interact Des Manuf* **2023**. <https://doi.org/10.1007/s12008-023-01354-0>.
- (112) Mokhena, T. C.; Sefadi, J. S.; Sadiku, E. R.; John, M. J.; Mochane, M. J.; Mtibe, A. Thermoplastic Processing of PLA/Cellulose Nanomaterials Composites. *Polymers* **2018**, *10* (12), 1363. <https://doi.org/10.3390/polym10121363>.
- (113) Chen, Z.; Zhou, J.; Jiang, Y.; Hu, Z.; Yin, S.; Wang, Q.; Innocent, M. T.; Xiang, H.; Zhu, M. Preparation of Form-Stable Silica/Polyethylene Glycol Composites Using Flash-Drying for Large-Scale Melt-Spun Fibers with Thermal Management Property. *Polymer Engineering & Science* **2023**, *63* (2), 454–466. <https://doi.org/10.1002/pen.26220>.
- (114) Barthod-Malat, B.; Hauguel, M.; Behlouli, K.; Grisel, M.; Savary, G. Influence of the Compression Molding Temperature on VOCs and Odors Produced from Natural Fiber Composite Materials. *Coatings* **2023**, *13* (2), 371. <https://doi.org/10.3390/coatings13020371>.
- (115) Cherifi, Z.; Zaoui, A.; Boukoussa, B.; Derdar, H.; El Abed, O. Z.; Zeggai, F. Z.; Meghabar, R.; Chebout, R.; Bachari, K. Ultrasound-Promoted Preparation of Cellulose Acetate/Organophilic Clay Bio-Nanocomposites Films by Solvent Casting Method. *Polym. Bull.* **2023**, *80* (2), 1831–1843. <https://doi.org/10.1007/s00289-022-04129-x>.
- (116) Tao, Y.; Wang, H.; Li, Z.; Li, P.; Shi, S. Q. Development and Application of Wood Flour-Filled Poly(lactic Acid Composite Filament for 3D Printing. *Materials* **2017**, *10* (4), 339. <https://doi.org/10.3390/ma10040339>.
- (117) Murphy, C. A.; Collins, M. N. Microcrystalline Cellulose Reinforced Poly(lactic Acid Biocomposite Filaments for 3D Printing. *Polymer Composites* **2018**, *39* (4), 1311–1320. <https://doi.org/10.1002/pc.24069>.

- (118) Ambone, T.; Torris, A.; Shanmuganathan, K. Enhancing the Mechanical Properties of 3D Printed Polylactic Acid Using Nanocellulose. *Polymer Engineering & Science* **2020**, *60* (8), 1842–1855. <https://doi.org/10.1002/pen.25421>.
- (119) Cataldi, A.; Rigotti, D.; Nguyen, V. D. H.; Pegoretti, A. Polyvinyl Alcohol Reinforced with Crystalline Nanocellulose for 3D Printing Application. *Materials Today Communications* **2018**, *15*, 236–244. <https://doi.org/10.1016/j.mtcomm.2018.02.007>.
- (120) Olam, M.; Tosun, N. 3D-Printed Polylactide/Hydroxyapatite/Titania Composite Filaments. *Materials Chemistry and Physics* **2022**, *276*, 125267. <https://doi.org/10.1016/j.matchemphys.2021.125267>.
- (121) Thurzo, A.; Gálfiová, P.; Nováková, Z. V.; Polák, Š.; Varga, I.; Strunga, M.; Urban, R.; Surovková, J.; Leško, L.; Hajdúchová, Z.; Feranc, J.; Janek, M.; Danišovič, L. Fabrication and In Vitro Characterization of Novel Hydroxyapatite Scaffolds 3D Printed Using Polyvinyl Alcohol as a Thermoplastic Binder. *International Journal of Molecular Sciences* **2022**, *23* (23), 14870. <https://doi.org/10.3390/ijms232314870>.
- (122) Karimipour-Fard, P.; Jeffrey, M. P.; Jones Taggart, H.; Pop-Iliev, R.; Rizvi, G. Development, Processing and Characterization of Polycaprolactone/Nano-Hydroxyapatite/Chitin-Nano-Whisker Nanocomposite Filaments for Additive Manufacturing of Bone Tissue Scaffolds. *Journal of the Mechanical Behavior of Biomedical Materials* **2021**, *120*, 104583. <https://doi.org/10.1016/j.jmbbm.2021.104583>.
- (123) Mihankhah, P.; Azdast, T.; Mohammadzadeh, H.; Hasanzadeh, R.; Aghaiee, S. Fused Filament Fabrication of Biodegradable Polylactic Acid Reinforced by Nanoclay as a Potential Biomedical Material. *Journal of Thermoplastic Composite Materials* **2023**, *36* (3), 961–983. <https://doi.org/10.1177/08927057211044185>.
- (124) Wang, Z.; Xu, J.; Lu, Y.; Hu, L.; Fan, Y.; Ma, J.; Zhou, X. Preparation of 3D Printable Micro/Nanocellulose-Polylactic Acid (MNC/PLA) Composite Wire Rods with High MNC Constitution. *Industrial Crops and Products* **2017**, *109*, 889–896. <https://doi.org/10.1016/j.indcrop.2017.09.061>.
- (125) Xu, W.; Pranovich, A.; Uppstu, P.; Wang, X.; Kronlund, D.; Hemming, J.; Öblom, H.; Moritz, N.; Preis, M.; Sandler, N.; Willför, S.; Xu, C. Novel Biorenewable Composite of Wood Polysaccharide and Polylactic Acid for Three Dimensional Printing. *Carbohydr Polym* **2018**, *187*, 51–58. <https://doi.org/10.1016/j.carbpol.2018.01.069>.
- (126) Tran, T. N.; Bayer, I. S.; Heredia-Guerrero, J. A.; Frugone, M.; Lagomarsino, M.; Maggio, F.; Athanassiou, A. Cocoa Shell Waste Biofilaments for 3D Printing Applications. *Macromol. Mater. Eng.* **2017**, *302* (11), 1700219. <https://doi.org/10.1002/mame.201700219>.
- (127) Dong, J.; Mei, C.; Han, J.; Lee, S.; Wu, Q. 3D Printed Poly(Lactic Acid) Composites with Grafted Cellulose Nanofibers: Effect of Nanofiber and Post-Fabrication Annealing Treatment on Composite Flexural Properties. *Additive Manufacturing* **2019**, *28*, 621–628. <https://doi.org/10.1016/j.addma.2019.06.004>.
- (128) Daver, F.; Lee, K. P. M.; Brandt, M.; Shanks, R. Cork–PLA Composite Filaments for Fused Deposition Modelling. *Composites Science and Technology* **2018**, *168*, 230–237. <https://doi.org/10.1016/j.compscitech.2018.10.008>.
- (129) Wasti, S.; Triggs, E.; Farag, R.; Auad, M.; Adhikari, S.; Bajwa, D.; Li, M.; Ragauskas, A. J. Influence of Plasticizers on Thermal and Mechanical Properties of Biocomposite Filaments Made from Lignin and Polylactic Acid for 3D Printing. *Composites Part B: Engineering* **2021**, *205*, 108483. <https://doi.org/10.1016/j.compositesb.2020.108483>.
- (130) *3D Printing Filaments Prepared from Modified Poly(Lactic Acid)/Teak Wood Flour Composites: An Investigation on the Particle Size Effects and Silane Coupling Agent Compatibilisation*. Journal of Physical Science. <https://jps.usm.my/3d-printing-filaments/> (accessed 2023-05-15).
- (131) Guo, R.; Ren, Z.; Bi, H.; Song, Y.; Xu, M. Effect of Toughening Agents on the Properties of Poplar Wood Flour/Poly (Lactic Acid) Composites Fabricated with Fused Deposition Modeling. *European Polymer Journal* **2018**, *107*, 34–45. <https://doi.org/10.1016/j.eurpolymj.2018.07.035>.
- (132) Fijoł, N.; Aguilar-Sánchez, A.; Mathew, A. P. 3D-Printable Biopolymer-Based Materials for Water Treatment: A Review. *Chemical Engineering Journal* **2022**, *430*, 132964. <https://doi.org/10.1016/j.cej.2021.132964>.

- (133) Deroiné, M.; Le Duigou, A.; Corre, Y.-M.; Le Gac, P.-Y.; Davies, P.; César, G.; Bruzard, S. Accelerated Ageing of Polylactide in Aqueous Environments: Comparative Study between Distilled Water and Seawater. *Polymer Degradation and Stability* **2014**, *108*, 319–329. <https://doi.org/10.1016/j.polymdegradstab.2014.01.020>.
- (134) Podkościelna, B.; Gargol, M.; Goliszek, M.; Klepka, T.; Sevastyanova, O. Degradation and Flammability of Bioplastics Based on PLA and Lignin. *Polymer Testing* **2022**, *111*, 107622. <https://doi.org/10.1016/j.polymertesting.2022.107622>.
- (135) Du, Y.; Zheng, J.; Yu, G. Influence of Thermally-Accelerated Aging on the Dynamic Mechanical Properties of HTPB Coating and Crosslinking Density-Modified Model for the Payne Effect. *Polymers* **2020**, *12* (2), 403. <https://doi.org/10.3390/polym12020403>.
- (136) Frigione, M.; Rodríguez-Prieto, A. Can Accelerated Aging Procedures Predict the Long Term Behavior of Polymers Exposed to Different Environments? *Polymers* **2021**, *13* (16), 2688. <https://doi.org/10.3390/polym13162688>.
- (137) Amza, C. G.; Zapciu, A.; Baci, F.; Vasile, M. I.; Nicoara, A. I. Accelerated Aging Effect on Mechanical Properties of Common 3D-Printing Polymers. *Polymers* **2021**, *13* (23), 4132. <https://doi.org/10.3390/polym13234132>.
- (138) Starkova, O.; Gagani, A. I.; Karl, C. W.; Rocha, I. B. C. M.; Burlakovs, J.; Krauklis, A. E. Modelling of Environmental Ageing of Polymers and Polymer Composites—Durability Prediction Methods. *Polymers* **2022**, *14* (5), 907. <https://doi.org/10.3390/polym14050907>.
- (139) Plota, A.; Masek, A. Lifetime Prediction Methods for Degradable Polymeric Materials—A Short Review. *Materials* **2020**, *13* (20), 4507. <https://doi.org/10.3390/ma13204507>.
- (140) ImageJ. ImageJ Wiki. <https://imagej.github.io/software/imagej/index> (accessed 2023-07-24).
- (141) Belhachemi, M.; Addoun, F. Comparative Adsorption Isotherms and Modeling of Methylene Blue onto Activated Carbons. *Appl Water Sci* **2011**, *1* (3), 111–117. <https://doi.org/10.1007/s13201-011-0014-1>.
- (142) Zhang, X.; Megone, W.; Peijs, T.; Gautrot, J. E. Functionalization of Electrospun PLA Fibers Using Amphiphilic Block Copolymers for Use in Carboxy-Methyl-Cellulose Hydrogel Composites. *Nanocomposites* **2020**, *6* (3), 85–98. <https://doi.org/10.1080/20550324.2020.1784600>.
- (143) Conoscenti, G.; Carrubba, V. L.; Brucato, V. A Versatile Technique to Produce Porous Polymeric Scaffolds: The Thermally Induced Phase Separation (TIPS) Method. *Arch Chem Res* **2017**, *01* (02). <https://doi.org/10.21767/2572-4657.100012>.
- (144) Fijoł, N.; Abdelhamid, H. N.; Pillai, B.; Hall, S. A.; Thomas, N.; Mathew, A. P. 3D-Printed Monolithic Biofilters Based on a Polylactic Acid (PLA) – Hydroxyapatite (HAp) Composite for Heavy Metal Removal from an Aqueous Medium. *RSC Adv.* **2021**, *11* (51), 32408–32418. <https://doi.org/10.1039/D1RA05202K>.
- (145) Fijoł, N.; Aguilar-Sánchez, A.; Ruiz-Caldas, M.-X.; Redlinger-Pohn, J.; Mautner, A.; Mathew, A. P. 3D Printed Polylactic Acid (PLA) Filters Reinforced with Polysaccharide Nanofibers for Metal Ions Capture and Microplastics Separation from Water. *Chemical Engineering Journal* **2023**, *457*, 141153. <https://doi.org/10.1016/j.cej.2022.141153>.
- (146) Pérez-Fonseca, A. A.; Robledo-Ortíz, J. R.; González-Núñez, R.; Rodrigue, D. Effect of Thermal Annealing on the Mechanical and Thermal Properties of Polylactic Acid–Cellulosic Fiber Biocomposites. *Journal of Applied Polymer Science* **2016**, *133* (31). <https://doi.org/10.1002/app.43750>.
- (147) Saito, T.; Isogai, A. TEMPO-Mediated Oxidation of Native Cellulose. The Effect of Oxidation Conditions on Chemical and Crystal Structures of the Water-Insoluble Fractions. *Biomacromolecules* **2004**, *5* (5), 1983–1989. <https://doi.org/10.1021/bm0497769>.
- (148) Lichtenstein, K.; Lavoine, N. Toward a Deeper Understanding of the Thermal Degradation Mechanism of Nanocellulose. *Polymer Degradation and Stability* **2017**, *146*, 53–60. <https://doi.org/10.1016/j.polymdegradstab.2017.09.018>.
- (149) Fijoł, N.; Mautner, A.; Grape, E. S.; Bacsik, Z.; Inge, A. K.; Mathew, A. P. MOF@Cell: 3D Printed Biobased Filters Anchored with a Green Metal–Organic Framework for Effluent Treatment. *J. Mater. Chem. A* **2023**, *10*.1039.D3TA01757E. <https://doi.org/10.1039/D3TA01757E>.

- (150) Karim, Z.; Hakalahti, M.; Tammelin, T.; P. Mathew, A. In Situ TEMPO Surface Functionalization of Nanocellulose Membranes for Enhanced Adsorption of Metal Ions from Aqueous Medium. *RSC Advances* **2017**, 7 (9), 5232–5241. <https://doi.org/10.1039/C6RA25707K>.
- (151) Si, R.; Wu, C.; Yu, D.; Ding, Q.; Li, R. Novel TEMPO-Oxidized Cellulose Nanofiber/Polyvinyl Alcohol/Polyethyleneimine Nanoparticles for Cu²⁺ Removal in Water. *Cellulose* **2021**, 28 (17), 10999–11011. <https://doi.org/10.1007/s10570-021-04236-4>.
- (152) Sehaqui, H.; de Larraya, U. P.; Liu, P.; Pfenninger, N.; Mathew, A. P.; Zimmermann, T.; Tingaut, P. Enhancing Adsorption of Heavy Metal Ions onto Biobased Nanofibers from Waste Pulp Residues for Application in Wastewater Treatment. *Cellulose* **2014**, 21 (4), 2831–2844. <https://doi.org/10.1007/s10570-014-0310-7>.
- (153) *European Union: Directive (EU) 2020/2184 of the European... - Google Scholar*. [https://scholar.google.com/scholar_lookup?title=Directive+\(EU\)+2020/2184+of+the+European+Parliament+and+of+the+Council+of+16+December+2020+on+the+quality+of+water+intended+for+human+consumption&author=European+Union+\(EU\)&publication_year=2020&journal=Of+f.+J.+Eur.+Union&volume=435&pages=1%E2%80%939362](https://scholar.google.com/scholar_lookup?title=Directive+(EU)+2020/2184+of+the+European+Parliament+and+of+the+Council+of+16+December+2020+on+the+quality+of+water+intended+for+human+consumption&author=European+Union+(EU)&publication_year=2020&journal=Of+f.+J.+Eur.+Union&volume=435&pages=1%E2%80%939362) (accessed 2023-03-08).
- (154) Svensson Grape, E.; Chacón-García, A. J.; Rojas, S.; Pérez, Y.; Jaworski, A.; Nero, M.; Åhlén, M.; Martínez-Ahumada, E.; Galetsa Feindt, A. E.; Pepillo, M.; Narongin-Fujikawa, M.; Ibarra, I. A.; Cheung, O.; Baresel, C.; Willhammar, T.; Horcajada, P.; Inge, A. K. Removal of Pharmaceutical Pollutants from Effluent by a Plant-Based Metal–Organic Framework. *Nat Water* **2023**, 1 (5), 433–442. <https://doi.org/10.1038/s44221-023-00070-z>.